3-2008

Investigation into Fretting Fatigue Under Cyclic Contact Load and in Conjuction with Fatigue of Titanium Alloy

Abdulla A. Al-Noaimi

IVESTIGATION INTO FRETTING FATIGUE UNDER CYCLIC CONTACT LOAD AND IN CONJUNCTION WITH PLAIN FATIGUE OF TITANIUM ALLOY

THESIS

Abdulla Al-Noaimi, Capt, Royal Bahraini Air Force

AFIT/GAE/ENY/08- M30

DEPARTMENT OF THE AIR FORCE
AIR UNIVERSITY

AIR FORCE INSTITUTE OF TECHNOLOGY

Wright-Patterson Air Force Base, Ohio

AFIT/GAE/ENY/08 - M30

**IVESTIGATION INTO FRETTING FATIGUE UNDER CYCLIC CONTACT LOAD
AND IN CONJUNCTION WITH PLAIN FATIGUE OF TITANIUM ALLOY**

THESIS

Presented to the Faculty

Department of Aeronautics and Astronautics

Graduate School of Engineering and Management

Air Force Institute of Technology

Air University

Air Education and Training Command

In Partial Fulfillment of the Requirements for the

Degree of Master of Science in Aeronautical Engineering

Abdulla Al-Noaimi

Capt, Royal Bahraini Air Force

March 2008

AFIT/GAE/ENY/08- M30

IVESTIGATION INTO FRETTING FATIGUE UNDER CYCLIC CONTACT LOAD AND IN CONJUNCTION WITH PLAIN FATIGUE OF TITANIUM ALLOY

Abdulla Al-Noaimi

Capt, Royal Bahraini Air Force

Approved:

_____/signed/_____   _____
    S. Mall (Chairman)   date

_____/signed/_____   _____
    S. Soni   (Member)   date

_____/signed/_____   _____
    V. Jain   (Member)   date

Abstract

In this study, an investigation of fretting fatigue behavior of titanium Alloy, Ti-6Al-4V, was carried out. This study includes experimental work followed by analysis using finite element method. Fretting fatigue occurs at the interface between two components that are undergoing a small amplitude oscillatory movements which result in a reduction of the material life, compared to the plain fatigue. Unlike most of the previous works, which were accomplished using constant applied contact load, this study will put more effort to investigate the effect of cyclic axial and normal contact loads on material life. Also, this study will account the effect of the phase difference between the axial and the normal contact loads into which not many studies are focused on. The primary goal of this study is to investigate the effect of phase difference between axial and normal contact loads on fretting fatigue behavior of Ti-6Al-4V alloy, as well as the effect of increasing the cylindrical pad radii. In addition, this study investigated in detail the effects of combined plain and fretting fatigue loading conditions on the life of material. This will lead to a better understanding of the behavior of titanium Alloy under different combinations of fretting fatigue and plain fatigue, using frequency of 10 HZ for both axial and contact loads. The crack initiation location and orientation at the contact surface were investigated and measured using the Optical and Scanning Electron Microscope (SEM). Cracks were always found to initiate on the contact surface and near the trailing edge in all tests. In order to use finite element analyses to determine the contact region state variable such as displacement, stress, and strain, a commercial software called ABAQUS was used. These variables were needed for the computation

of fretting fatigue parameters. The fatigue parameters; such as the axial stress range, effective stress, and modified shear stress range (MSSR), were analyzed to predict the fatigue life. It was observed that as ratio of plain fatigue to fretting fatigue increases the fretting fatigue life increases. Also, the MSSR parameter was effective in predicting the crack initiation, crack initiation orientation, and fatigue life under the fretting fatigue condition.

Acknowledgments

Table of Contents

The introduction chapter will discuss the definition of the fretting fatigue phenomenon, negative effects of fretting fatigue, importance of this study, the objective and purposes of this study, and the methodology used to model the

Axial-Normal Force Vs Time

There are many factors that can affect the martial under fretting fatigue, which makes the study of fretting fatigue complicated. Different studies have been conducted and each concentrated on one of these to have a deeper understanding of the contribution of this fracture on the fretting fatigue condition. This section

In a study conducted by Lee [8], the effect of variable contact load on fretting fatigue behavior of titanium alloy was investigated. The study concluded that the tangential load stayed in phase with the axial load and the contact load affected only the magnitude of the tangential load and had no effect on the phase or the frequency of the tangential load. In addition, the study showed that the fatigue life was primarily dominated by the axial load and that the magnitude and frequency of the contact load had no significant effect on fatigue life and MSSR parameter. Fatigue life data from both constant and variable contacts loads were the same. In addition, the crack initiated near the trailing edge, and the crack

$$\tau = -\frac{\sigma_{xx} - \sigma_{yy}}{2} \sin(2\theta) + \tau_{xy} \cos(2\theta) \qquad (2.29)$$

28 ...... The Smith-Watson-Topper (SWT) parameter can be expressed as follows:

The function the peak-valley compensator (PVC), in the software of the test machine, was used during each test for both contact load and axial load in order to reduce variation between command and feedback signals sensed by the test machine. After failure of the specimen, by using the date collected, the tangential

In this chapter the details of finite element analysis that is needed for conducting analysis of fretting fatigue tests will be discussed. This chapter will include the

Finite Element Analysis (FEA) is a numerical procedure that is used to determine the fretting fatigue parameters by calculating the state of strain, stress, and displacement at the contact area. Using this procedure, a body can be represented by a discrete system containing many elements which are connected to each

other by the nodes. At these nodes the governing equations can be solved to give the solution of the strain, stress, and displacement at the contact interface. As was discussed earlier in the thesis, configuration, two cylindrical bodies were used with the assumption that their radii are very large in comparison to the contact width (r >> a), in order to use analytical solutions such as "Ruiz" program. In addition, the contacting bodies are assumed to have infinite boundaries. An infinite half-space assumption in fretting fatigue analysis is

This section discusses the results of fatigue life that were determined from this study. This section will discuss the followings; combination of plain fatigue and fretting fatigue, fretting fatigue life, the use of the MSSR parameter as a predictive parameter, pad geometry effect on fatigue life, and effect of out of

Two experiments were done under the combinations between the fretting fatigue and the plain fatigue condition. Tables 5.5 and 5.6 show the fatigue life for these experiments. Test # 16 was conducted under fretting fatigue condition with a constant contact load of 3336 N, and a cyclic axial load with maximum magnitude of 564 MPa and minimum magnitude of 56.4 MPa. During this test, 5,000 fretting fatigue cycles was applied first followed by 1,000 plain fatigue cycles and this continued on till fracture of the specimen occurred. The fatigue life of this test was 44,656 cycles. On the other hand, Test # 17 was conducted with the same contact and axial loads applied in test # 16 but with 5,000 fretting fatigue cycle followed by 100,000 plain fatigue cycles. The fatigue life of this test was 350,937 cycles. Results from previous study conducted by Al-Majali [30] were used in conjunction with results from present study. Figure 5.26 shows that plotting results from test # 16 and test # 17 which reflect that plain fatigue increases the life of titanium specimen while fretting fatigue decreases the life of titanium specimen. The ratios of plain fatigue to that of fretting fatigue were calculated for these tests and plotted, as shown in Figure 5.26. On the other hand, it can concluded from Figure 5.27 that there is no history effect as long as the total cycles are the same, since it shows the same trend as that in Figure 5.26 This means that there will be no effect on fretting fatigue life whether some of fretting fatigue was applied at first and continued by plain fatigue and the process kept alternating or finishing all fretting fatigue cycles first followed by

This section will discuss the following; the effect of the axial stress range and the effective axial stress, shear stress range, the use of MSSR parameter on fatigue

The axial stress range can be defined as the difference between the maximum and the minimum axial stress. On the other hand, the effective stress can be

$$\sigma_{effective} = \sigma_{max}(1-R)^m \qquad\qquad (6.1)$$

The reason that the MSSR parameter was adopted in this study because it is the most effective parameter in predicting the fatigue life, the crack initiation location, and the crack initiation orientation for this present study. As concluded in previous sections, MSSR was very effective parameter in predicting the crack initiation location and orientation because it does take into consideration both

normal and shear stress and is independent of pad geometry. This section will discuss the effect of MSSR on the fatigue life. By then, the result will be compared to previous studies.

The result of MSSR calculation and the fatigue life for the titanium alloy from this study and previous studies are tabulated in Table 5.12 and 5.15. Looking at these tables, results from constant applied load condition and variable applied contact load condition from the previous studies as well as the phase difference condition from this present study were tabulated. Figure 5.40 shows the graphical results of MSSR and fatigue life which reflect the effect of MSSR on the fatigue life from present study while Figure 5.41 shows the same graphical results from present study as well as previous studies. Figure 5.40 shows that MSSR S_N curve did collapse all date together, unlike S_N curves from axial stress range and effective stress. It can be noticed from Figure 5.41 that values of MSSR data lie within the scatter band, except for data from Majali [30] which are out of the scatter from all the other studies. From Figure 5.41, it can be concluded that MSSR parameter was very effective as a tool that can be used to predict fretting fatigue life, because it did take into consideration contact stresses. Also, it can be concluded that MSSR was an excellent parameter to predict crack initiation location as well as crack initiation orientation.

The investigation into the effect of out of phase on the fatigue life of titanium alloy is one of the purposes of this study. The phase difference between the axial and the contact loads improves the fretting fatigue life. However this improvement depends on the applied axial load. For example, under higher magnitude of applied axial stress, the improvement of the fatigue life is not so much. On the other hand, under lower applied axial stress condition the fatigue life might be doubled. The fatigue life of the out of phase condition proved to be higher. It can be concluded that the results from this present study were very close to the previous studies. Also, it can be noticed that all values lie within the scatter band.

In this chapter, the summary of this study are presented. This chapter will include the conclusion of the analyzed and discussed results from this present study as well as recommendation for future work which can be accomplished

There is a lot of work that has been accomplished to better understand the fretting behavior of the titanium alloy Ti-6Al-4V since this material is used in gas turbine engines. In previous studies, most of them assumed that the applied contact load is constant, while a little effort has been conducted under variable contact load. Trying to look into mechanics of components in the turbine engine fretting fatigue phenomenon is a very difficult area to study due to the complicated oscillatory movements at the contact region which result from the application of both the axial and the contact loads. These loads can be applied in any condition; variable contact load, in-phase, an alternate between plain fatigue and fretting fatigue, or phase lag between the axial and the contact load. In order to have a better understanding of the behavior of fretting fatigue, investigating the fretting fatigue with phase difference and combination of fretting fatigue and

Test # 16 and test # 17 were conducted under combinations between fretting fatigue and plain fatigue. In both tests; the contact load was kept constant at 3336 N, while the axial stress range was kept in between 564 MPa and 56 MPa. In addition, fifteen tests were conducted with phase difference between the applied axial load and the applied contact load. Eleven out of these fifteen tests were conducted using 50.8 mm pads while the rest were conducted using 304.8 mm pads. In these experiments; the maximum axial load was varied between 564 MPa and 413 MPa and the applied contact load was kept constant between 4448 N and 2224 N. Also, the selected phase angles were: 0 degree, 45 degree, and 90

All of the experiments were conducted by using Ti-6Al-4V alloy specimens, which has Poison's ratio of 0.33, modulus of elasticity of 126 GPa, and dimension of 3.81 mm thickness and 6.35 mm width. a computer controlled bi-axial servo-hydraulic machine was used to control the applied load condition and their frequencies and phase angle by using a peak valley compensator to reduce the variation between control and feedback signals. The outputs of various data were monitored and saved continuously until failure of the specimen occurred.

The resulting tangential loads were found as the half difference between the lower axial loads and the upper grip loads. After the specimen failed, the contact half width of the failed specimen was determined by using the lower magnification microscope. After that, the Scanning Electron Microscope (SEM) was used to examine the fracture surface area, locate the crack initiation location, and measure the crack initiation orientation. And prior to SEM the contact half width of the failed specimen was determined by using the lower magnification

List of Figures

List of Tables

List of Symbols

a	contact half-width
$a_{analytical}$	contact half-width carried out from analytical solution
a_{Exp}	contact half-width measured from experiments
A	a specimen's cross section area
b	a specimen's half thickness
c	stick zone boundary
$c^{'}$	fatigue ductility exponents
d	specimen thickness
E	modulus of elasticity
f	coefficient of friction
FEA	finite element analysis
FP	Findley Parameter
h	depth of penetration
HCF	High Cyclic Fatigue
k	the curvature
L	specimen overall length
MPT	Multi-Purpose Test Software
MSSR	modified shear stress range fatigue predictive parameter
N_f	numbers of fatigue cycles to break a specimen into two pieces
N_i	numbers of fatigue cycles to crack initiation
p	contact pressure distribution in the contact zone

P	applied contact loads
P_0	maximum contact pressure or Hertzian Peak Pressure
P_{Freq}	frequency of the applied contact loads
P_{max}	maximum applied contact loads
P_{min}	minimum applied contact loads
PVC	Peak Valley Compensator
q	surface shear stress distribution
Q	tangential loads
Q_{max}	maximum tangential loads
Q_{min}	minimum tangential loads
r	fretting pad radius
R	stress ratio
R_1	radius of fretting pad
R_2	radius of fretting specimens
R_σ	stress ratio of axial stress
R_ε	strain ratio
R_τ	shear stress ratio
SEM	scanning electronic microscopy
SSR	Shear Stress Range
SWT	Smith-Watson-Topper parameter
σ_{xx}	normal stress along x-direction
σ_{xy}	shear stress on x-y plane
σ_{yy}	normal stress along y-direction
u	displacement
V_{lower}	lower axial load

V_{upper}	upper axial load
w	specimen width
w(x)	weight function
Y_0	the depth within a specimen where residual stress is zero
β	Dundurs' parameter
ε_a	total strain amplitude
ε_f'	fatigue ductility coefficient
ε_{max}	maximum strain
ε_{min}	minimum strain
ε_{xx}	strain induced by the axial stress
ν	Poisson's ratio
θ	direction of stress in a material, observed angle of orientation
ϕ	phase angle
$\Delta\sigma$	axial stress range
$\Delta\varepsilon$	plastic strain amplitude
$\Delta\tau$	shear stress range
σ	normal stresses at a given point with a specific orientation
$\sigma_{1,2}$	principal normal stresses
σ_{axial}	applied axial stress
σ_{eff}	effective axial stress
σ_f'	fatigue strength coefficient
σ_{max}	maximum applied axial stress
σ_{min}	minimum applied axial stress

$(\sigma_{xx})_{axial}$	x-direction normal stress contributed from axial load
$(\sigma_{xx})_{contact}$	x-direction normal stress contributed from contact load
$(\sigma_{xx})_{tangential}$	x-direction normal stress contributed from tangential load
σ_y	yield strength
τ	shear stress at a given point with a specific orientation
τ_{max}	maximum shear stress at a given point

IVESTIGATION INTO FRETTING FATIGUE UNDER CYCLIC CONTACT LOAD AND IN CONJUNCTION WITH PLAIN FATIGUE OF TITANIUM ALLOY

I. Introduction

The introduction chapter will discuss the definition of the fretting fatigue phenomenon, negative effects of fretting fatigue, importance of this study, the objective and purposes of this study, and the methodology used to model the fretting fatigue mechanism.

1.1. Fretting Fatigue

Material failure can take many forms. The most common are wear, corrosion, deformation, and fracture. When a cyclic load is subjected to a component and results in the separation of the two components into two or more pieces, this failure is called plain fatigue. On the other hand, when there is a contact between two surfaces while there is small amplitude oscillatory movement and one of both surfaces subjected to cyclic stresses, then this kind of failure is called fretting fatigue. Simply, fretting fatigue is the phenomenon when a cyclic stress is applied to a component in contact with one another which causes a small amplitude oscillatory movement and a tangential force resisting these movements. Under fretting fatigue, shear and tensile stress will increase at the contact zone, producing surface defects, which act as stress concentration sites that promote crack nucleation. Fatigue loading coupled with pressure between two touching components causes premature crack nucleation and accelerated crack growth causing components under fretting fatigue to fail

unexpectedly at stress levels well below their plain fatigue limit or at fewer life cycles than predicted by plain fatigue analysis.

Failure in component due to fretting fatigue is characterized by four stages; which are characterized by four regions: crack initiation, crack propagation due to bulk and contact stresses, crack propagation due to bulk stresses only, and finally fracture. The crack will initiate in stage or region I. After it appears the crack will penetrate the material at an angle and will propagate into the sub-surface. In stage or region II, the crack will progress deeper into the material and the contact stress reduces making the crack propagate at an angle in a direction normal to the axial stress. In stage or region III, the crack progresses until rapture. Finally, stage or region IV is the zone of failure when the stress intensity factor is critical or the crack reaches the outer edge of the part. Fretting fatigue reduces the material life time; therefore, many aircraft industries are interested in the investigation of the fretting fatigue phenomenon.

1.2. Negative Effects of Fretting Fatigue

Fretting Fatigue could result in a significant reduction in aircraft and engine components' service life and eventually leads to their premature failure, and this is because it accelerates crack propagation. This can lead to components failure if not detected. Because of a lack of understanding of fretting fatigue, engine maintenance technicians need to spend greater efforts looking for cracks that may or may not be propagating on the blades. If cracks are missed, the lives of the air crew will be endangered. In order to prevent such failures, more strict maintenance procedures

must be followed, which increases the maintenance cost in addition to maintenance time. The US Air Fore spends an estimated $ 20 Million annually on these preventive measures [9]. In addition, designers may compensate for this danger in the form of thicker, heavier, less efficient blades, which can lead to a more costly engine, by making these dovetail joints more robust than may actually be necessary.

1.3. Importance of This Study

An aircraft is subject to cyclic loads through wing loading, atmospheric turbulence, and cabin pressurization. On the other hand, the propulsion and hydraulic systems also experience cyclic loads. Air Forces from around the world are interested in this subject because fretting fatigue is the cause of many of the failures that occur in turbine engines, due to high cycle fatigue failure. The location where each turbine blade connects to the outer annulus is where components could undergo fretting fatigue, which is called the dovetail joint as shown Figure 1.1. The turbine blades experience cyclic loading in the form of vibrations while at the dovetail joint two surfaces are in contact and potentially rub and slip against each other. Gaining a better understanding of how fretting fatigue affects Ti-6Al-4V, the material of most turbine blades, turbine design engineers could make a more efficient and improved engine, and pilots will be safer with a reduced chance of in-flight engine damage. As a result of this understanding, detection and prediction will be made easier for maintenance technicians. Simply, more research in the fretting fatigue area could provide a clearer view of the crack initiation mechanism that will help in increasing the life time of components as well as reducing the maintenance costs. Different areas in fretting

3

fatigues have been investigated in order to have a better understanding of the phenomenon.

1.4. Purpose and Objectives

Many studies have been conducted done on titanium alloys to investigate the effect of fretting fatigue. Those studies aimed to provide a better understanding of the fretting fatigue phenomenon and thus do give a clearer picture of the crack initiation mechanism. This clearer picture will help in developing technique that will enable to increase the life time of titanium alloy and increase service life of components made of it. Each of the previous studies investigated the effects of different variables and factors on fretting fatigue of titanium alloy which included: different contact pads geometry, different phase angles, different setting of temperature, different load frequencies, and different axial and fretting loads [11, 12, 13, 14, 30]. However, there are many more variables and factors which need to be investigated.

There are four specific goals of this study. The first goal is to investigate the effect of the domination of fretting fatigue cycles versus the domination of plain fatigue cycle on the engine component's life. Figure 1.2 illustrates the process of combination of fretting fatigue and plain fatigue, by using three parts. The first part of this figure shows that cyclic axial stress will continue in the same manner in both fretting fatigue and plain fatigue periods. The second part of this graph shows how shear force goes in a cyclic manner as well in the fretting fatigue period but goes to zero at the plain fatigue period. The third part of this figure shoes how the normal force is constant during the fretting fatigue period then goes zero at the plain fatigue period. The second goal is to investigate the effects of different phase angles between

4

cyclic axial load and cyclic contact load on the engine component's life. Figure 1.3 illustrate the difference between in-phase and out-phase process. In this figure, it can be seen that there is a phase angle between the peak of the plot of cyclic axial load and the peak of the plot of the cyclic contact load, which is called theta. When this phase angle exist, this case is called out-phase condition. On the other hand, when theta is zero, this case is called in-phase condition. The third step is to investigate the effects of changing the fretting pad from 50.8 mm radius to 304.8 mm radius on the engine component's life. The fourth is to investigate the effect of different levels of cyclic axial loads on the engine component's life. This will be the first study to investigate the effect of fretting fatigue using fretting pads of 304.8 mm radius, different phase angles, and cyclic axial and cyclic contact loads on titanium alloy. Previous studies conducted the same affect using cyclic axial and constant contact loads.

The frequency of both the axial and the applied contact loads is 10 Hz. In the present study, both the contact and the axial loads are cyclic in all tests, except one case when using a combination of fretting fatigue and plain fatigue. The results of this research will be investigated to see how the fatigue life, crack initiation location, and crack initiation orientation are affected under these conditions. This study would provide important information that will allow researchers in the future to investigate further the fretting fatigue behavior of titanium alloy under more complex conditions.

1.5. Methodology

In order to link a real problem of the failure of aircraft turbines to theory and put it into practice, a method is needed to model the geometry of the disk and blade attachment in the turbine section. Imitating the components' exact geometry and loading conditions is a complex task, and can be time consuming as well as expensive. Therefore, a simplified cylinder-on-flat model was adopted for the experimental setup of this study as illustrated in Figure. 1.4. This model will be used in this study, in order to investigate the effect on fretting fatigue using different variables.

The specific magnitude of the axial loads and contact loads can be applied using a bi-axial servo-hydraulic machine, which is discussed with full detail in the next chapter. Optical and Scanning Electron Microscopes (SEM) will be used to examine the fracture surface, contact half-width, crack initiation location, and crack initiation orientation. Finite Element Analysis (FEA) will be used to calculate local fretting variables, such as: stress, strain, and displacement. In addition, several predictive parameters will be evaluated to test their effectiveness to predict fatigue life, crack location, and crack initiation orientation on components under fretting fatigue.

Figure 1.1 **Blade/Disc Dovetail Joint in a Turbine Engine**
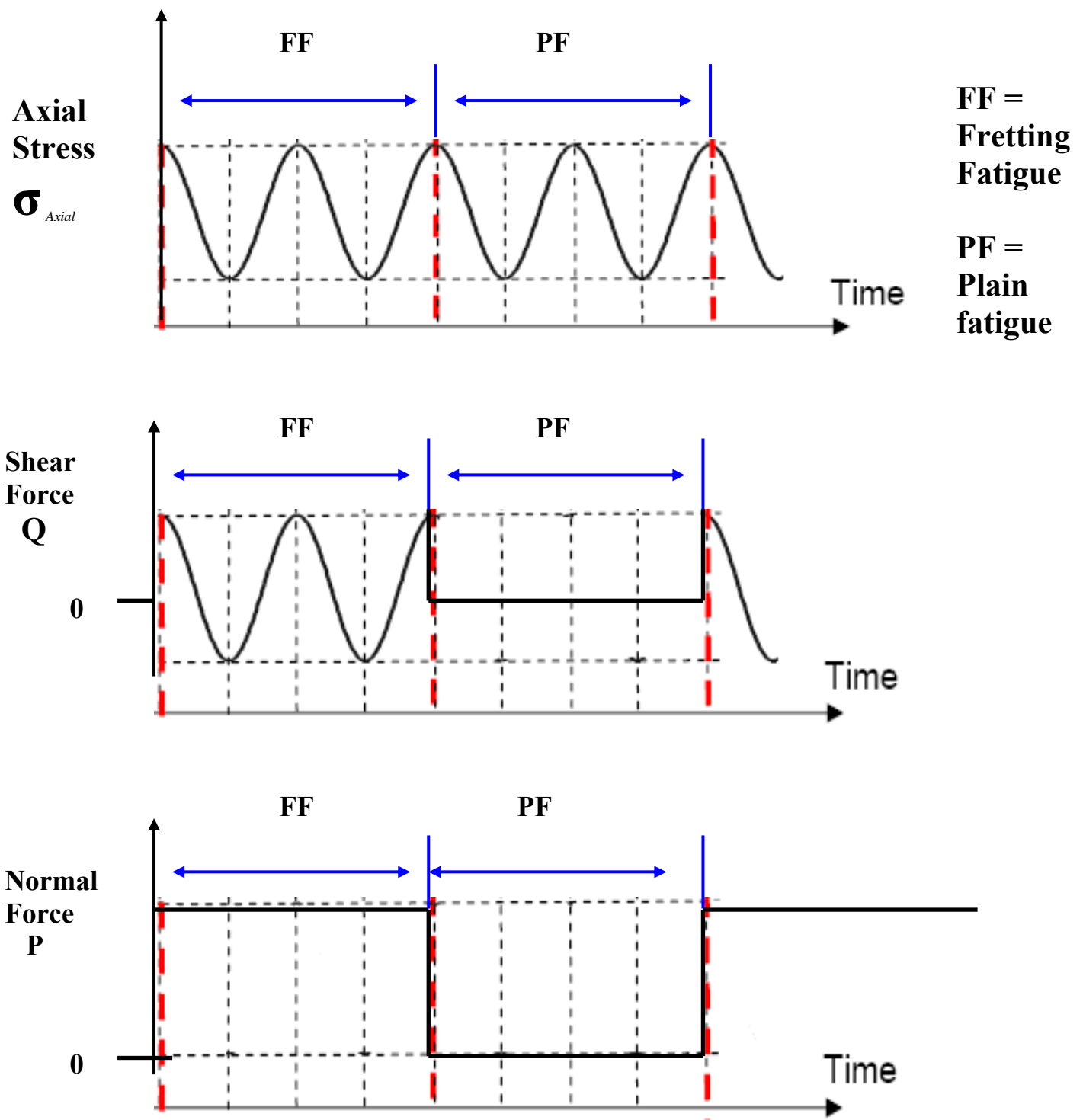
Figure 1.2 Illustration of Combined Fretting Fatigue & Plain Fatigue

8
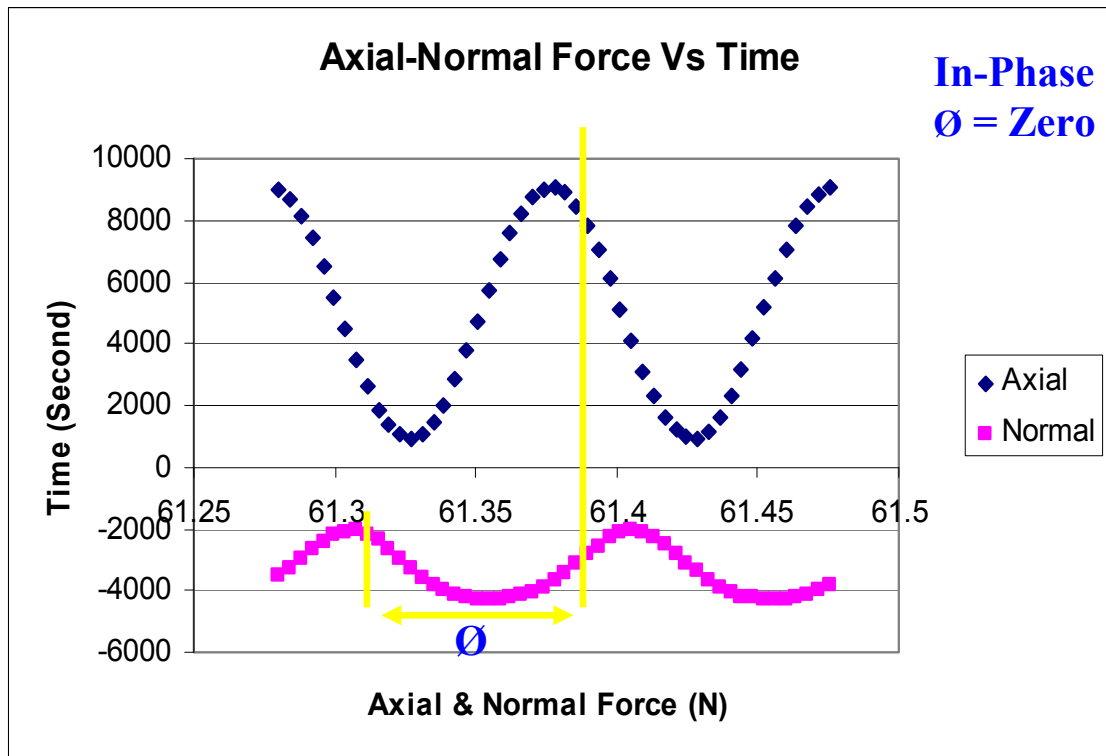
Figure 1.3 **Illustration of Phase Angle (Ø) Between Applied Axial Load &**
Contact Load – Test # 8

Fixed End

Leading Edge Area

Q: Tangential Force

Normal
Load

P

Fretting Pad

Trailing Edge Area

Specimen

Axial Stress σ_{Axial}
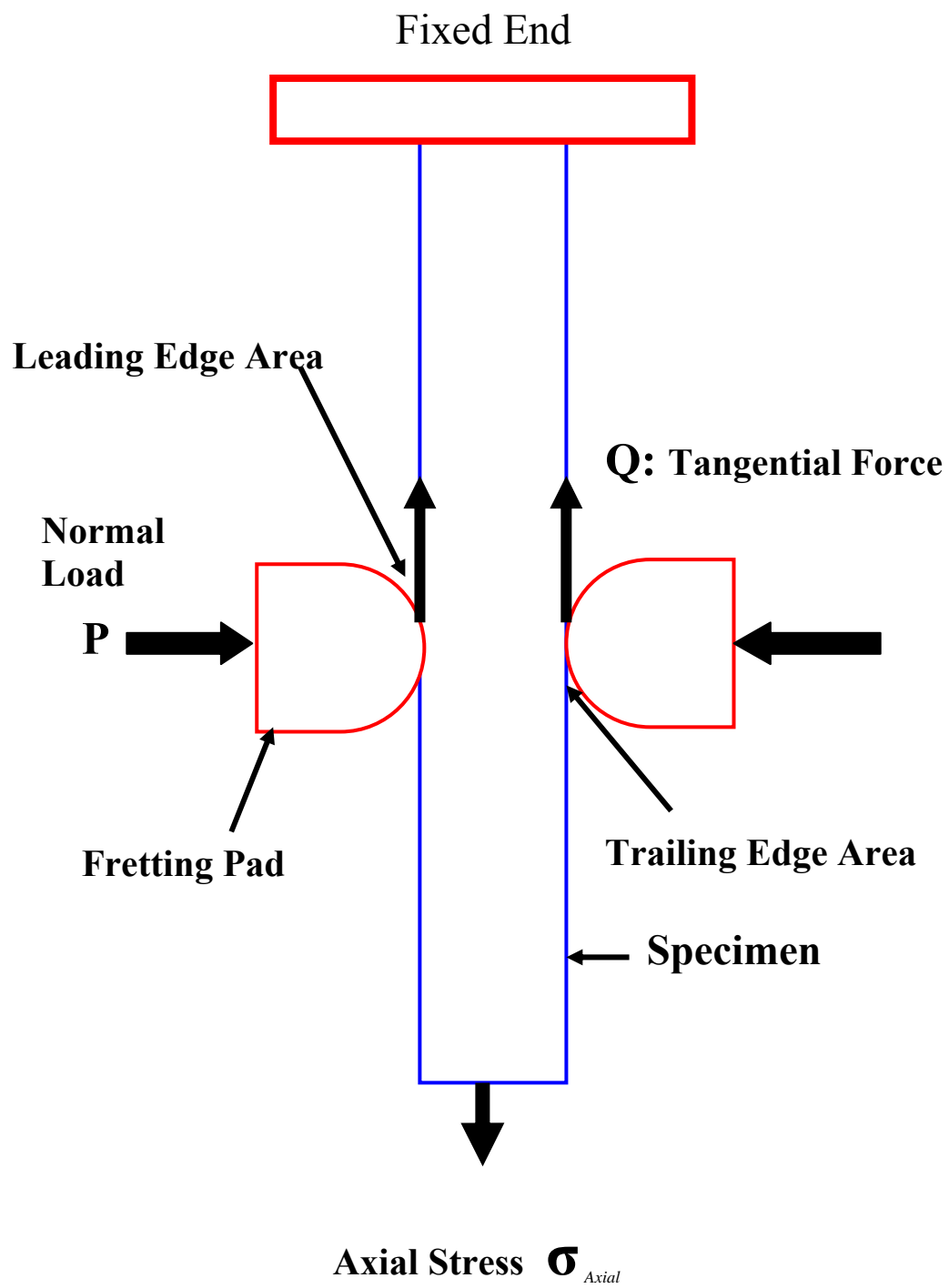
Figure 1.4 Fretting Fatigue Model

II. Background

This chapter will provide an overview by reviewing fundamental concepts of fretting fatigue developed and tested on titanium alloy. First fretting fatigue mechanics will be addressed and discussed. Second, fretting fatigue factors that can affect the material under fretting fatigue will be discussed. Third, parameters which help to predict the fretting fatigue life are explained. In addition, the crack initiation mechanism will be addressed and discussed. Then, gross slip and partial slip will be discussed.

2.1. Fretting Fatigue Configuration

The fretting fatigue configuration has been developed and simplified by several previous studies, as shown in Figure 1.2 in the previous chapter. In this fretting fatigue configuration, the fretting specimen and pads are presented as two mechanical components in contact with each other. The specimen is gripped at one end and subjected to axial stress (σ_{axial}) while the fretting pads are pressed against the specimen by the applied contact load P. This applied contact load is perpendicular to the axial load. By using the software installed in the servo hydraulic machine, the applied axial load can be controlled to produce fatigue loads with different frequencies, waveforms, magnitudes, phase angles, and stress ratios to simulate the load conditions that are needed. Also, the contributing variables of fretting fatigue can be tested using different pad geometry if needed.

When an axial load and a contact load are applied, a tangential load known as shear load (Q) is induced along the contact surface. This tangential load forces pads

and specimens to move relative to each other in a partial slip condition, instead of gross slippage, defined as half of the difference between the applied axial load and the load measured at the gripped end of specimens. As a result of fretting fatigue, a contact region along the contact surface of a pad and specimen is created. The side of the contact region near the applied axial loads is called the trailing edge, while the other side near the fixed end is called the leading edge. Contact half-width, a, incorporates both stick-zone (c) and partial slip zones while the center of contact width is called the origin of x-direction, as shown in Figure 2.1. During this study, a similar fretting fatigue configuration where cylindrical-end pads in contact with a flat specimen was used. This configuration will be discussed in greater detail in Chapter III.

2.2. Contact Mechanics

Fretting fatigue configuration can be modeled by a cylindrical-end body in contact with a flat body which is a cylinder with infinite radius. For the purpose of understanding the different variables involved, Figure 2.2 shows a two-dimensional picture of the experimental setup. The specimen is represented by the rectangular shape in the middle while the two rounded bodies on the two sides of the specimen are the fretting pads. The specimen has a cross sectional area A, thickness d, half thickness b, and is subjected to an axial load of σ_{axial}. The fretting pads have a constant radius r in the cross sectional plane, and are subjected to a normal load P. The presence of friction between the pads and the specimen results in surface shear force, Q. When the normal load is applied, the length of the contact area is known as the contact width, 2a. Also, half of the contact is called the contact semi-width, a.

There are three zones that account for the contact area. The first two zones are called slip zones. These two zones are located on both sides where the relative tangential motion occurs, and the shear stress is given by:

$$q(x,y) \ = \ -\,f\,p(x,y) \qquad\qquad (2.1)$$

In this equation, f is the coefficient of friction, and p is the direct stress. The third zone is called the stick zone, and is located in the middle between the two previous zones. This is where the particles of the two bodies are adhered, and the applied shear force Q is less than the resulted friction force and is given by:

$$Q \ < \ f\,P \qquad\qquad (2.2)$$

In equation 2.2, P is the normal load.

Hills and Nowell [1] found that the relative displacement in normal direction $v_1(x) - v_2(x)$, Where the two bodies are in contact with each other and there is an application of normal force P in y-direction and shearing force Q in x-direction, is given by:

$$\frac{1}{A}\frac{\partial h}{\partial x} \ = \ \frac{1}{\pi}\int\frac{p(\zeta)d\zeta}{x-\zeta} \ \ -\,\beta\,q(x) \qquad\qquad (2.3)$$

Where $h(x)=v_1(x)-v_2(x)$ is the amount of overlap that would occur if the contacting bodies could penetrate each other freely. In equation 2.3, q represents the surface

shear stress while p represents the pressure in the contact zone. Also, A represents the composite compliance

$$A = 2 \left\{ \frac{1-v_1^2}{E_1} + \frac{1-v_2^2}{E_2} \right\}$$
(2.4)

In addition, Dundurs' parameter, β, is given by :

$$\beta = \frac{1}{A} \left\{ \frac{(1-2v_1)(1+v_1)}{E_1} - \frac{(1-2v_2)(1+v_2)}{E_2} \right\}$$
(2.5)

Where E and v are the material modulus of elasticity and Poisson's ratio respectively.

Similarly, relative tangential displacement can be written as

$$g(x) = u_1(x) - u_2(x)$$
(2.6)

Thus, equation (2.3) can be expressed in terms of g(x) as follow:

$$\frac{1}{A}\frac{\partial g}{\partial x} = \frac{1}{\pi}\int \frac{q(\zeta)d\zeta}{x-\zeta} + \beta\, p(x)$$
(2.7)

However, $\beta = 0$ in this case, since the contact bodies are made of the same material. Equations 2.3 and 2.6 can be simplified to:

$$\frac{1}{A}\frac{\partial h}{\partial x} = \frac{1}{\pi}\int_{-a}^{a}\frac{p(\zeta)d\zeta}{x-\zeta} \qquad (2.8)$$

$$\frac{1}{A}\frac{\partial g}{\partial x} = \frac{1}{\pi}\int_{-a}^{a}\frac{q(\zeta)d\zeta}{x-\zeta} \qquad (2.9)$$

When fretting begins between the contacting bodies after application of the normal load, certain pressure distribution, p(x) will be created. By inverting equation 2.8, the contact load distribution found to be as follow:

$$p(x) = -\frac{\omega(x)}{A\pi}\int_{-a}^{a}\frac{h'(\zeta)d\zeta}{\omega(\zeta)(\zeta-x)}+C\omega(x) \qquad (2.10)$$

Since there is no singularity at the edges in this study, the C is assumed to be zero. Where weight function ω(x) can taken to be:

$$\omega(x) = \sqrt{a^2 - x^2} \qquad (2.11)$$

Also, the amount of overlap in freely interpenetrating bodies h(x) is assumed to be:

$$h(x) = \Delta - \frac{1}{2}k*x^2 \qquad (2.12)$$

Where Δ is a constant and k is the curvature given by following:

$$k = \frac{1}{R_1}+\frac{1}{R_2} \qquad (2.13)$$

R_1 and R_2 are the radii of the contacting surfaces.

h'(x) can be can be written as:

$$\frac{dh}{dx} = -k * x \tag{2.14}$$

By using equations 2.11 and 2.14 and inserting then in equation 2.10, the result will be as following:

$$p(x) = -\frac{\sqrt{a^2 - x^2}}{A\pi} \int_{-a}^{a} \frac{k\zeta d\zeta}{\sqrt{a^2 - \zeta^2}(\zeta - x)} \tag{2.15}$$

By integrating equation 2.15, the following equation gives the distribution load as follows:

$$p(x) = -\frac{k}{A}\sqrt{a^2 - X^2} \tag{2.16}$$

Integrating the total contact length on equation 2.16 will result in the following:

$$P = \frac{\pi k a^2}{2A} \tag{2.17}$$

Hence, the contact-width a can be written as:

$$a^2 = \frac{2PA}{\pi k} \tag{2.18}$$

16

While the peak contact pressure can be written as:

$$p(x) = -P_0 \sqrt{1 - (\frac{x}{a})^2}$$

(2.19)

P_0 is the maximum peak pressure and can be written as:

$$p_0 = \frac{2P}{\pi a}$$

(2.20)

Since the fretting pad is assumed to have $R_1 = \infty$, have a flat surface, then equation 2.18 can be simplified further:

$$a = \sqrt{\frac{8PR_1}{\pi} \frac{1 - v^2}{E}}$$

(2.21)

In addition, σ_{xx}, the axial stress resulting from the applied contact load P, can be written in Cartesian coordinates as:

$$(\sigma_{xx})_{contact} = -p_0 \{\frac{\sqrt{a^2 - x^2}}{a}\}$$

(2.22)

In Figure 2.1, the stick and slip shown are shown. The slip zones are located between –a and -c as well as c and a while the stick zone is bounded by –c and c. To put it in simple words, the stick zone is a area where the particles of the fretting bodies, the specimen and the pad, move together. The stick zone in fretting fatigue is

17

determined by the contact pressure, contact geometry, and coefficient of friction. The result of the forces in the stick zone contributes to remotely applied stresses in the vicinity of contact surface and premature crack initiation.

The stick zone accounts for the entire contact from –a to a before applying any tangential force. Knowing this, equation 2.7 will equal zero and will give the solution to the shear stress distribution along the contact surface and can be written as:

$$q(x) = \frac{C}{\sqrt{a^2 - x^2}} \qquad (2.23)$$

where C=Q/π, and Q is the total shear stress along the contact length and can be calculated by integrating the shear stress distribution:

$$Q = \frac{fp_0\pi}{2a}(a^2 - c^2) \qquad (2.24)$$

The stick zone size can be obtained as follows:

$$\frac{c}{a} = \sqrt{1 - |\frac{Q}{fP}|} \qquad (2.25)$$

2.3. Fretting Fatigue Factors

There are many factors that can affect the martial under fretting fatigue, which makes the study of fretting fatigue complicated. Different studies have been

conducted and each concentrated on one of these to have a deeper understanding of the contribution of this fracture on the fretting fatigue condition. This section will discuss some of these fretting fatigue factors.

2.3.1. Coefficient of Friction

Coefficient of Friction results when a contact load P is applied on the pad against the specimen while increasing the axial load until gross slip occurs, and is mainly dependent on the applied normal load. The ratio between the contact load and tangential load is known the dynamic coefficient of friction, and this ratio can be calculated as follows:

$$f = Q/P \qquad\qquad (2.26)$$

As concluded in a previous study, Iyer and Mall [3] reported that the experimental stabilized static coefficient of friction was determined to range from 0.37~0.46 for Ti-6Al-4V. Usually, during a fretting fatigue test, the coefficient of friction is usually stabilized after 5,000 to 10,000 fretting fatigue cycles. Also, studies by Lykins et al [5], and Iyer and Mall [6] found that the variation of friction coefficient from 0.45 - 0.7 caused relatively small variation on fretting fatigue. This variation caused twenty percent 20% increase in strain range.

In Addition, Namjoshi [7] showed that by increasing coefficients of friction from 0.5 to 0.8 there was no effect on crack initiation location prediction from the Modified Shear Stress Range Parameter (MSSR) parameter. On the other hand,

MSSR always predicted crack orientation at about ±45˚ for a cylindrical-end and only about 32% increase in MSSR was observed compared 12% increase in MSSR under flat-end pad geometry. Finally, a study by Lee [8] concluded that the friction coefficient is equal to 0.34 and 0.45 when applying a 2224 N and 4448 N contact load respectively. Using this result, the coefficient of friction can be assumed to be constant to simplify the fretting fatigue analysis in finite element analysis. Therefore the magnitude of 0.5 was used in this study as the coefficient of friction in finite element analysis.

2.3.2. Contact Pad Geometry

In a study by Namjoshi [7, 9, 10], varying pad geometry showed to affect the fatigue life of Ti-6Al-4V by using fretting contact pads with three different radii and two different flat- end- with- radius- edge contact pad geometry. The study showed that the fretting fatigue life was significantly reduced compared to plain fatigue life despite pad geometry. In addition, the study showed that the crack initiation location was found at the contact surface near the trailing edge with orientation at about either -45˚ or +45˚ under variation of ±15˚ from the direction perpendicular to the applied axial load. On the other hand, there was no significant correlation between pad geometry/load conditions and crack initiation location/orientation. Also a study be Lee [8] showed that fretting pads of 304.8 mm radius resulted in less fretting fatigue life compared to other experiments conducted with fretting pads with two inches radius, using the same axial and normal loads.

2.3.3. Axial Load Frequency and Contact Pressure

A study by Iyer [3] investigates the effect of varying the magnitude of the applied contact load and the applied axial load frequency on Ti-6Al-4V. The study showed that when the contact load was increased from 1338 N to 3567 N, the fretting fatigue life has was reduced at 1 Hz, yet it wasn't affected at 200 Hz. In addition, the study showed that by increasing the axial load frequency from 1 Hz to 200 Hz and keeping the applied contact load at a constant value of 1338 N, the fretting fatigue life was reduced. Also, at 1338 N applied contact load a wear-plastic deformation across the entire contact region was found, while at 3567 N applied contact load a clear dominate stick zone and a narrow slip zone with little debris was observed . It was also observed that crack initiation location was found near the trailing edge in all tests on the contact surface.

Fretting fatigue loading results in an amplified stress range in the vicinity of contact region due to the local build-up of compressive stresses upon loading and unloading. The decrease of fretting fatigue life by increasing the contact pressure can be related to the increase in the local stress range amplification along the contact surface.

2.3.4. Elevated temperature

A study conducted by Lee et al. [13, 14] was done to investigate Ti-6Al-4V specimens under influence of temperature at 25˚C, 100˚C, and 260˚ C. The study concluded that there was no effect on fretting fatigue life from raising the temperature

21

to 260˚. And the cracks always initiated at the trailing edge on the contact surface. Also, there was no noticeable effect on changing the coefficient of friction and higher temperature as well as longer exposure time induced larger stress relaxation.

2.3.5. Environment Corrosion

A study conducted by Waterhouse and Dutta [15] showed that fretting fatigue life under 1% NaCl solution corrosion is reduced at higher alternating stresses but it is improved at lower stress regime when compared to tests under dry conditions. Wharton and Waterhouse [16] explained this phenomenon by showing that at higher stresses, environment corrosion increases crack propagation, resulting in a reduced fatigue life, but the protective corrosive debris which remained on the fretting contact surface under lower stresses can retard crack initiation and improve fatigue life. In addition, a study conducted by Hoeppner et al. [17] showed a greater reduction on fatigue life in 3.5% NaCl solution than in distilled water or air. Also, a study done by Lietch [18] found that under dry and seawater conditions, seawater corrosion fretting fatigue life is reduced under low cycle fatigue; on the other hand it improved under high cycle fatigue.

2.3.6. Cyclic Contact Load

In a study conducted by Lee [8], the effect of variable contact load on fretting fatigue behavior of titanium alloy was investigated. The study concluded that the tangential load stayed in phase with the axial load and the contact load affected only

22

the magnitude of the tangential load and had no effect on the phase or the frequency of the tangential load. In addition, the study showed that the fatigue life was primarily dominated by the axial load and that the magnitude and frequency of the contact load had no significant effect on fatigue life and MSSR parameter. Fatigue life data from both constant and variable contacts loads were the same. In addition, the crack initiated near the trailing edge, and the crack initiation orientation was the same as for the constant contact load.

2.4. Fatigue Parameters

Fatigue parameters were developed on the basis of stress or strain history of the plain fatigue configuration. These techniques can be extended to fretting fatigue data. Hence, these parameters can be used to predict the location of the initiation crack, crack initiation angle, and how many cycles will be required for this crack to occur. Using this data, engineers can design components with enhanced resistance to fretting fatigue. A fretting fatigue condition is associated with high cycle fatigue (HCF), where a large fraction of fatigue life is spent in crack nucleation and growth to a detectable size while only a small fraction of life is spent in the crack propagation from detectable size to a critical size. As a result, unlike using damage tolerant approach for predicting fatigue life under low cycle fatigue regime, an alternative approach is required to predict HCF crack initiation behavior.

2.4.1. Critical Plane Based Fatigue Approach

The most important predictive parameters are the stresses occurring at the
critical plane. The critical plane models are based on the theory that a crack will
initiate on a particular plane, called the critical plane. On the critical plane, normal
stress opens cracks that reduce the friction between the crack surfaces and shear
stress, inducing dislocation movement along slip lines. This will result in nucleation
and growth of cracks. Therefore, the method goes about finding the maximum shear
strain amplitude and the plane on which it acts and then using the maximum normal
stress on this plane to determine the effect of a mean stress. In a current study,
Namjoshi et al. [7] found that the initiation of a fretting crack is a function of the
shear stress on the critical plane and that the fretting fatigue life is effected by the
normal stress acting upon the same plane. Research has shown that this method is
accurate in estimating the crack size in Ti-6Al-4V, though it will be difficult to
measure these stresses experimentally. Therefore, an approach is used which is based
on combination of analytical solutions and FEA output data to determine such
parameters.

At a specific point, the in-plane principal stresses acting at a specific point can
be calculated as follows:

$$\sigma_{1,2} = \frac{\sigma_{xx} - \sigma_{yy}}{2} \pm \sqrt{(\frac{\sigma_{xx} - \sigma_{yy}}{2})^2 + \tau_{xy}^2} \qquad (2.26)$$

$$\tau_{max} = \sqrt{(\frac{\sigma_{xx} - \sigma_{yy}}{2})^2 + \tau_{xy}^2} \qquad (2.27)$$

Where σ_1 and σ_2 are the maximum and minimum principal normal stresses that acting
on the principal planes and σ_{yy}, τ_{xy} are stress components at a local point. Also, τ_{max} is

the maximum shear stress at a given point, which always acts on a plane 45° from the orientation of principal planes.

The critical plane is defined as the plane where a fatigue parameter has its maximum value. Therefore, in order to evaluate critical plane-based fatigue parameters, shear stresses and local normal are computed as follows

$$\sigma = \frac{\sigma_{xx} + \sigma_{yy}}{2} + \frac{\sigma_{xx} - \sigma_{yy}}{2}\cos(2\theta) + \tau_{xy}\cos(2\theta) \tag{2.28}$$

$$\tau = -\frac{\sigma_{xx} - \sigma_{yy}}{2}\sin(2\theta) + \tau_{xy}\cos(2\theta) \tag{2.29}$$

By using equation 2.28 and 2.29, a good fatigue parameter can be formulated in order to predict fatigue life, crack initiation location, and crack initiation orientation.

2.4.2. Plain Fatigue

In the low cycle regime Coffin [20] and Manson [21] expressed the relationship of life in the plastic area as:

$$\left(\frac{\Delta\varepsilon}{2}\right)_p = \varepsilon_f'(2N_f)^{c'} \tag{2.30}$$

Where N_f is the number of strain reversals to failure, 1/2 cycle =1 reversal, $(\Delta\varepsilon/2)_p$ is the plastic strain amplitude, c' is the fatigue ductility exponent, and ε_f' is the fatigue ductility coefficient.

On the other hand, Basquin [22] found that stress vs. fatigue life relationship can be correlated for the elastic as follows:

$$\left(\frac{\Delta\varepsilon}{2}\right)_e = \frac{\sigma_f'}{E}(2N_f)^{b'}$$

(2.31)

where σf' is the fatigue strength coefficient, E is modulus of elasticity, $(\Delta\varepsilon/2)_e$ is the elastic strain amplitude, b' is the fatigue strength exponent, and N_f is the number of strain reversals to failure.

Solving for the strain life from equation 2.31 will lead to the following:

$$\varepsilon_a = \frac{\sigma_f'}{E}(2N_i)^{b'} + \varepsilon_f'(2N_i)^{c'}$$

(2.31)

where N_i is the cycles to crack initiation and ε_a is total strain amplitude. This equation can be used for constant strain ratio conditions while the following equation can be used when different strain ratios are applied as stated by Walker [23]:

$$\varepsilon_{max,R_\varepsilon} = \varepsilon_{max}(1-R_\varepsilon)^m$$

(2.32)

where R_ε is the strain ratio ($R_\varepsilon=\varepsilon_{min}/\varepsilon_{max}$), $\varepsilon_{max,R\varepsilon}$ is the maximum strain corrected for the strain ratio, m is the material fitting parameter that was chosen to collapse plain fatigue crack initiation data at different strain ratios, and ε_{max} is the maximum strain.

A caution to be noted, Lykins [5] proved that this parameter could predict the number of cycles to crack initiation and crack initiation location along a contact surface, but could not predict crack initiation orientation.

2.4.3. Stress Range and Effective Stress

Predictive parameters based on global boundary conditions such as contact load, tangential load, and far field stresses are favored in some fields because global boundary conditions are more readily controlled. Some of these parameters are stress range and effective stress.

The stress range for the applied axial load can be expressed as:

$$\Delta\sigma = \sigma_{max} - \sigma_{min} \tag{2.33}$$

Since equation 2.33 does not account for the effect of mean stress or stress ratio, Namjoshi et al. [4] discovered another method using effective stress to account for the effects from stress ratio as well as residual stress as follows:

$$\sigma_{eff} = (\sigma_{max} + \sigma_{residual}^{tensile})(1 - \frac{\sigma_{min} + \sigma_{residual}^{tensile}}{\sigma_{max} + \sigma_{residual}^{tensile}})^m \tag{2.34}$$

where σ_{eff} is the effective stress taking into account the effect from stress ratio and residual stress. The effect of mean stress or stress ratio is important to account for because it is relevant to fatigue strength. In equation 2.34, m was found by Lykins [5]

to be 0 .45. Mall et al. [10, 24] showed that this only collapse fretting fatigue life data into a single curve while Andrew [11] showed that this equation was able to collapse fretting fatigue life into a single curve under variable contact load as will as constant contact load conditions.

In addition, Lee et al. [12] concluded that this equation worked well in fretting fatigue life prediction under elevated temperature up to 260˚ C. Since equation 2.33 and 2.34 do not account for the stress concentration effect occurring at the trailing edge of contact region and multi-axial loading conditions induced by fretting fatigue, critical plane-based predictive parameters are needed.

2.4.4. Smith-Watson-Topper Parameter (SWT)

The Smith-Watson-Topper (SWT) parameter can be expressed as follows:

$$SWT = \frac{\left(\sigma_f^{'}\right)^2}{E} * \left(2N_i\right)^{2b'} + \sigma_f^{'}\varepsilon_f^{'}\left(2N_i\right)^{b'+c'} \tag{2.35}$$

where $\sigma_f^{'}$ is fatigue strength coefficient, ε_f' is fatigue ductility coefficient, b_f' is fatigue strength exponent, c' is fatigue ductility exponent, N_i is cycles to crack initiation, and E is the elasticity modulus. Equation 2.35 is usually referred to as the strain life equation. This equation has been modified by Szolwinski and Farris [25] by using critical plane approach equation is widely known as Smith-Watson-Topper (SWT) parameter, which can be expressed follows:

$$SWT = \sigma_{\max}\varepsilon_a \quad or \quad \max(\sigma_{\max}\varepsilon_a) \tag{2.36}$$

Where ε_a is the normal strain amplitude to a critical plane, and σ_{max} is the stress normal to a critical plane. SWT parameter asserts crack initiation occurs on the plane where the product of σ_{max} and ε_a is maximal. By using the computed local stress and strain from finite element analysis of the fretting fatigue experiments, this parameter was calculated at all planes ranging from $-90^o \le \theta \le +90^o$, which provided this parameter's maximum value. The SWT parameter was found effective in predicting the number of cycles to crack initiation and crack initiation location with strong dependence on pad geometry [10, 24, 25, and 26], yet it did not provide good agreement with crack initiation orientation.

2.4.5. Findley Parameter (FP)

Crack initiation mechanism in multiaxial loading fatigue conditions is influenced by both normal and shear stresses. Findley's study [27] concluded that there is a multi-axial fatigue parameter affected from the normal stress on a critical plane in addition to the shear stress and can be expressed as follows:

$$FP = \tau_a + k\sigma_{max} \tag{2.37}$$

Where k is an influence factor calculated from 35 from plain fatigue data and found to be 0.35, and τ_a is stress amplitude defined as:

$$\tau_a = (\tau_{max} - \tau_{min})/2 \tag{2.38}$$

Where τ_{max} is the minimum shear stress and τ_{min} is the maximum shear stress. Findley Parameter was calculated at all planes ranging from $-90^o \leq \theta \leq +90^o$ from computed stresses and strains obtained from finite element analysis.

Findley Parameter could predict crack initiation location, yet was not able to predict fretting fatigue life from plain fatigue data as the concluded by Mall et al. [10, 24] applying specimens with different geometry pads under fretting fatigue conditions. Also, the predicted crack orientations were different from experimental observations.

2.4.6. Shear Stress Range Parameter (SSR)

Shear Stress Range Parameter (SSR) accounts for only the maximum and minimum shear stress on the critical plane. To calculate this parameter, the shear stress should be calculated along all planes ranging from $-90^o \leq \theta \leq 90^o$ from the state of stress (σ_{xx}, σ_{yy}, τ_{xy}) computed from FEA by using the following equation:

$$\tau = -\frac{\sigma_{xx} - \sigma_{yy}}{2} \sin 2\theta + \tau_{xy} \cos 2\theta \qquad (2.39)$$

$\Delta\tau = \tau_{max} - \tau_{min}$ was computed at all planes and at all points in the contact region, where $\tau_{max} - \tau_{min}$ are shear stresses due to the applied maximum and minimum axial load. Since the mean stress or stress ratio also affects fretting fatigue behavior, this

effect on the critical plane was taken care of by incorporating a technique introduced

by Walker [X] as follows:

$$(SSR = \Delta\tau_{crit}) = \tau_{max}(1 - R_\tau)^m \qquad (2.40)$$

where R_τ is the shear stress ratio (τ_{min} / τ_{max}) at the critical plane τ_{min} is the minimum

shear stress, τ_{max} is the maximum shear stress, and m is a fitting parameter determined

as mentioned before to be 0.45. It was showed that SSR, for specimens with different

pad geometry by Mall et al. [10, 24], was useful in conjunction fretting fatigue life

with plain fatigue life. Also, SSR can correlate crack initiation location and

orientation with experimental observations very well.

2.4.7. Modified Shear Stress Range Parameter (MSSR)

The Modified Shear Stress Range Parameter (MSSR), by combing maximum

normal stress on a critical plane of maximum SSR into the original SSR, generally

acts in opening the crack surface. It is simply a modified version of the SSR

parameter. MSSR is considered by many researchers in the field to be the premier

predictive parameter of fretting fatigue behavior, and it is known to eliminate the

effect of pad geometry. This parameter is needed to predict the crack initiation

location, the fatigue cycles to occur, and the crack initiation orientation at the same

time and can be expressed as follows:

$$MSSR = A\Delta\tau_{crit}^B + C\sigma_{max}^D \qquad (2.41)$$

where $\Delta\tau_{crit}$ is calculated from equation 2.39 and σ_{max} is the maximum normal stress on the critical plane of the SSR parameter. A, B, C, D are fitting constants that can be determined by curve fitting approach. These constants are determined empirically by as A = 0.75, B = 0.5, C = 0.75, and D = 0.5 [10]. The Modified Shear Stress Range Parameter was calculated at all planes ranging from $-90^{o} \leq \theta \leq +90^{o}$ from computed stresses and strains obtained from finite element analysis. These calculations provided the critical plane, where this parameter is the maximum.

From looking at the previous studies [10,19,24], MSSR was found to be the only critical plane-based parameter eligible in predicting crack initiation location, crack initiation orientation, and fatigue life. It was proved that MSSR was able to satisfactorily characterize fretting crack initiation orientation and location independent of contact geometry for two values of coefficient of friction, 0.5 and 0.8. by Namjoshi et al. [7]. In conclusion, MSSR parameter proved to be an effective fatigue predictive parameter while investigating crack initiation behavior of Ti-6Al-4V under fretting fatigue phenomenon, and thus was adopted as the fatigue parameter to be investigated in fretting fatigue behavior prediction. It was found that the accuracy of this parameter was due to taking into consideration both the effect of shear stress as well as normal stress in the case of multiaxial fatigue loading condition. In this study, MSSR is calculated in order to measure its ability, as a fretting fatigue parameter, to predict fatigue life, crack location and crack initiation orientation of Ti-6Al-4V.

2.5. Crack Initiation Mechanism

It has been demonstrated from previous studies that the primary crack, which causes failure in the specimen, always initiated near the trailing edge on the contact

surface. Also it has been demonstrated that there are usually some smaller secondary cracks that do not grow enough to develop further to cause failure. The initiation angles are ± 45 Deg ± 15 Deg from a perpendicular to the axial loading direction. In addition, maximum shear stress range can occur on two planes orthogonal to each other, one in the positive quadrant and the other in the negative one. Therefore, for every state of stress, there are two critical shear stress planes with equal possibility of crack orientation and only local microstructure property may make one plane preferred over the other. Fretting fatigue crack was proved by previous studies initiated and propagated in inter-granular manner, under fretting fatigue conditions. Also, crack behavior was found to be independent of pad geometry and fretting load conditions.

2.6. Gross Slip and Partial Slip

During a fretting fatigue process starts, the two mating bodies experience slip, long before a stick zone is formed. Under this condition, the pads and specimen are relatively free to slip against each other. After some time, fretting either turns into either gross slip or partial slip condition. Partial slip occurs when no gross relative displacement observed, rather only small slip zones exist near the edges of contact. On contrast, gross slip occurs when the two contacting surfaces are in full sliding mode across the contact zone and the resulting damage is called fretting wear. In the center of contact, the surface of the specimen and the pads are welding together. Figure 2.2 shows the two zones.

2.7. Summary

Fretting fatigue occurs between two components in contact with each other and reduces the fatigue life when compared to plain fatigue. Several studies have been conducted to develop analytical solutions and experiments to give a better understanding of fretting fatigue phenomenon by changing some of the contributed factors thought to have an effect on the fretting fatigue behavior. Some of these contributing factors are coefficient of friction, elevated temperature, fretting pad geometry, shot-peening process, axial load condition with different frequencies, contact load condition, and environmental corrosion.

Most of the previous works were accomplished using constant applied contact load. Unlike the previous studies, this study would focus more effort to investigate the effect of variable axial and normal loads on material life. Also, this study did account the effect of the phase difference between the axial load and the contact load into which not many studies focused on. The primary goal of this study was to investigate the effect of phase difference between axial and normal loads on fretting fatigue behavior of Ti-6Al-4V alloy, as well as the effect of increasing the cylindrical pad radii. In addition, this study investigated in detail the effects of combined plain and fretting fatigue loading conditions on the life of test material.
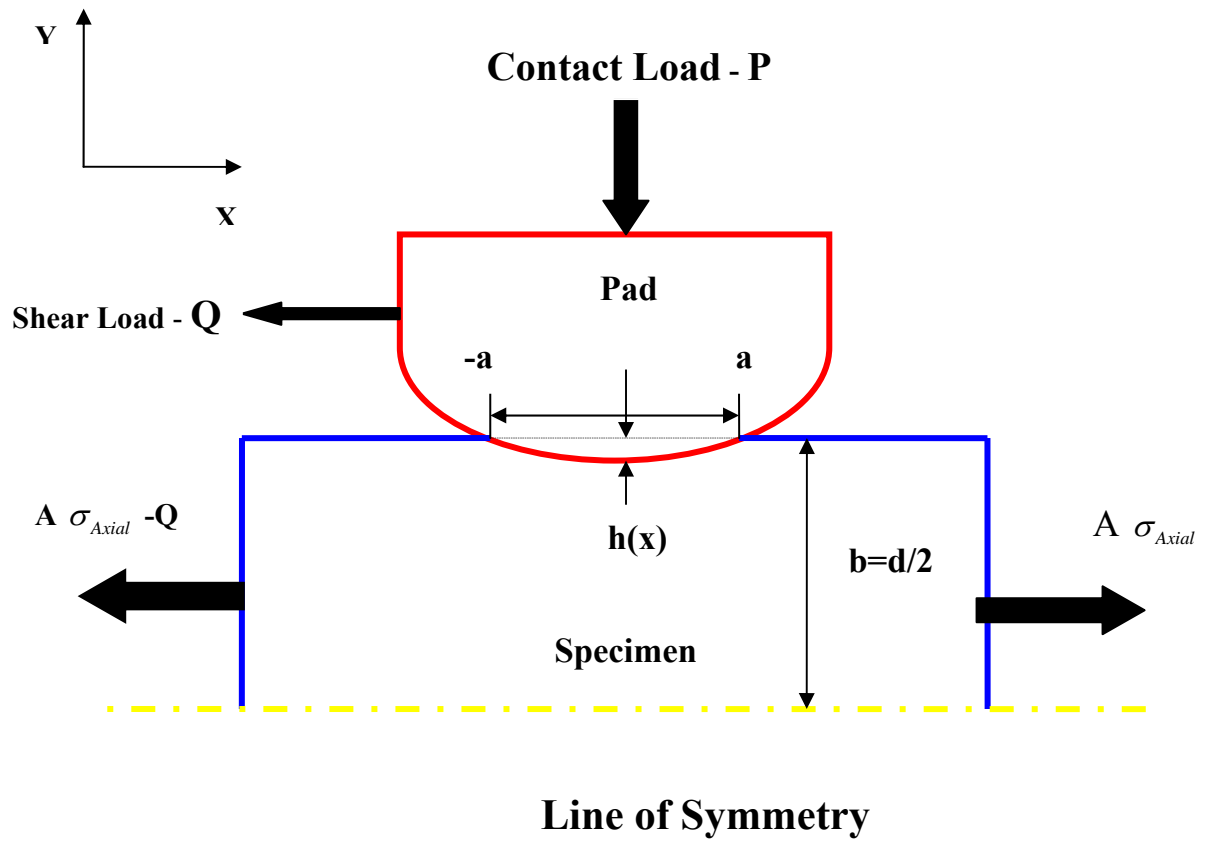
Figure 2.1 Free Body Diagrams of Two Bodies under Fretting Fatigue Loads

Y

X

Contact load - **P**

Stick Zone   **Pad**

Shear force - **Q**

$A\sigma_{Axial}$ **-Q**

-a -c   c a

Slip Zone

b= d/2

$A\sigma_{Axial}$

Specimen

Line of Symmetry
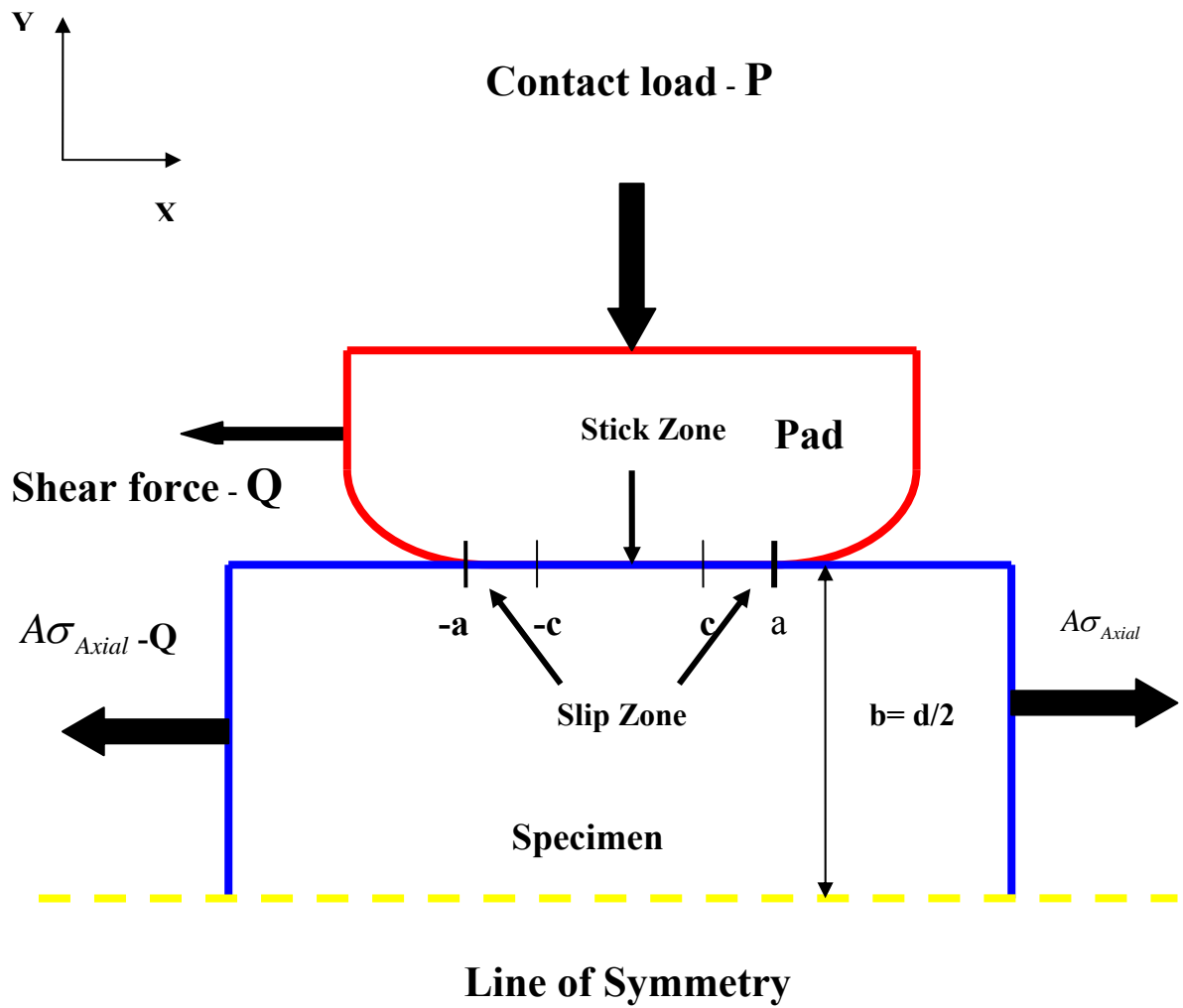
Figure 2.2 Diagram Distinguishing the Slip and Stick Zones

III. Experimental Configuration

This chapter documents the experimental procedure and setup used in this study to investigate the behavior of Ti-6Al-4V under fretting fatigue as well as under combined fretting fatigue and plain fatigue loading conditions. These tests were conducted under tension-tension fatigue conditions. The sections to be discussed are: the test set up, the material details and the geometry of both the specimen and the pad that were used in this work, the test procedure and load determination, and the determination of crack initiation and the crack initiation orientation .

3.1. Test Set-up

During this study, a bi-axial servo-hydraulic test machine was used as depicted in Figure 3.1. This machine consists of a rigid steel fixture frame, a 100 KN lower axial hydraulic servo actuator, and a 5 KN contact hydraulic servo actuator. These two actuators are controlled by Multi Test System MTS 793.10 Multi-Purpose Test Software (MPT) which allows the users to vary the magnitude, frequency, waveform, and phase lag between these two actuators. A schematic diagram of the above test machine is shown in Figure 3.2 which shows that the fretting fixture holding the blocks to keep a pair of pads in the precise alignment and prevent them from moving freely.

During a load cycle, the contact pads undergo small relative movement with respect to the specimen, and during this process cause fretting action on the face of the specimen. Therefore, alignment becomes of such a critical concern, therefore testing and alignment should be checked before every test. Such process may seem

easy but in reality it can be hard to align, and making the two pads on each side touch the specimen exactly at its center becomes tricky as it that is important to ensure that both loads are perpendicular to each other.

3.2. Specimen and Pad Geometry

Figure 3.3 illustrate both the dimensions dog-bone specimen and the pad. The specimen's length is 228.6 mm, thickness 3.81 mm, width 6.35 mm, and cross section area is $24.1935\,mm^2$. In the other hand, two pad geometries have been used. The first has one cylindrical end with radius of 50.8 mm at one end and with a flat end at the other side, and has thickness and width of 9.525 mm. The second has one cylindrical end with radius of 304.8 mm at one end and with a flat end at the other side, and has thickness and width of 9.525 mm. Both the specimens and the pads used in this study were made up from Ti-6A1-4V. Both the dog-bone specimens and the pads are cut by the wire electrical discharge method.

3.3. Material Properties

Ti-6A1-4V was preheated and treated in a solution at $935^o C$ for 105 minutes, then cooled in air, afterwards vacuum annealed at $705^o C$ for two hours, and cooled again in argon. As result, a micro structure showed 60 % by volume of α (HCP) phase (platelets) and 40 % by volume of β (BCC) phase matrix. Also, the yield strength (σ_y) of the material is 930 MPa, the measured grain size is about 10 μm, the Poisson's ratio (υ) of 0.33, Brinell hardness number of 302, and the elastic modulus (E) of 126 GPa.

3.4. Test Procedure

At first, on both sides of the specimen, a pair of pads is mounted into the fixture holding blocks. Before running any tests, the pads are aligned to ensure pads' surfaces are in perpendicular contact with the specimen. I found it that the sensitive tape was not that much effective in ensuring this procedure. The best method I found was to draw a line that is exactly in the center of the specimen, by the help of an electronic caliper. After that, another line should be drawn exactly in the center of the fretting pads and by then making sure that the line drawn on the specimen and the line drawn on the fretting pad are parallel. Next, the specimen was then taken out from hydraulic machine, and a warm-up procedure programmed in MPT was executed to warm up the test machine for at least 30 minutes to ensure hydraulics are well functioning., by using the displacement control for the axial load actuator. Once warm-up done, the specimen is mounted and clamped into the test fixture through the upper and lower grips. Next, the program was executed to run the actual test and there will be gradual application of both the fretting load and of the axial load, until the maximum σ_{axial} is achieved in case of the axial load.

The induced tangential load was determined by half of the difference between the lower axial load and upper axial load. The actuator cycles then in a periodic fashion (sinusoidal) between the maximum and minimum loads at the frequency of 10Hz, until failure of the specimen, when it broke into two pieces. After the failure of the specimen, the number of fretting fatigue cycles were taken down as the specimen's fatigue life. After being done with the test, the following data can be found; the upper axial load, the lower axial load, the running time, the fretting fatigue

cycles, applied contact load, and the displacement. By then, the data can be saved in Microsoft excel document for convenience. Table 3.1 summarizes all the tests that have been conducted with specific details.

3.5. Load Determination

The function the peak-valley compensator (PVC), in the software of the test machine, was used during each test for both contact load and axial load in order to reduce variation between command and feedback signals sensed by the test machine. After failure of the specimen, by using the date collected, the tangential load can be calculated as follows:

$$Q = \frac{V_{lower} - V_{upper}}{2} \qquad (3.1)$$

Where Q is the tangential load, V_{upper} is the upper axial load, and V_{lower} is the lower axial load. Figure 3.4 shows the tangential loads versus the axial loads for a desired number of cycles for tests five and six. On the other hand, Figure 3.5 shows the tangential loads versus the axial loads for a desired number of cycles for test seventeen. In these Figure, the curve which known as the fretting hysteresis loops indicates that the partial slip conditions have been met after approximately 100 fretting fatigue cycles. On the other hand, Figure 3.6 shows the same for test seventeen while Figure 3.7 shows the maximum and minimum tangential loads versus the life cycles as shown for tests five and six, It can be notices from these curves that the test started to be in a steady state condition at the first hundreds cycles of fretting

40

fatigue cycles. Therefore, the magnitude of the maximum and minimum tangential loads suspending to the maximum and minimum axial loads were taken at a 10,000 cycles as an input to both the analytical solution of Ruiz program and the Finite Element Analysis (FEA), which will be discussed in chapter IV.

On the other hand, the coefficient of friction, f, can be found as the ratio between the tangential load Q and the applied normal load P as follows:

$$f = Q/P \qquad\qquad (3.2)$$

The coefficient of friction has to be determined for subsequent use in the Finite Element Analysis. In this study, this coefficient of friction was found to be ranged between 0.11-0.37, for the 50.8 mm pads. On the other hand, the coefficient of friction was found to be ranged between 0. 22-0.34, for the 304.8 mm pads. Therefore, for simplification, a coefficient of friction of 0.5 will be adopted in the analysis of Finite Element Analysis.

3.6. Crack Initiation and Orientation

Upon failure of the specimen, the contact region and the fracture surface of the failed specimen should be investigated. A lower magnification microscope, in order to locate the crack initiation, was used to take a photo of the scar. This scar resulted from the contact mechanism between the specimen and the pad. Also, this microscope was used to take a general picture of the fracture surface of the specimen. It was noticed during this study, that the crack always initiates at or very near the trailing edge of the

contact region where the stress concentration in the x-direction is maximum and

x/a =1 as shown in Figure 3.8. This Figure shows that the location of the crack

initiation is near the trailing edge, and the contact-half- width for this test was

measured experimentally to be between 0.75-0.78 mm, for 50.8 mm pads. On the

other hand, the contact-half- width for 304.8 mm pads was measures experimentally

to be between 1.92-1.95 mm. This value of the contact half- width is needed in FEA

to find the required stresses at the contact area.

On the other hand, Scanning Electron Microscope (SEM) was used in order to

see this area in a higher magnification a Scanning Electron Microscope (SEM). It has

to be noted that the specimen should be should be cut along the y-direction by using a

saw machine to reach a length of around 10 mm in x-direction in order for the

specimen to be fit inside the .By Using SEM, the crack initiation zone is at first noted

as the area with discoloration on the failed specimen surface. The precision saw

machine must be used in this procedure and the specimen should be sectioned

laterally along the x-axis as close as possible to the center of the estimated crack

initiation zone. It will be helpful if more material is shaved off until a clear SEM

picture which will ease the process of crack initiation orientation evaluation along the

contact. Hence, the experimentally found angles and locations will be compared to the

angles predicted through fretting fatigue parameters.
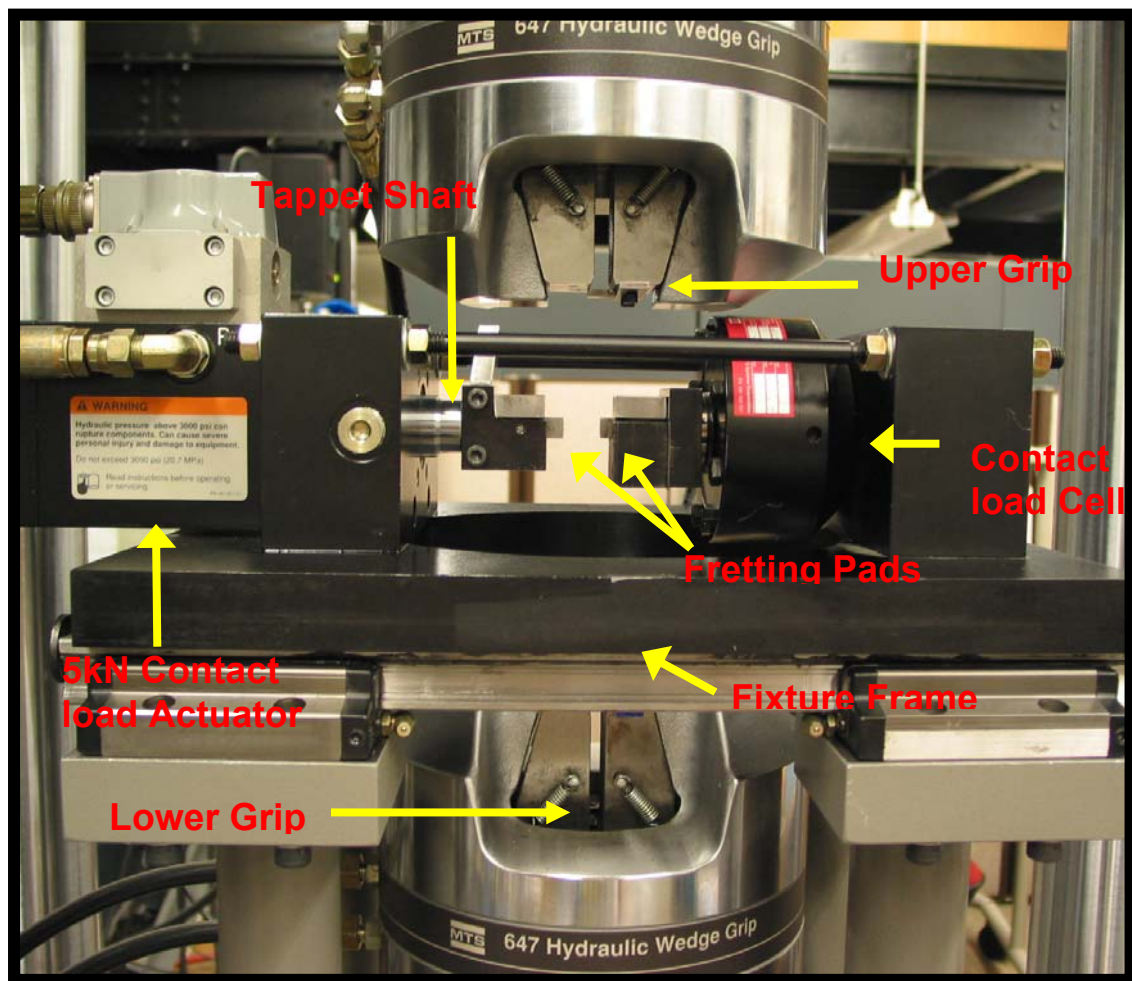
Figure 3.1 Fretting Fatigue Test Machine
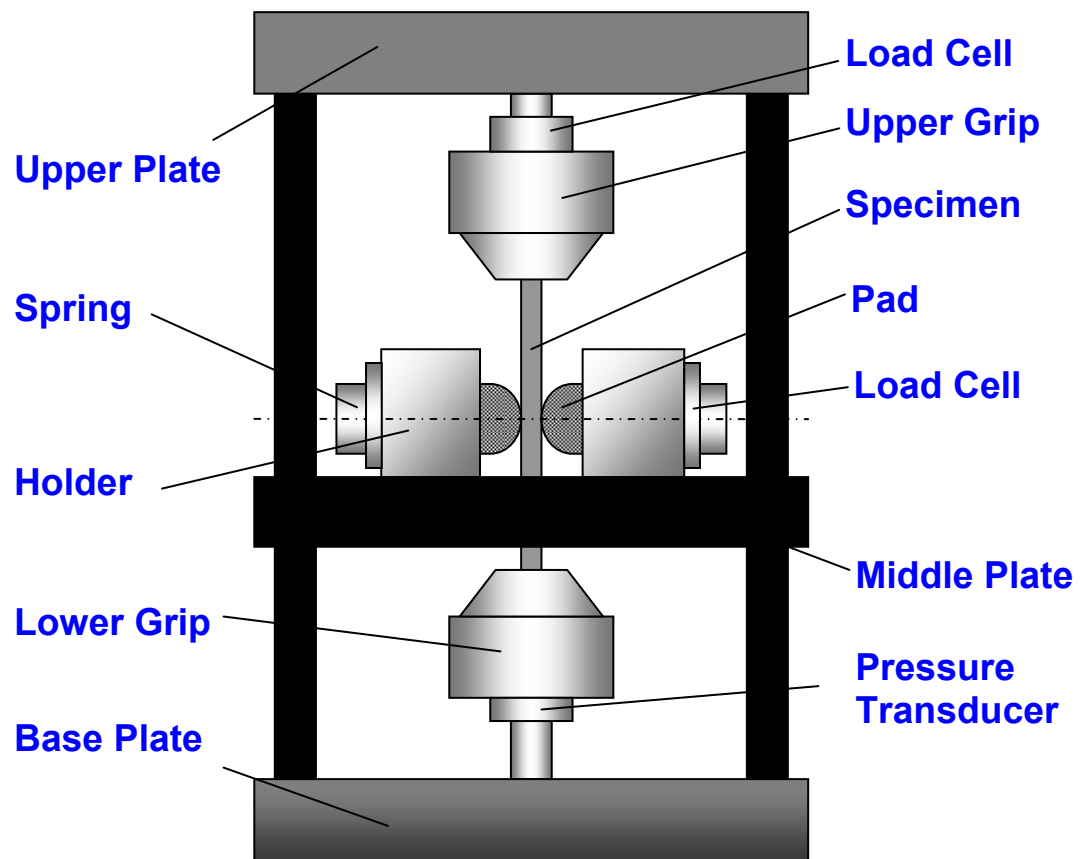
Figure 3.2 Schematic Diagram of Biaxial Fretting Fatigue Set-Up
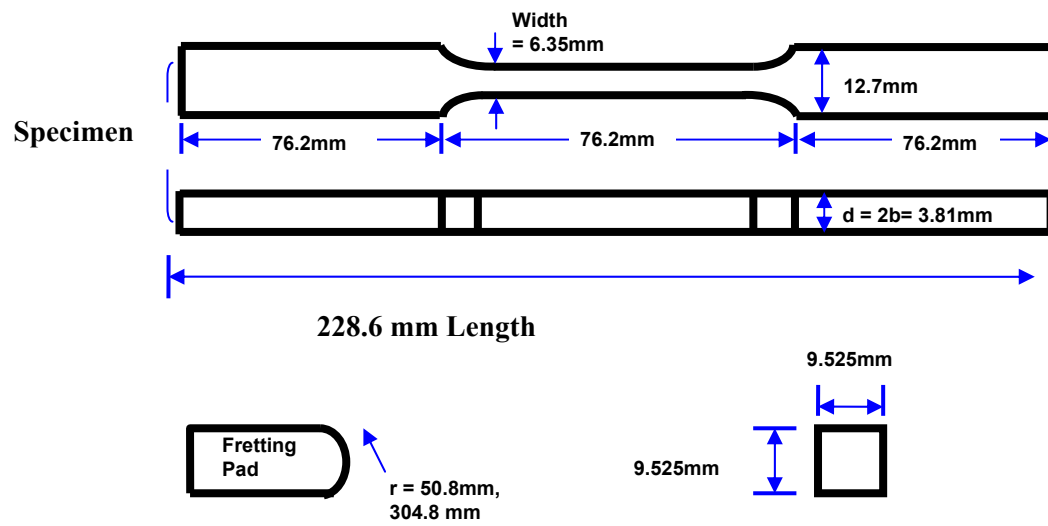
Figure 3.3 Specimen and Pad Dimensions and Geometry

Axial Load Vs Shear Force (0 Deg 413MPa)

In-phase

Axial Load Vs Shear Force (45 Deg 413 MPa)
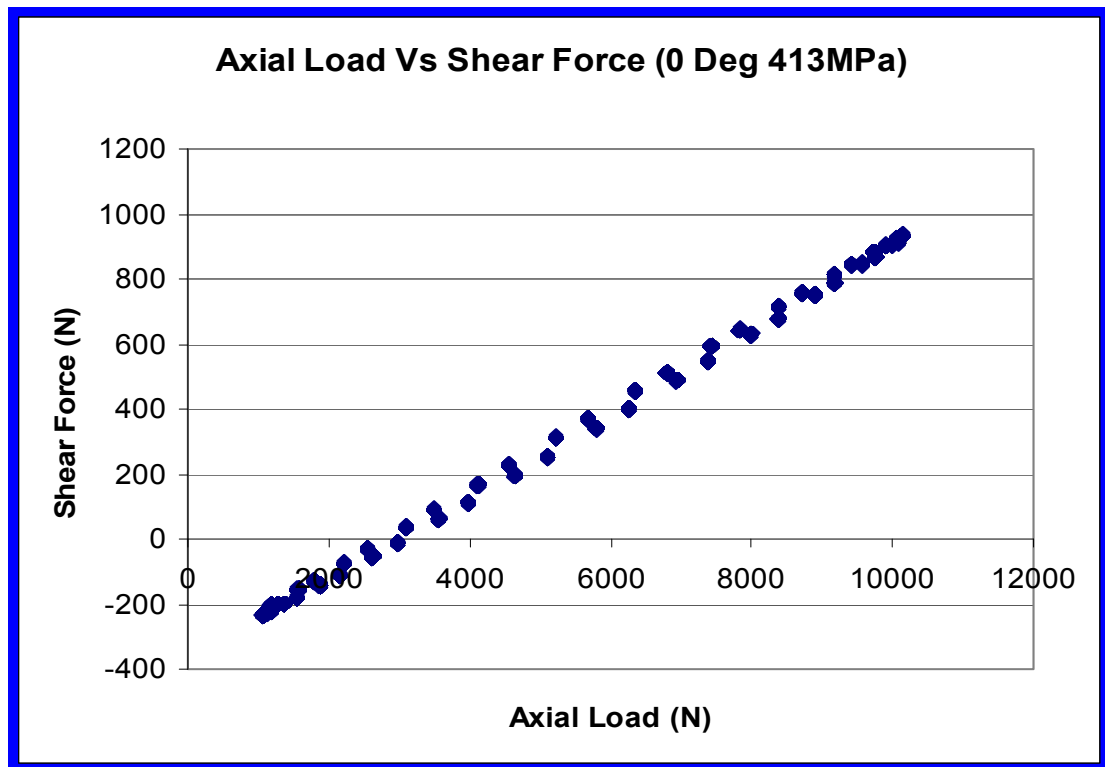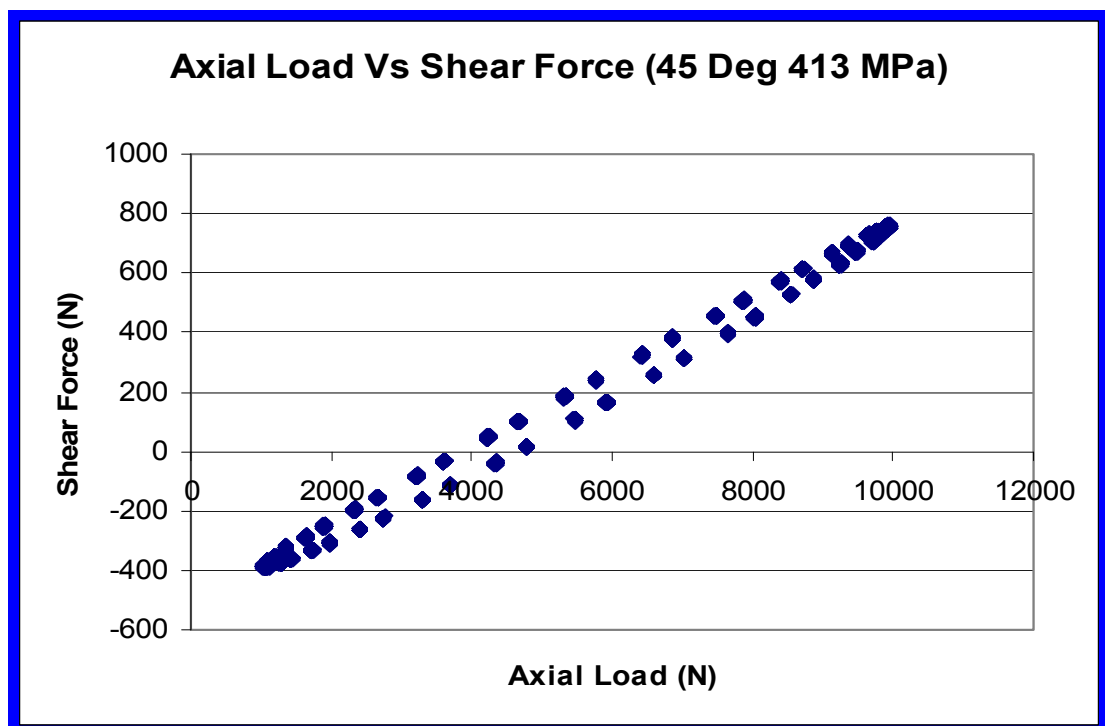
Out of phase

Figure 3.4 Axial Load Vs Shear Force for Test # 5 & 6
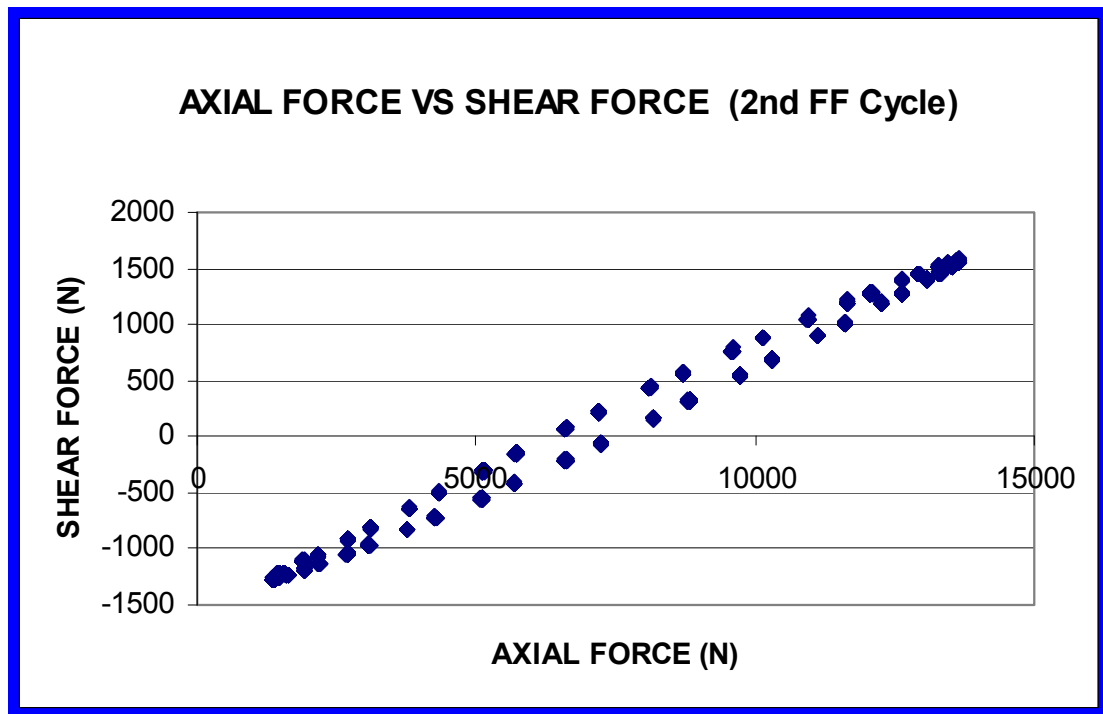
Figure 3.5 Axial Load Vs Shear Force for Test # 17
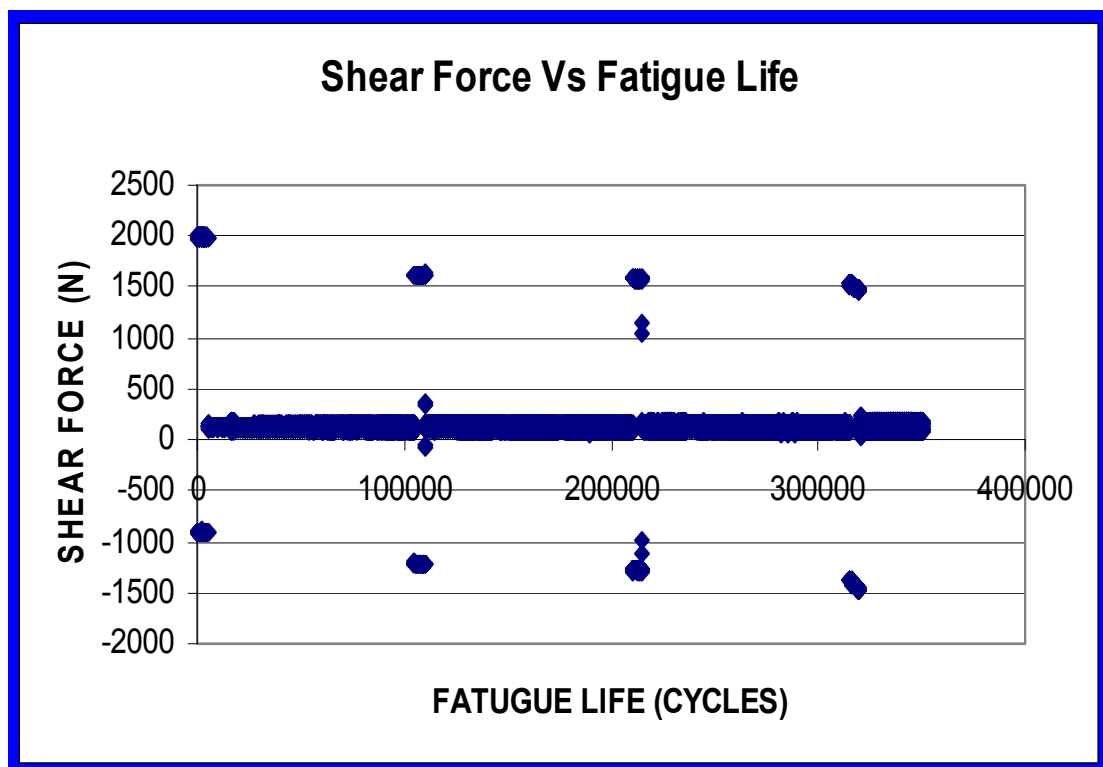
Figure 3.6 Shear Force Vs Fatigue Life for Test # 17
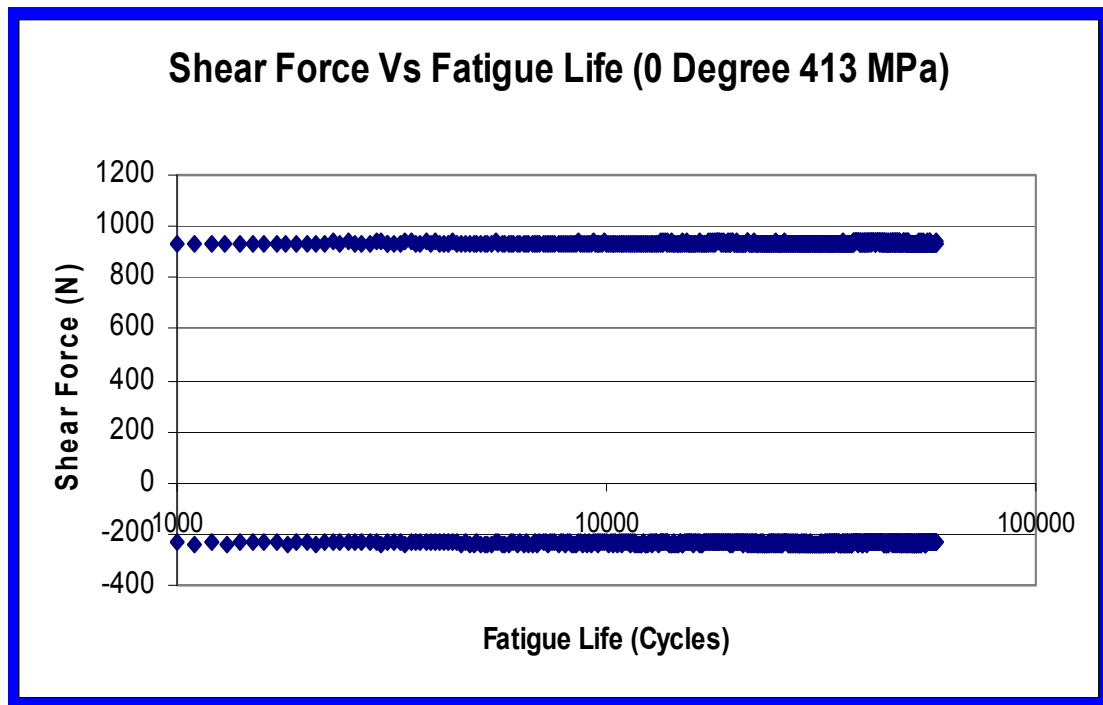
In-phase
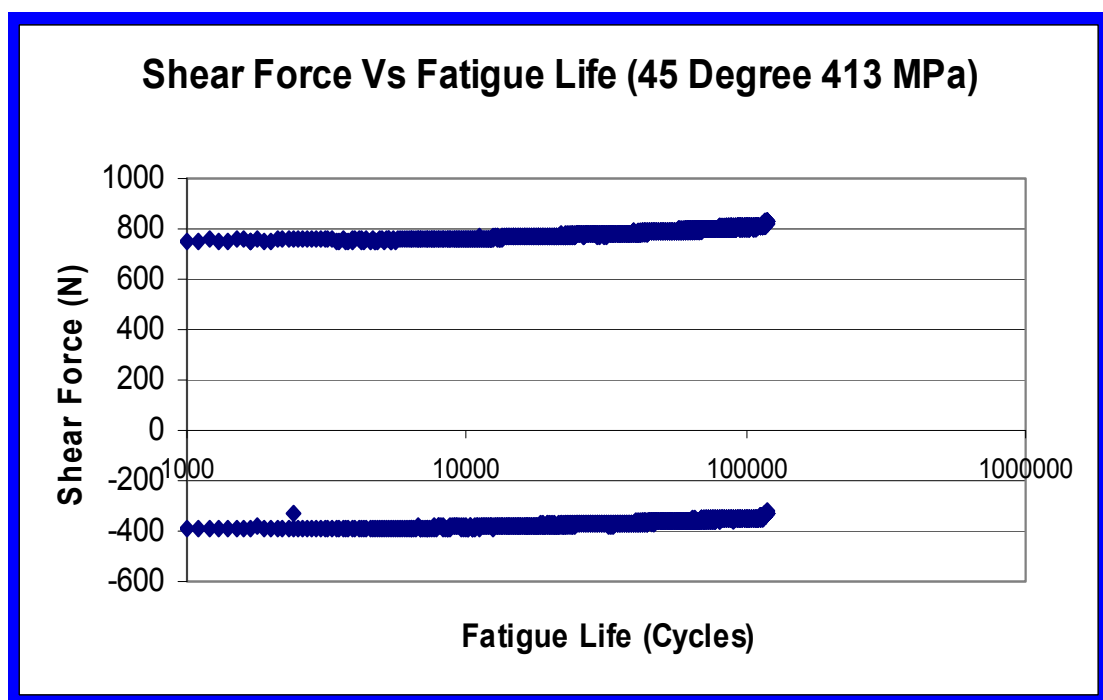
Out of phase

Figure 3.7 Shear Force Vs Cycles Fatigue Life for Test # 5 & 6

48
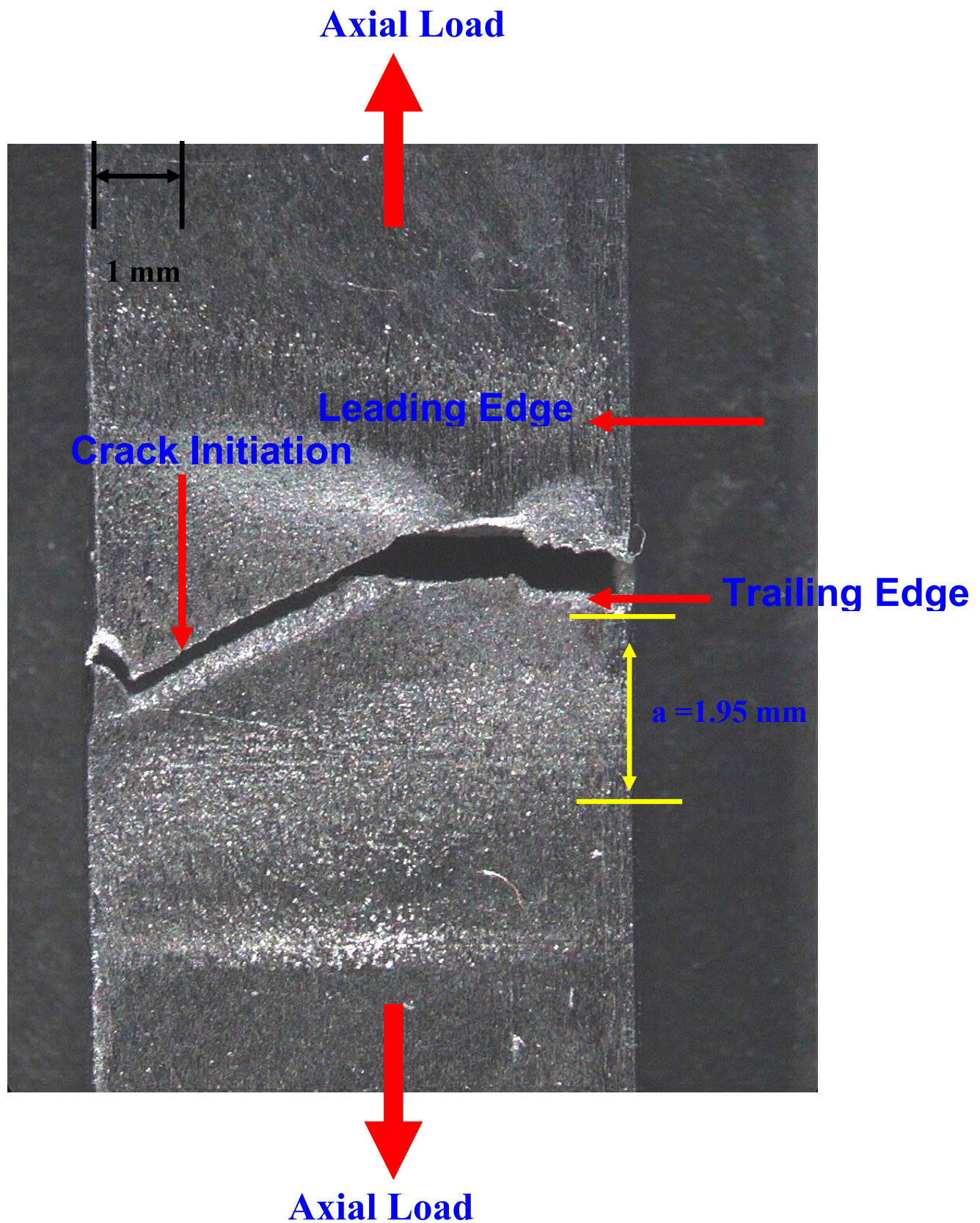
Figure 3.8 Crack Initiation Location for Test # 16
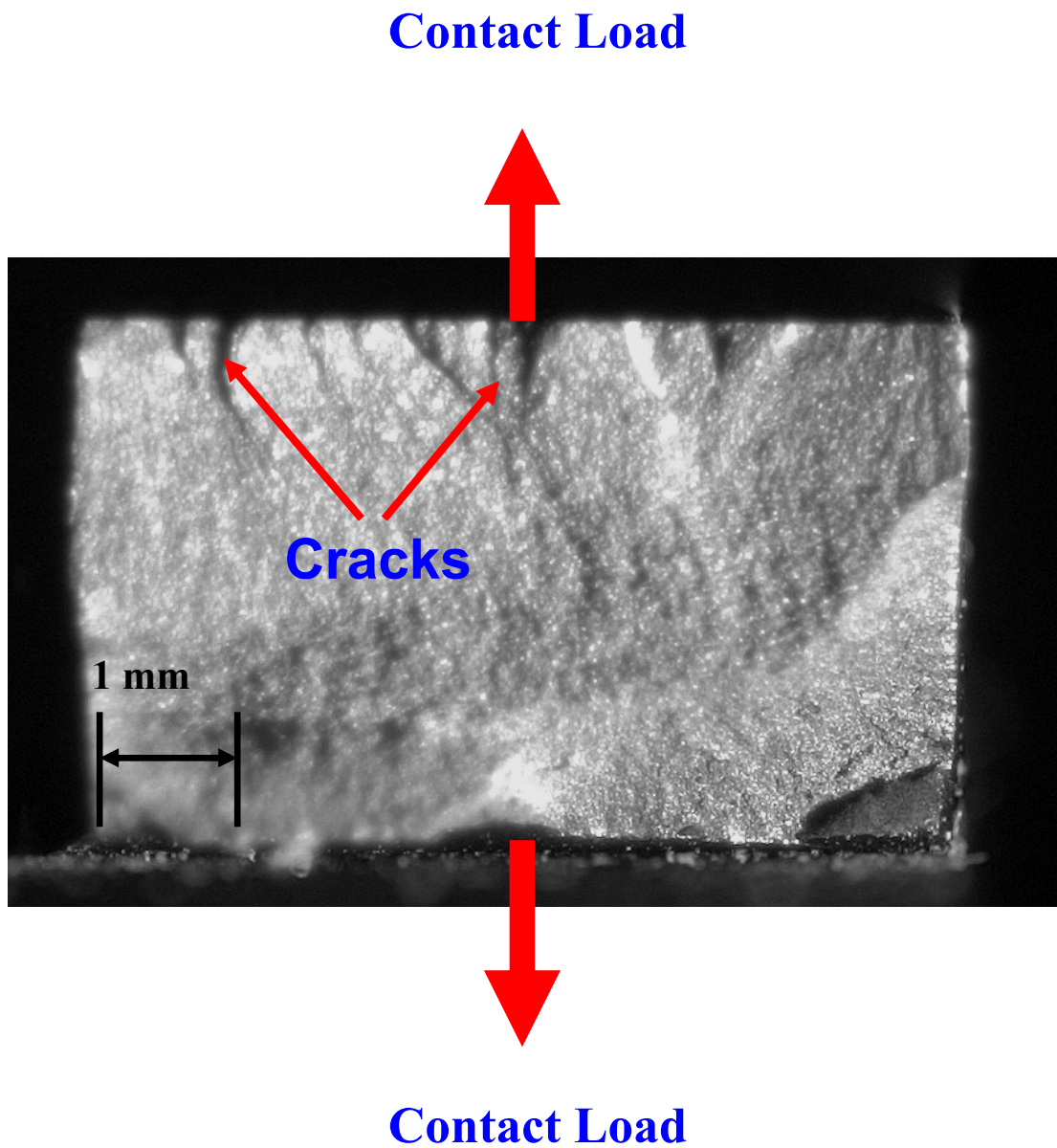
Figure 3.9 Fracture Surface of Failed Specimen for Test # 7

Table 3.1 Input Loads and Phase Angles

Test	σ_{max}	σ_{min}	P_{max}	P_{min}	Q_{max}	Q_{min}	ΔQ	Θ	N_f
	(MPa)	(MPa)	(N)	(N)	(N)	(N)	(N)	deg	(Cycle)
1	564	56	4,448	2,224	410	-890	1,300	0	47,421
2	564	56	4,448	2,224	819	-413	1,232	45	70,118
3	564	56	4,448	2,224	611	-597	1,208	90	74,168
4	413	41	4,448	2,224	934.1	-229.7	1,164	0	58,574
5	413	41	4,448	2,224	939	-235	1,174	0	61,578
6	413	41	4,448	2,224	754	-390	1,144	45	118,960
7	413	41	4,448	2,224	110	-715	825	90	159,422
8	376	37	4,448	2,224	1189	-283	1,472	0	83,989
9	376	37	4,448	2,224	648	-383	1,031	45	124,238
10	376	37	4,448	2,224	680	-380	1,060	45	116,238
11	376	37	4,448	2,224	58.3	-682.3	741	90	158,555
12	450	40	4,448	2,224	1168	-198	1,366	0	52,422
13	450	40	4,448	2,224	1086	-250	1,336	0	54,889
14	450	40	4,448	2,224	1049	-221	1,270	45	107,214
15	450	40	4,448	2,224	858	-264	1,122	90	144,303
16	564	56	508	3,336	-	-	-	-	44,656
17	564	56	508	3,336	-	-	-	-	350,397

IV. Finite Element Analysis

In this chapter the details of finite element analysis that is needed for conducting analysis of fretting fatigue tests will be discussed. This chapter will include the requirements of FEA, FEA model, load inputs, and MSSR calculations.

4.1. Requirement for Finite Element Analysis

Finite Element Analysis (FEA) is a numerical procedure that is used to determine the fretting fatigue parameters by calculating the state of strain, stress, and displacement at the contact area. Using this procedure, a body can be represented by a discrete system containing many elements which are connected to each other by the nodes. At these nodes the governing equations can be solved to give the solution of the strain, stress, and displacement at the contact interface. As was discussed earlier in the thesis, configuration, two cylindrical bodies were used with the assumption that their radii are very large in comparison to the contact width (r >> a), in order to use analytical solutions such as "Ruiz" program. In addition, the contacting bodies are assumed to have infinite boundaries. An infinite half-space assumption in fretting fatigue analysis is defined as half specimen thickness (b)/ contact half-width (a) >10

In this case, the latter assumption's basis, known as the half space assumption is violated since the specimen's thickness, b, is less than ten times the contact half width, a. In this study, the pads have two constant radii; 50.8 mm and 304.8 mm, while the specimen is attributed an infinite radius. Therefore, another procedure, that

52

doesn't require an infinite half space assumption, is required to have a solution of the fretting fatigue parameters.

As a numerical solution, finite element analysis can be used to achieve this goal, and the result can be checked to match the analytical solution obtained from "Ruiz" program, yet not necessary. This explains the importance and the rule of finite element analysis as a vital step for conducting quantitative analysis in this study.

4.2. Finite Element Model Description

By using a software called ABAQUS, four nodes plain strain quadrilateral elements were used instead of eight node elements in order to eliminate the oscillation in the stress state along the contact interface introduced by the mid-side node of the eight node element. In this study two different models were used, one model to suit the set of experiments using pads with 50 mm radius while the second model was used to suit the set of experiments using pads with 304.8 mm radius. The fretting fatigue configuration used in this study can be modeled as shown in Figure 4.1 and Figure 4.2 by using this software. Both models mainly consist of three parts: the fretting specimen, the fretting pad, and the rigid body to constrain the pad from rotation. In addition, this model is formulated in two dimensions and because of its symmetry about x-axis, only one half of the contact configuration has been modeled to save the time and the memory resources. The contact condition was developed by using "master-slave" interfacial algorithm for modeling the finite element model. In contact region, the master segment and slave nodes were used to establish the contact

algorithm that was used to determine how the loads were transferred. The specimen is restricted from vertical movement at the bottom surface and only free to roll in the x-direction and along the gripped end while fixed at its far end in the negative x-direction. In addition, the fretting pad is constrained in the x and y direction by pad holder while the half space of fretting specimen was constrained in the x and y direction along its boundary. The master surface is chosen to be the fretting pad while the slave one is the fretting specimen. The top nodes of the pad are forced to move in unison in the y-direction. Also, A Multi-point constraint (MPC) was applied to the pad and specimen in the first model to keep it from rotating due to the application of loads, this was not necessary in the second model.

The material properties for the pad and the specimen were 0.33 as a Poisson's ratio and 126 GPa as modulus of elasticity, while the stiffness of the rigid constraint body was selected very small of 5 Pa and 0.3 as Poisson's ratio. This selection ensures that it has a minimum effect on the pads and the specimen in order to improve the convergence of the finite element analysis. The length of specimen is 288.6 mm, the half thickness b of the specimen is 1.905 mm, the thickness d of the specimen is 3.81 mm.

By changing certain geometric coordination in the ABAQUS input files, the mesh of the pad and the specimen were refined incrementally from the center of contact surface, since in fretting fatigue condition, the contact region is the most critical area where it is required to find the governing variables; such as the stress, strain, and displacement. The mesh near contact surface was refined to increase the accuracy of the stress, strain, and displacement distribution profile. On the other hand,

a course mesh far away from the contact region is designed in order to save the time as well as the memory resources. Since the focus of the analysis is the stress, strain, and displacement distribution profile, such refinement is necessary in order to encompass any tiny change in those values that could turn out to be crucial to understanding the fretting fatigue process in titanium.

According to previous studies as [18], it was concluded that there is a slight difference in a coefficient of friction which doesn't generate much deviation in stress profile, contact half-width. In addition, it was concluded that the experimental dynamic coefficient of friction was found to be ranged between 0.1107~0.3733 for Ti-6Al-4V. As a result, the coefficient of friction of 0.5 was used in all calculations in this study which is a value that is higher than the largest magnitude of the calculated of Q/P ratio in order to have a converging numerical solution.

4.3. Load Inputs

It was noticed that the fretting fatigue steady state condition was always met after the first hundreds cycles of fretting fatigue cycles. Because of that, the load conditions at 10,000 cycles in all tests, not including a plain fatigue condition, were selected to be as inputs to FEA in order to insure that all fretting fatigue variables including contact load, tangential load, axial load, and coefficient of friction were selected from the stable condition. Also, the maximum contact load was applied initially at the first step and kept constant until step 2 to avoid the gross slip condition. The maximum axial and tangential loads then followed as the second step. The frequency for all loads in all conditions of this study was constant of 10 Hz. After

Step 2, the applied loads were simulated as a sinusoidal wave function with predetermined peak/valley values for the axial, the contact, and the measured tangential loads. The input loads for all test is shown in Table 4.1. Also, the details of the applied loads sequence and the numbering systems for the seven steps that were needed for the all tests in this study are showed Figures 4.3 and Figure 4.4. In addition, applied load sequence with two steps for the second model for the set of experiments using pads with 304.8 mm radius are showed in Figure 4.5 and Figure 4.6.

4.4. MSSR Calculation

It was discussed in section 2.7.2 that the MSSR parameter was the most effective parameter in predicting the fretting fatigue life, crack initiation orientation, and crack initiation location. Also, it was discussed that MSSR can take the effects of multi-axial loading and the stress concentration at the trailing edge into consideration. As a result, MSSR is validated in this study as the only critical plane-based parameter. Finite Element Analysis stress outputs were used in the calculation of MSSR superimposed with the corresponding residual along all planes ranging from $-90^o \leq \theta \leq 90^0$ at 0.1^0 increment throughout the whole specimen, where θ is the orientation at which stress state in material is observed.

Two steps were needed to the MSSR. These steps were computed as the maximum and minimum values at the peak and the valley of the axial, tangential, and contact loads. It is by then, as discussed more fully in the next chapter, analyzed for its location, orientation, and correlation with fretting fatigue life under cyclic axial

and variable contact load conditions. In order to get MSSR, two set of files need to be used in MSSR program, one that contain maximums stresses and other than contain minimum stresses. Figure 4.7 shows profile stress for Test 3 using step three, while Figure 4.8 shows profiles stress for test one, using step four. In the same manner, Figure 4.9 and Figure 4.10 shows profile stress for maximum and minimum stresses, for test thirteen.
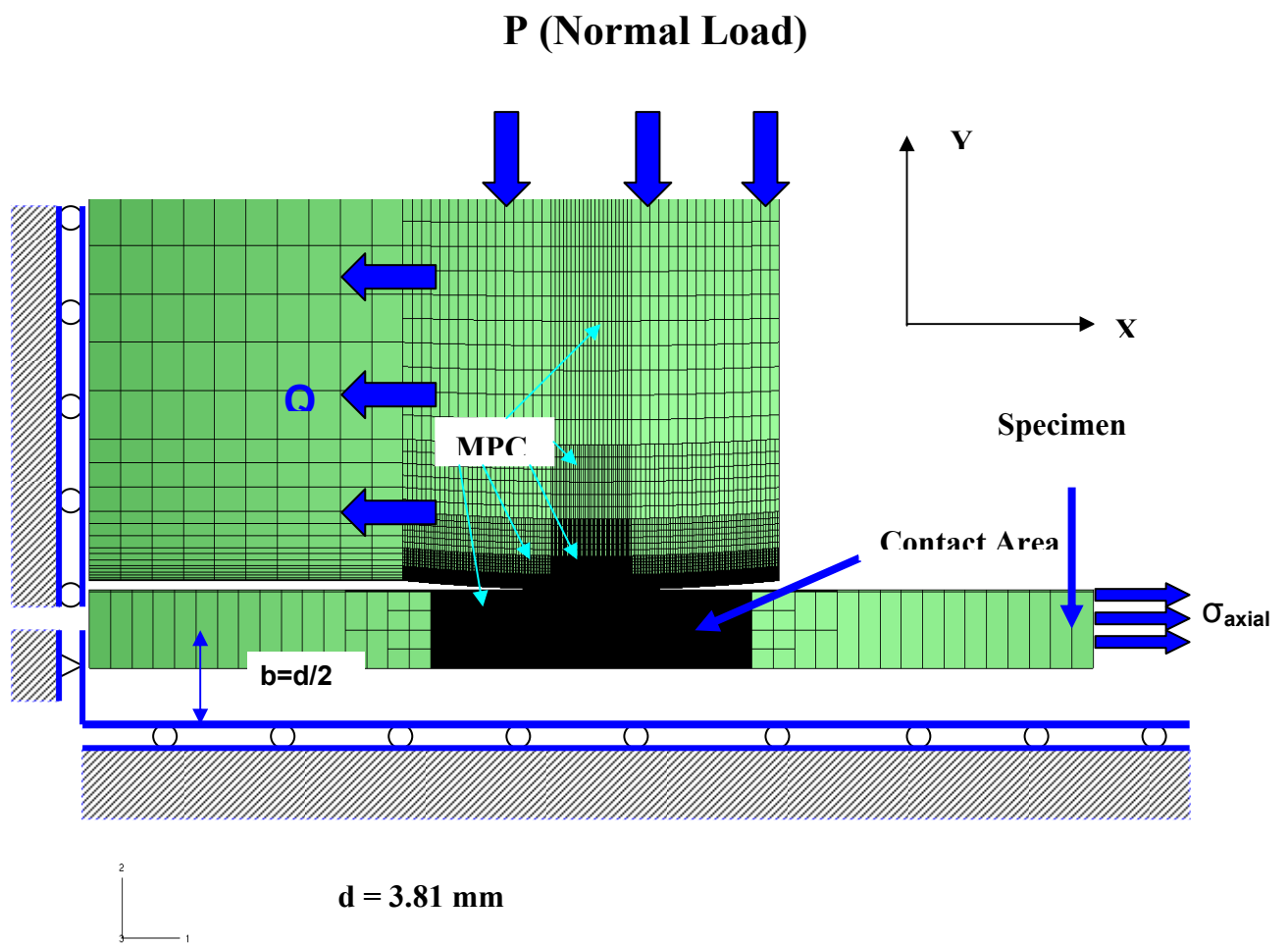
Figure 4.1 Finite Element Model with Load and Boundary Conditions for 50.8 mm Radius Pad Configuration
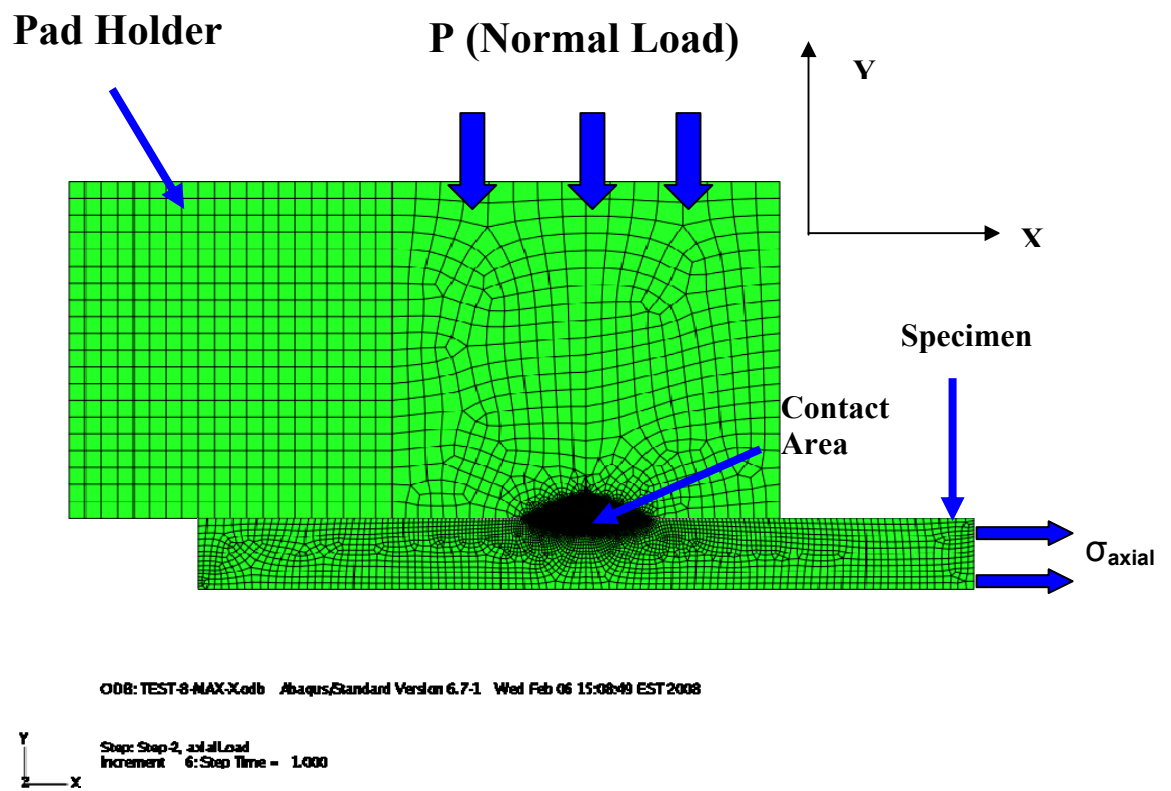
Figure 4.2 Finite Element Model for 304.8 mm Radius Pad Configuration
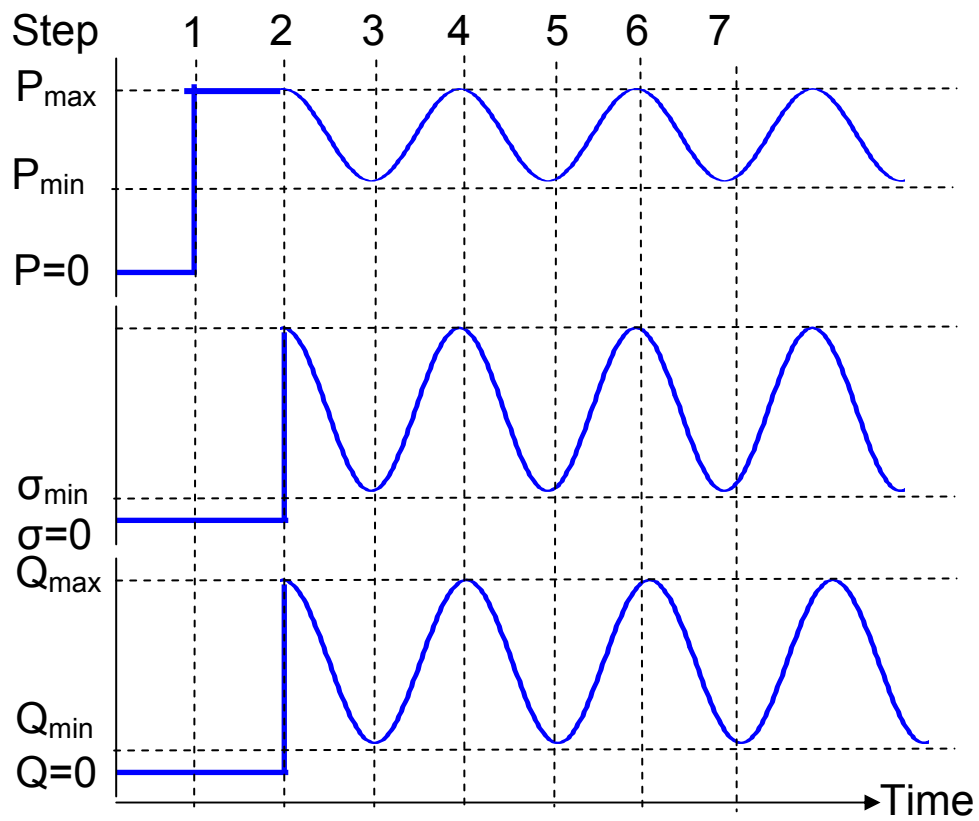
Figure 4.3 Load Step Used In FEA for In-Phase Condition
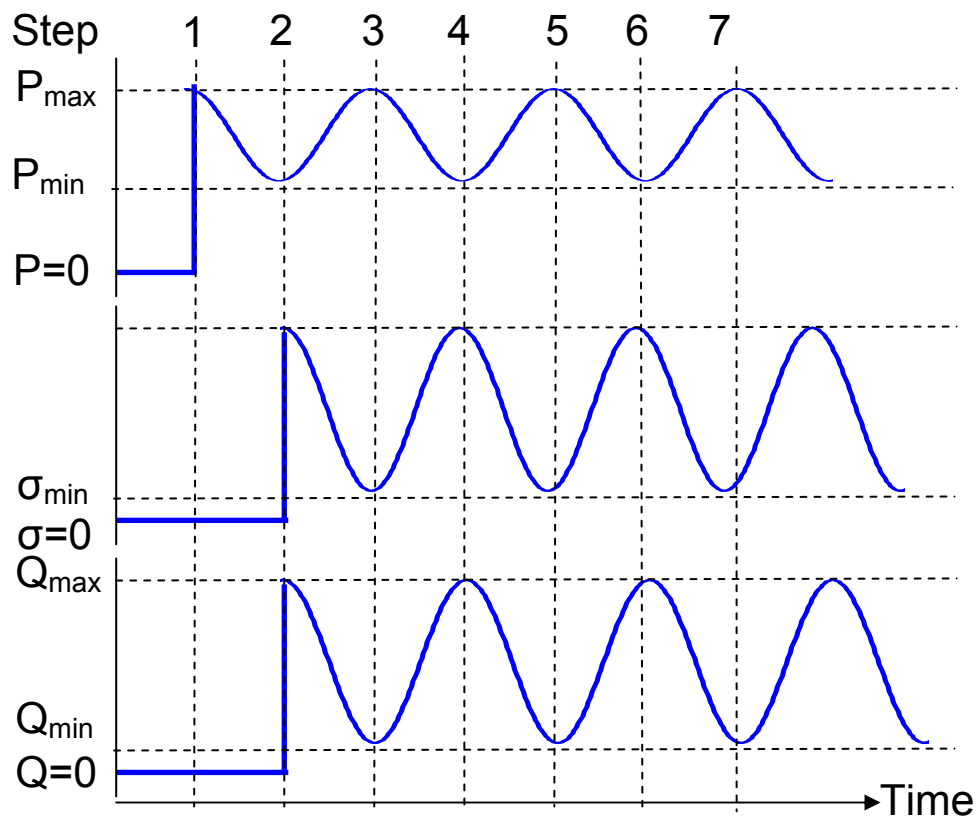
Figure 4.4 Load Step Used In FEA for Out-Phase Condition

Figure 4.5 Load Configuration for Maximum Axial Load Condition
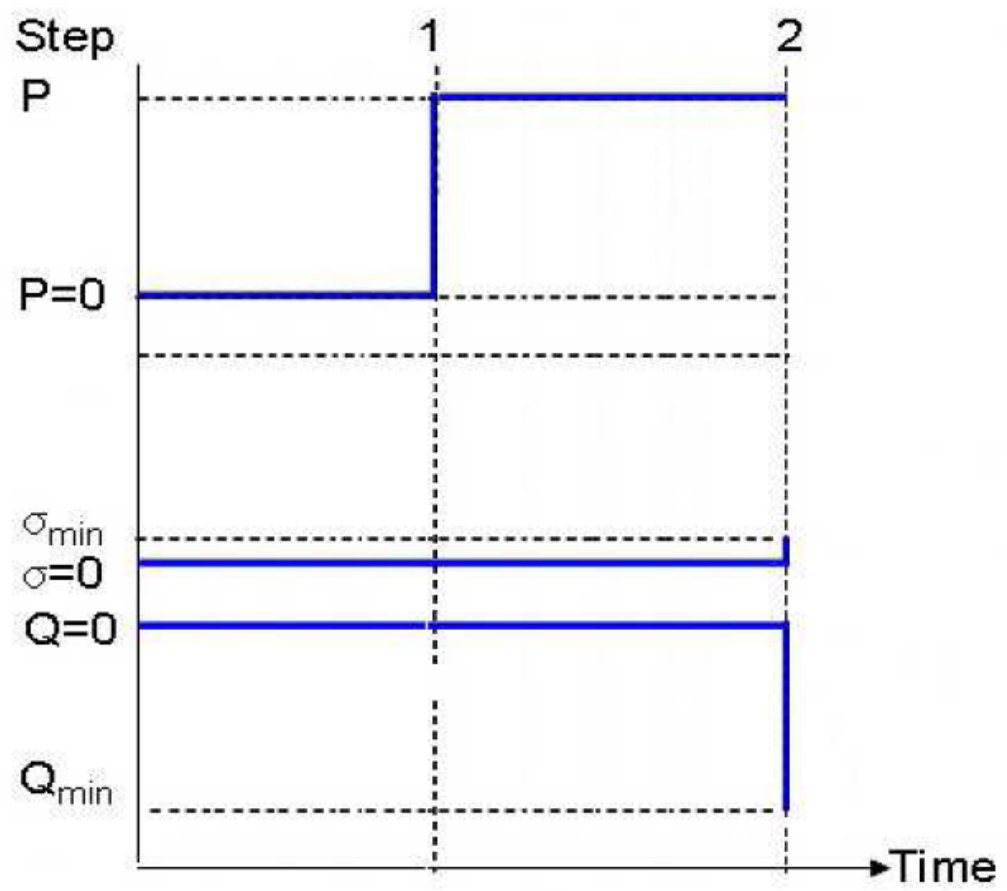
Figure 4.6 Load Configuration for Minimum Axial Load Condition
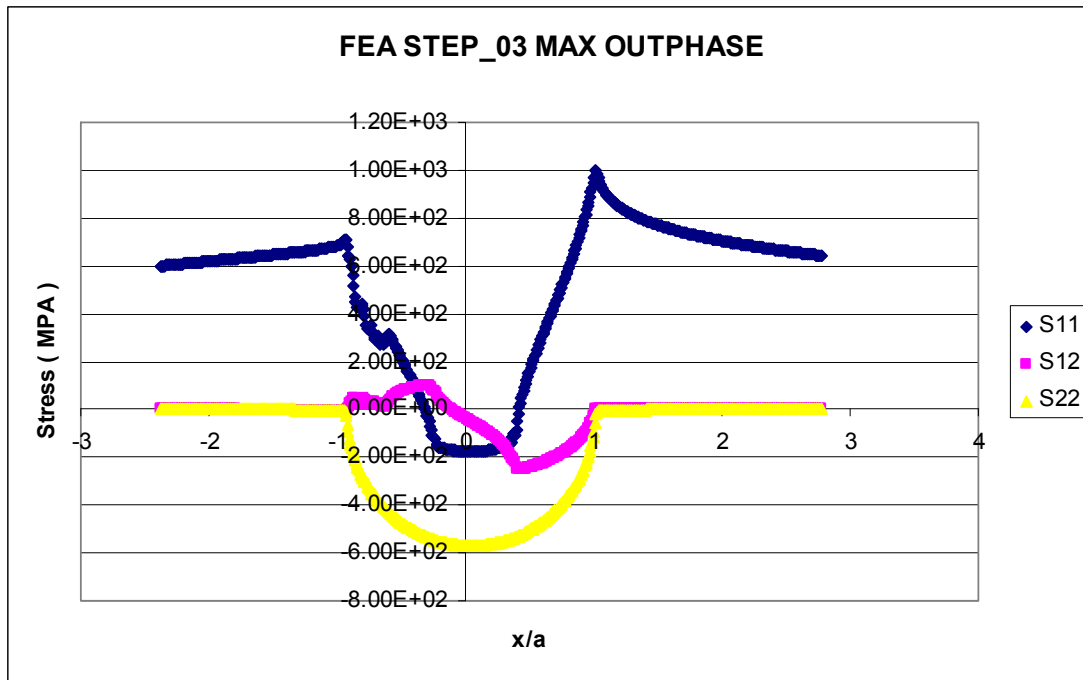
Figure 4.7 FEA Profile Stress for Test # 3, Step 3
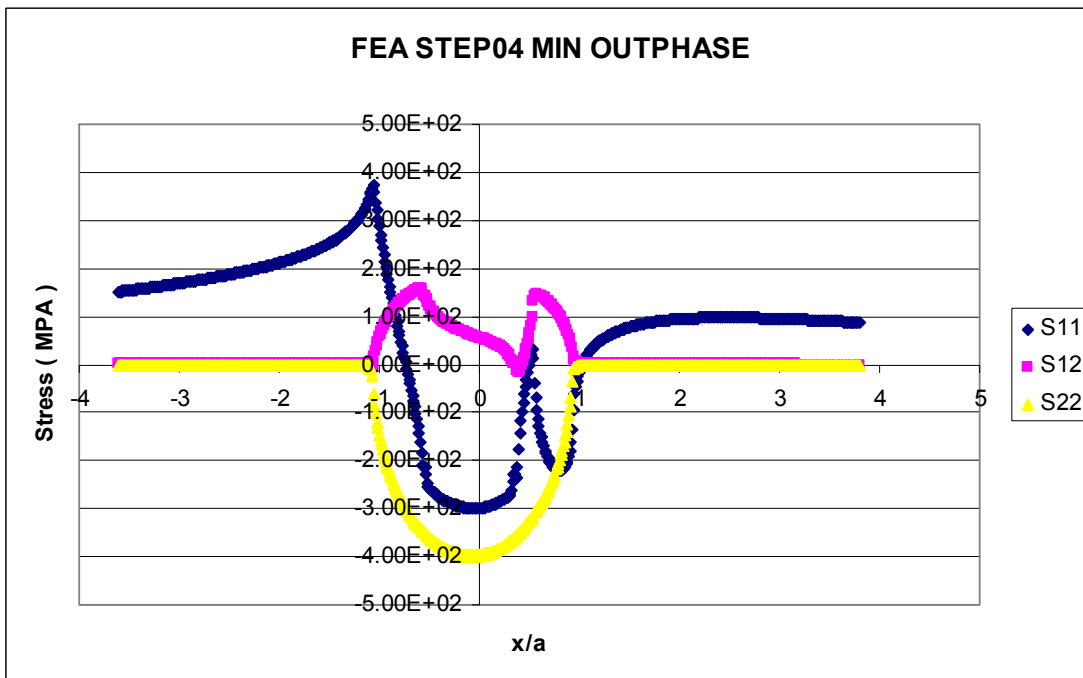
Figure 4.8 FEA Profile Stress for Test # 3, Step 4
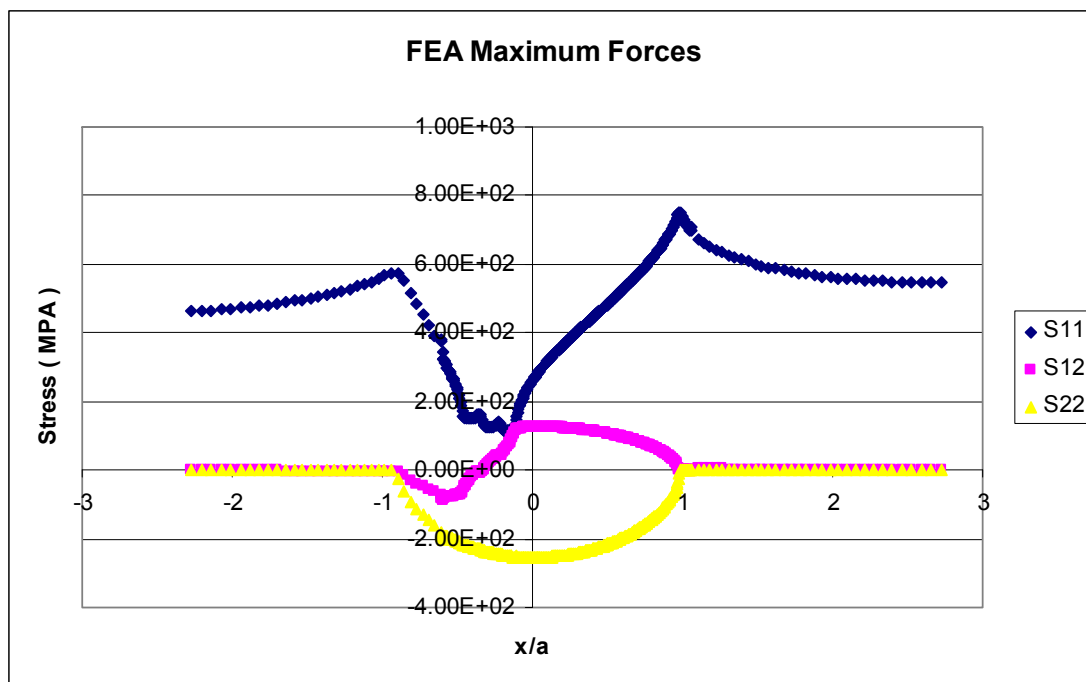
Figure 4.9 FEA Profile Stress for Test # 13, Maximum Forces
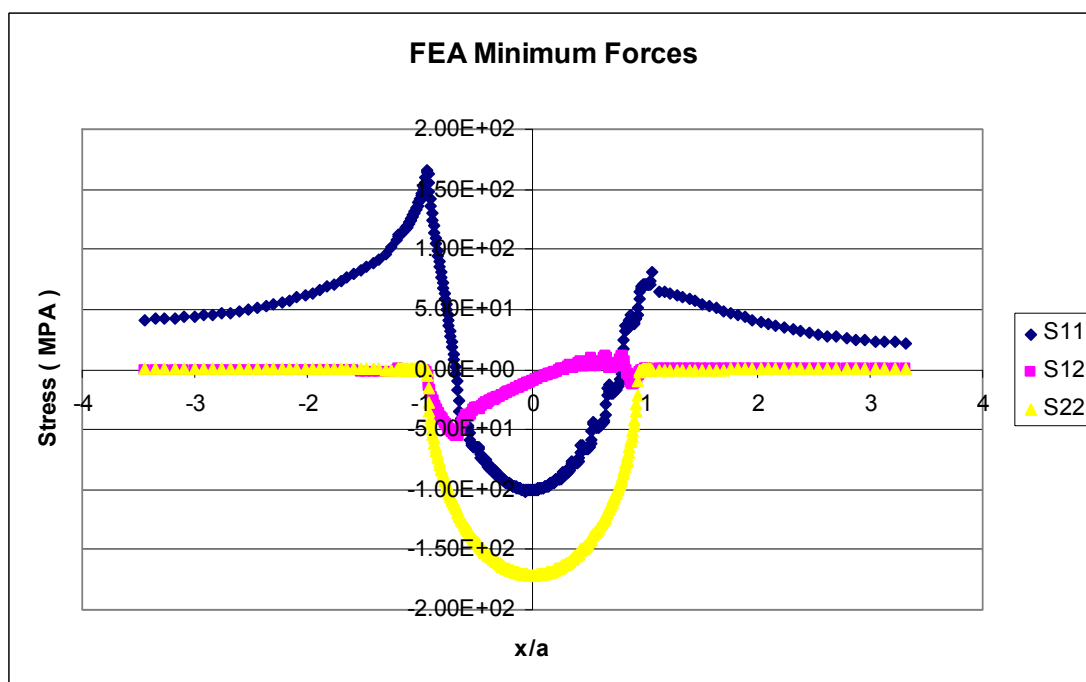
Figure 4.10 FEA Profile Stress for Test # 13, Minimum Forces

Table 4.1 Input Loads for FEA

Test Number	Diameter (mm)	σ_{max} (MPa)	σmin (MPa)	P_{max} (N)	P_{min} (N)	Phase Angle (Deg)	Q max	Q min
1	50.8	564	56	4448	2224	0	410	-890
2	50.8	564	56	4448	2224	45	819	-413
3	50.8	564	56	4448	2224	90	611	-597
4	50.8	413	41	4448	2224	0	934.1	-229.7
5	50.8	413	41	4448	2224	0	939	-235
6	50.8	413	41	4448	2224	45	754	-390
7	50.8	413	41	4448	2224	90	110	-715
8	50.8	376	37	4448	2224	0	1189	-283
9	50.8	376	37	4448	2224	45	648	-383
10	50.8	376	37	4448	2224	45	680	-380
11	50.8	376	37	4448	2224	90	58.3	-682.3
12	304.8	450	40	4448	2224	0	1168	-198
13	304.8	450	40	4448	2224	0	1086	-250
14	304.8	450	40	4448	2224	45	1049	-221
15	304.8	450	40	4448	2224	90	858	-264

V. Results and Discussion

In this chapter, the results of this study are discussed. This chapter will include the experimental results of both the phase difference between the axial cyclic load and the cyclic contact load and the combinations of fretting fatigue and plain fatigue, Finite Element Analysis (FEA), MSSR outputs, fretting fatigue life, fretting fatigue predictive parameters, crack initiation mechanism, and phase difference effect.

5.1. Experimental Results

In this section the following experimental results are discussed: fretting fatigue condition, Q/P ratio, tangential load, fracture surface, contact half-width, crack initiation location, and crack initiation orientation.

During this study, fifteen experiments were conducted on titanium alloy Ti- 6A1-4V. Eleven of these experiments were done with the phase difference between the axial cyclic load and the cyclic contact load at different axial stress range and different phase angle for contact pads of 50.8 mm, while four experiments were done under similar conditions using contact pads of 304.8 mm. On the other hand two more experiments were done with combinations of the fretting fatigue and the plain fatigue conditions by using cyclic axial load and constant contact load. Full details of these seventeen testes and their results are tabulated in Table 5.1. As seen in this table, test number sixteen and seventeen, which were done under combinations of fretting fatigue and plain fatigue condition, were not included in FEA or MSSR analysis.

67

5.1.1. Fretting Fatigue Condition

In order to determine the fretting fatigue conditions, the hysteresis loops between the tangential and the axial loads can be used. Figures 5.1 and 5.2 show the hysteresis loop of test # 8 (in-phase) and test # 9 (out-phase). On the other hand, Figures 5.3 and 5.4 show the maximum and minimum tangential load variation with respect to the fatigue cycles for test # 8 and test # 9. It can be noticed from these figures that the partial slip condition of the fretting fatigue was met after a few hundreds of the fretting fatigue cycles. Therefore, the required partial slip condition was met for fretting fatigue tests.

In addition, Figure 5.5 shows one of the tests that used combination of fretting fatigue and plain fatigue condition, which was done under constant contact load. This figure shows that the steady state condition for test # 16 has been met after a few hundreds of cycles. In this test, five thousands cycles of fretting fatigue was applied and after that one thousand cycles of plain fatigue did follow and the process was repeated till failure occur. On the other hand, Figure 5.6 for test # 17, shows the same number of fretting fatigue cycles that were applies in test # 16 but with one hundred thousands cycles of plain fatigue followed and the process will keep repeating till failure occur.

In all tests that were conducted in this study, the steady state condition of the fretting fatigue was met after a few hundreds cycles of fretting fatigue cycles, including test # 16 and test # 17 that relied on combination of fretting fatigue and plain fatigue condition. Hence, this result insures that all fretting fatigue variables

including axial load, tangential load, and coefficient of friction, were in a steady state condition till the failure of the specimen occurred.

5.1.2. Q/P

In each test, the maximum value of Q/P is considered to be the dynamic coefficient of friction between the specimen and the pad. Since the largest value of dynamic coefficient of friction was close to 0.4 in all the tests conducted in this study, a higher value of 0.5 was used in FEA analysis. Table 5.1 shows the maximum value of Q/P for all tests. It can be concluded using this table that the greatest value of Q/P was found to be in the in-phase condition, while the least value in the out of phase condition. This conclusion indicates that the out of phase condition has less friction than other conditions and the in-phase condition has the most friction. In Figure 5.7, the variation of Q/P with respect to the time for test # 4 is illustrated which is a sinusoidal wave as it follows the variation of the axial and the tangential loads.

It can be concluded that the Q/P ratio under fretting fatigue condition is varying over time, and could not be treated as a constant at all. For the purpose of finite element analysis, the coefficient of friction for tests conducted in this study was selected to be 0.5. Also, it can be noticed from Table 5.2 that the maximum value of Q/P decreases going from in-phase condition to out of phase condition.

5.1.3. Tangential load

As discussed in chapter III; the tangential load can be determined as the half of difference between the lower applied axial load and the load measured at the upper grip. For this reason, it was expected that the tangential load will follow the axial load in sinusoidal pattern, phase, and frequency. The tangential load vary in the same manner at the same time and at the same angle for conditions where there was no phase lag between the cyclic axial load and the cyclic contact loads. All the loads; tangential, axial, and contact, vary in the same manner at the same time and at the same angle as shown in Figure 5.8. On the other hand the tangential load varies in the same manner as the axial load and there was no effect from the applied contact load on the phase of tangential load for conditions where there was a phase lag between the cyclic axial load and the cyclic contact load, as shown Figures 5.9, for test # 9. It can be concluded that the contact load only affects the magnitude of the tangential load. Also, it can be concluded that the contact load had no effect on its phase angle or wave shape.

It was noticed that the shear stress range, which is the difference between the maximum and the minimum tangential stress, for the out of phase condition is less than that for the in-phase condition, as shown in Figure 5.10. Also, it can be noticed from this figure that when shear stress range decreases fretting fatigue life increases. On the other hand, by studying the relation between the phase angle and the shear stress range it was concluded that that the shear stress range decreases by increasing the phase lag until the phase angle reaches 90°, as shown in Figure 5.11. Therefore, it can be concluded that the greatest magnitude is at the in phase condition, while the

least magnitude of the shear stress range is under the out of phase condition. Finally, it can be said that the phase lag in general reduces the shear stress range which could have the most effect on fretting fatigue.

5.1.4. Contact Half-Width

As shown in equation 2.20, the applied contact load is the only parameter that affect the contact-half-width, a, as and there was no effect from the axial load conditions. Figure 5.12 is a photo of the specimen from test four, which shows the partial slip zones and stick zone at the contact region, using 50.4 mm contact pads. The fretting fatigue scars shown identify clearly a "stick zone" in the center area with darker thin lines on the edges denoting "partial slip" zones at the leading and the trailing edges of the contact area.

With tests using 50.8 mm contact pads, it was difficult to measure the contact half-width, a, since it has a very small length. Also, severe slip condition at the final stage of fretting fatigue test was a factor in that. For tests # 1 through test # 11 as well as test # 16 and test #17, different magnitudes of the contact half-width was determined each time during the measurement and most of these values were ranged between 0.75 mm ~ 0.82 mm. On the other hand, the theoretical values of contact half-width for these tests were all about 0.8055 mm. In addition, contact half-width values, for experiments with pad radius of 304.8 mm were between 1.92 mm and 1.95 mm for test # 12 through test # 15. On the other hand, the theoretical values of contact half-width for these tests were all about 1.9609 mm. All these values were tabulated in Table 5.3.

5.1.5. Fracture Surface Area

In order to examine the fracture surface of the cross sectional area of the specimens by taking a higher magnification pictures, the Scanning Electron Microscope (SEM) was used during this study. Figure 5.13 shows the fracture surface along with its four distinguishable regions that were created during the crack initiation and propagation for test four. In Figure 5.14 through Figure 5.16, these regions can be seen, by using the Scanning Electron Microscope. In Figure 5.14, it can be noticed that there was debris in region one due to the created wear from the damaged surface of the contact mechanism that nucleates the initial crack. Region one is where the crack initiated and grew at an early stage. On the other hand, Figure 5.15 shows stiriation of region two, which represents the main region for the crack propagation. Also, Figure 5.16 shows the large dimples with grain boundary of region three. Region four is where unstable crack growth occurred, were commonly associated with ductile tearing and shear slip, resulting in catastrophic failure.

5.1.6 Crack Initiation Location

Determination of the location of the initiated crack is one of the important issues in fretting fatigue. During all tests conducted in this study, which failed due to fretting fatigue condition, the crack initiation location always occurred at or very near the trailing edge of the contact region where $x/a = +1$ along the x-direction. Figure 5.17 shows that the crack initiated at the trailing edge of the contact area for test # 12. On the other hand, Figure 5.18 shows that this crack has been initiated at the contact surface where it is shown as darker area than other areas for test # 5.

The trailing edge area is the point where the maximum axial load is applied. Because of that, this axial load will propagate any crack that was initiated with a critical size at the trailing edge area. In a study conducted by Magaziner [28], it was found that that the crack nucleates in the trailing edge area due to the stress concentration forming at the boundary of the stick zones due to the shifting of the stick zone.

The crack initiation location, that was determined from the MSSR, for experiments using 50.8 mm pads, was at x/a = 1.1 for the in-phase condition and at out of phase condition. On the other hand, for experiments using 3.4.8 mm pads, crack imitation location was at x/a = 0.99.

5.1.7 Crack Initiation Orientation

From previous studies [7, 9, 10], the crack initiation orientation for titanium Ti-6Al-4V alloy under constant applied contact load is known to be about $+45^o \pm 15^o$. In general, there are two types of cracks that are found in a fretting fatigue specimen, primary and secondary ones. The first type is the crack that leads to failure, whilst the other type does not, but is also detectable by the SEM along the contact surface. Also, in a study conducted by Lee [8], for the test conducted under variable applied contact load with frequency of 2.5 Hz, while the axial load frequency is 10 Hz, found that the crack orientation was 40°. Lee did conclude that the variable contact load under different frequencies didn't alter crack initiation orientation significantly from constant contact load.

In this study; one test was examined for the crack initiation orientation by using SEM. The crack initiation orientation for test # 5 was found to be 42° as shown in Figure 5.18. This value is very close to the one of the previous studies.

5.1.8 Effect of Out of Phase Loading

There are several effects of out of phase condition on fretting fatigue. First, the partial slip condition of the out of phase was met after the first hundreds cycles of fretting fatigue cycles. This was valid as well for the in-phase condition. Second, the Q/P ratio was found to be smaller for out of phase conditions than for in-phase condition. Third, under both in-phase or out of phase condition, the tangential load was varying in the same manner as the axial load. The only effect from the contact load was on the magnitude of the tangential load. Fourth, under any phase condition the crack initiation location was always found to be at the trailing edge of the contact region. Also, the fracture surface topography consisted of four distinguishable areas.

5.2. Finite Element Analysis Results

Finite Element Analysis (FEA) model has been used to determine numerically the stress, strain, and displacement distribution within the contact region of the specimen, as mentioned in chapter IV. As an input into FEA, the load condition of the applied axial and contact loads, and the corresponding tangential load for each test were used, this is shown in Table 4.1. In this section the following will be discussed: axial stress state, distribution of normal stress, distribution of shear stress, stress profiles, and out of phase effect on stress profile.

5.2.1. Axial Stress State, σ_{xx}

By looking at equation 2.39, we can conclude that the total axial stress along the contact surface between the fretting specimen and the fretting pad depends on the applied contact load and the resulting tangential load as well as the applied axial load. Figure 5.19 shows the axial stress σ_{xx} for test # 1 (in-phase) and test # 3 (out of phase), those have been under the same applied axial stress. It can be concluded from this graph that the maximum value for σ_{xx} for in-phase condition is more than that of out of phase condition, which could affect the fretting fatigue life. It can be noticed that the maximum value of σ_{xx} is reached at the trailing edge at a location of x/a around 0.95 for the 50.8 mm pads and around 0.93 for 304.8 mm pads. All the previous points are located inside the stick zone in a location called the trailing edge. Also, it can be noticed that maximum compressive value of σ_{xx} occurs always at the center of contact region for both tests conduced with 50.8 mm pads as well 304.8 mm pads.

Looking again at Figure 5.19, the curve almost linearly slopes up to a tensile stress peak which is almost at the edge of the contact zone at the positive x-direction from the center of the contact area. Continuing from that point on, σ_{xx} continues to decrease until it eventually goes back to the remotely applied bulk stress at the end. On the other hand, σ_{xx} slopes up less rapidly to a lower peak and then gradually decreases until it eventually reaches the remotely applied bulk stress as well in the negative x- direction. Same observations can be seen in Figure 5.22 and 5.23.

5.2.2. Distribution of Normal Stress σ_{yy}

In Figure 5.20, the distribution of the normal stress σ_{yy} FEA output for test number # 1 and test # 3 can be seen. It can be noticed that maximum value for σ_{yy} for in-phase condition different from that for out of phase condition. This is because during the in-phase condition; if the axial load was at its maximum magnitude, the contact load would be at its maximum magnitude. However; during the out of phase condition if the axial load was at its maximum magnitude the contact load would be at its minimum magnitude. From this graph, it can be noticed that the local normal stress reaches a maximum compressive value at the very center of contact, with symmetry towards both edges of the contact area. Also, it can be noticed that the stress increases parabolically to reach zero, approximately at the edge of the contact zone. Same observations can be seen in Figure 5.22 and 5.21.

5.2.3. Distribution of Shear Stress σ_{xy}

It is helpful to try to understand how the maximum load condition was met, whether it is based on axial or contact load. Most previous studies were done under a constant contact load, so the maximum condition was based on the maximum axial load. On the other hand, in those studies where the applied contact load was variable, the maximum load condition was based on the maximum axial load. The reason behind this was because the maximum contact load was met at the same time when the maximum axial load was met. This was also the case in the in-phase conditions. This will leave us to think of what should be the maximum load condition under the out of phase case.

76

.   The answer can be found from the distribution of the shear stress, since the

distribution for both the axial stress and the normal stress didn't give the same

answer. This can be found by comparing shear forces from step 3 that represent

maximum axial load conditions for both test # 1 and test # 3. In test # 1 (in phase),

step number 3 represent the minimum axial load and the minimum contact load. On

the other hand, in test # 3 (out of phase) step number 3 represents the maximum axial

load condition and the minimum contact load condition, while step number 4 is the

minimum axial load condition and the maximum contact load condition. Figure 5.21,

shows shear forces from test # 1 and test # 3 that are both taken from step 3 from FEA

results. In Figure 5.21, it can be noticed that the maximum axial load condition for the

out of phase condition is close to the one of the in-phase condition and both of them

result in a shear stress close to each other. Therefore, the maximum axial load

condition in this study was also assumed the maximum load condition.

In addition, it can be noticed from that for σ_{xy} distribution along the contact

surface that the local normal stress and shear stress are linked. It can be noticed from

Figure 5.21 that the maximum values for σ_{xy} are reached somewhere between the

center of contact and the trailing edge, in the positive x-direction. Also, all the

specimens run under this present study failed at a location between the position of

maximum shear stress and maximum axial stress where shear stress is decreasing

parabolically until it reaches zero values outside the contact area. Same observations

can be seen in Figure 5.22 and 5.23.

5.2.4 Out of Phase Effect on Stress Profile

It can be concluded from results from previous section that the maximum load condition of the out of phase condition, as the in-phase condition, at the maximum axial load condition. Also, at the same axial stress the axial stress concentration factor for the out of phase condition is lower than the in-phase condition. Finally, there was no effect from the sequence of the applied loads and the only effect is from the magnitude of these loads.

5.3. MSSR Calculation

Being the most effective parameter used to predict the material fatigue life, the crack initiation location, and the crack initiation orientation, the MSSR was adopted in this study. All test results from finite element analysis were formulated to be used as an input into the MSSR calculations. To be able to use the MSRR calculations, only two steps of the load application are needed; one is at the maximum magnitude, while the other one is at the minimum magnitude. This section will discuss the determination of the maximum MSSR and the effect of MSSR on the crack initiation location.

The determination of the MSSR needed two steps. Table 5.4 shows the final results for MSSR for test one through fifteen. Figure 5.24 shows the maximum MSSR for tests those conducted under in-phase and out of phase conditions. It can be concluded from this figure that the MSSR values for the out of phase condition is slightly higher than these in-phase condition at a given stress level, yet the difference

is very small and trivial. There are two reasons. The first reason is that MSSR depends on both the axial stress and shear stress as shown in equation 2.46. The second reason is that MSSR doesn't depend on the maximum of any of them but it depends on the combination between them as well as the arbitrary constants A, B, C, and D.

Figure 5.25 demonstrate the MSSR variation with fretting fatigue life for both in-phase and out of phase conditions. It can be noticed from Figure 5.25 that MSSR values increases as axial stress increase. On the other hand, it can be noticed that MSSR values increases as fretting fatigue life decreases.

5.4. Fatigue Life

This section discusses the results of fatigue life that were determined from this study. This section will discuss the followings; combination of plain fatigue and fretting fatigue, fretting fatigue life, the use of the MSSR parameter as a predictive parameter, pad geometry effect on fatigue life, and effect of out of phase condition.

5.4.1. Plain Fatigue and Fretting Fatigue Life

Two experiments were done under the combinations between the fretting fatigue and the plain fatigue condition. Tables 5.5 and 5.6 show the fatigue life for these experiments. Test # 16 was conducted under fretting fatigue condition with a constant contact load of 3336 N, and a cyclic axial load with maximum magnitude of 564 MPa and minimum magnitude of 56.4 MPa. During this test, 5,000 fretting fatigue cycles was applied first followed by 1,000 plain fatigue cycles and this

continued on till fracture of the specimen occurred. The fatigue life of this test was 44,656 cycles. On the other hand, Test # 17 was conducted with the same contact and axial loads applied in test # 16 but with 5,000 fretting fatigue cycle followed by 100,000 plain fatigue cycles. The fatigue life of this test was 350,937 cycles. Results from previous study conducted by Al-Majali [30] were used in conjunction with results from present study. Figure 5.26 shows that plotting results from test # 16 and test # 17 which reflect that plain fatigue increases the life of titanium specimen while fretting fatigue decreases the life of titanium specimen. The ratios of plain fatigue to that of fretting fatigue were calculated for these tests and plotted, as shown in Figure 5.26. On the other hand, it can concluded from Figure 5.27 that there is no history effect as long as the total cycles are the same, since it shows the same trend as that in Figure 5.26 This means that there will be no effect on fretting fatigue life whether some of fretting fatigue was applied at first and continued by plain fatigue and the process kept alternating or finishing all fretting fatigue cycles first followed by plain fatigue.

5.4.2. Fretting Fatigue Life

This section will discuss the following; the effect of the axial stress range and the effective axial stress, shear stress range, the use of MSSR parameter on fatigue life, and a comparison between this study and the previous studies.

5.4.2.1 Axial Stress Range and Effective Stress

The axial stress range can be defined as the difference between the maximum and the minimum axial stress. On the other hand, the effective stress can be found using the following equation:

$$\sigma_{effective} = \sigma_{max}(1-R)^m \qquad (6.1)$$

where m is 0.45. The results of fatigue life with respect to the axial stress range and the effective stress for this study and the previous studies. [8, 12, and 29] were summarized in tables 5.7 though 5.10. After that, the values in these tables have been plotted. Figure 5.28 illustrate the relationship between the axial stress range and fretting fatigue life from present study. It can be concluded from Figure 5.28 that as the axial stress range decreases fretting fatigue life increases, for both in-phase and out of phase condition. Also, it can be noticed that the S_N curve for the axial stress range did not collapse the data together, rather three segregated curves were formed which reflect that using axial stress range as a predictive parameter for this present study is not effective. This is due to the reason that axial stress range does not account do contact stresses. On the other hand, Figure 5.29 illustrate the relationship between the effective axial stress and the fatigue life. It can be concluded from Figure 5.29 that as the effective axial stress decreases fretting fatigue life increases, for both in-phase and out of phase condition. In addition, Figure 5.30 shows that fretting fatigue life for out of phase condition is higher than that of in-phase condition for the same axial load. Also, it can be noticed that the S_N curve for effective stress did not collapse the data together, rather three segregated curves were formed which reflect

that using effective stress as a predictive parameter for this present study is not effective. This is due to the reason that effective stress does not account do contact stresses.

On the other hand, at the same axial load condition, the fretting fatigue tests conducted under phase difference (45 & 90 degree) shows higher fretting fatigue life than that of in-phase condition. This is illustrated in Figure 5.31, 5.32, and 5.33 which reflects that this conclusion is valid for both experiments done with 50.8 mm contact pads as well as for experiments done with 304.8 mm contact pads. Simply, fretting fatigue life increases when the phase angle increases for the same applied axial load condition. On the other hand, at different axial load condition and same phase angle, Figure 5.34 and Figure 5.35 shows for different axial load condition and same phase angle, the fretting fatigue life decreases for higher axial load condition.

Figures 5.36 and 5.37 illustrate a comparison between this present study and the previous studies in term of S_N Curve in the basis of the axial stress range and effective stress. It can be noticed that the results from this study lie in the scatter band as the previous studies.

5.4.2.2 Shear Stress Range

The average shear stress range can be defined as the difference between the maximum and the minimum shear stress. The average shear stress range results for all tests were tabulated in Table 5.11, for those conducted under fretting fatigue condition. Figure 5.37 shows the average shear stress with respect to the fatigue life. It can be noticed from this figure that the fatigue life increases as the shear stress

range decrease, despite of the phase condition even in-phase or out of phase condition. In addition, it can be concluded from Figure 5.38 that the shear stress range decreases as phase angle increases.

5.4.2.3 MSSR Predictive Parameter

The reason that the MSSR parameter was adopted in this study because it is the most effective parameter in predicting the fatigue life, the crack initiation location, and the crack initiation orientation for this present study. As concluded in previous sections, MSSR was very effective parameter in predicting the crack initiation location and orientation because it does take into consideration both normal and shear stress and is independent of pad geometry. This section will discuss the effect of MSSR on the fatigue life. By then, the result will be compared to previous studies.

The result of MSSR calculation and the fatigue life for the titanium alloy from this study and previous studies are tabulated in Table 5.12 and 5.15. Looking at these tables, results from constant applied load condition and variable applied contact load condition from the previous studies as well as the phase difference condition from this present study were tabulated. Figure 5.40 shows the graphical results of MSSR and fatigue life which reflect the effect of MSSR on the fatigue life from present study while Figure 5.41 shows the same graphical results from present study as well as previous studies. Figure 5.40 shows that MSSR S_N curve did collapse all date together, unlike S_N curves from axial stress range and effective stress. It can be noticed from Figure 5.41 that values of MSSR data lie within the scatter band, except for data from Majali [30] which are out of the scatter from all the other studies. From

Figure 5.41, it can be concluded that MSSR parameter was very effective as a tool that can be used to predict fretting fatigue life, because it did take into consideration contact stresses. Also, it can be concluded that MSSR was an excellent parameter to predict crack initiation location as well as crack initiation orientation.

5.4.3 Pad Geometry Effect on Fatigue Life

Changing the radius of the cylindrical pads from a high curvature value 50.8 mm to merely flat pads 304.8 mm did have different effect on the fatigue life. It was noticed that changing the pad radius from 50.8 mm to 304.8 mm did decrease the retting fatigue life.

5.4.4 Effect of Out of Phase on Fretting Fatigue

The investigation into the effect of out of phase on the fatigue life of titanium alloy is one of the purposes of this study. The phase difference between the axial and the contact loads improves the fretting fatigue life. However this improvement depends on the applied axial load. For example, under higher magnitude of applied axial stress, the improvement of the fatigue life is not so much. On the other hand, under lower applied axial stress condition the fatigue life might be doubled. The fatigue life of the out of phase condition proved to be higher. It can be concluded that the results from this present study were very close to the previous studies. Also, it can be noticed that all values lie within the scatter band.

Figure 5.1 Hysteresis Loop for Test # 8 (In-Phase) Axial Load 376-37 (MPa)
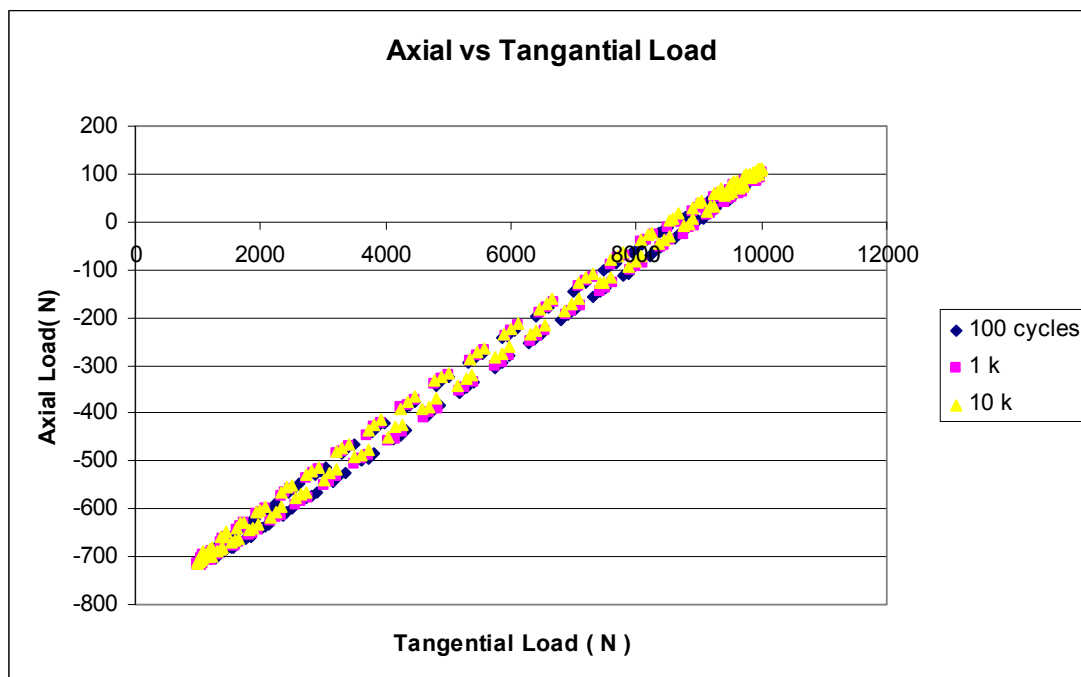
Figure 5.2 Hysteresis Loop for Test # 7 (Out-Phase) Axial Load 413-41 (MPa)
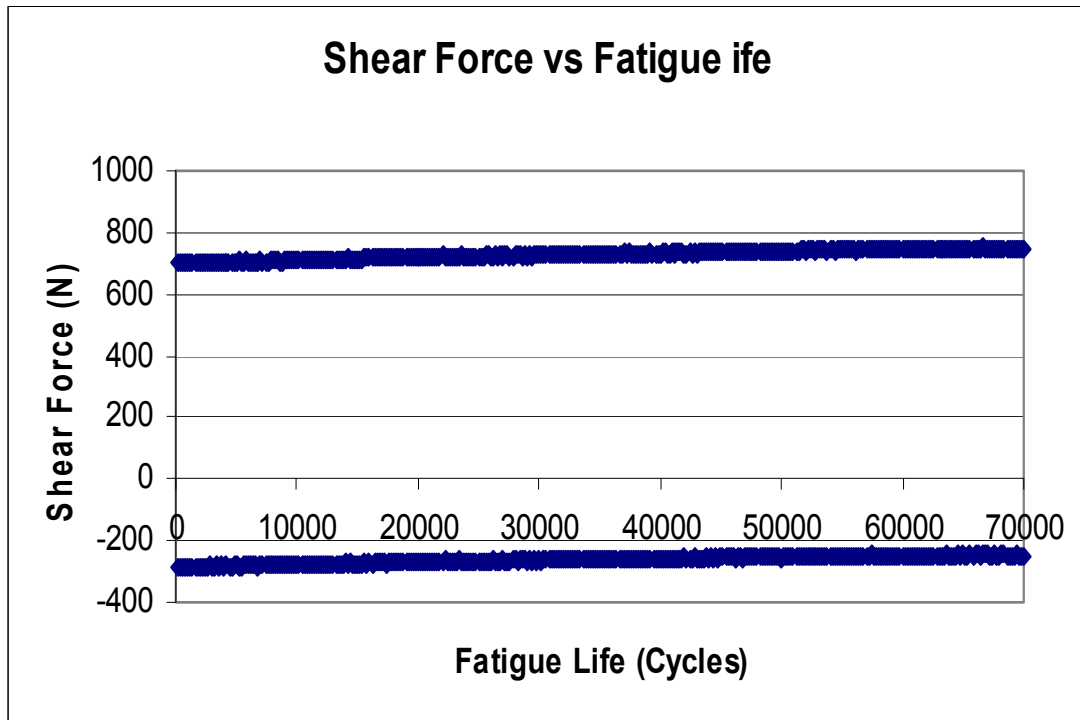
Figure 5.3 Shear Force vs. Fatigue Life for Test # 8 (In-Phase) Axial Load 376-37 (MPa)
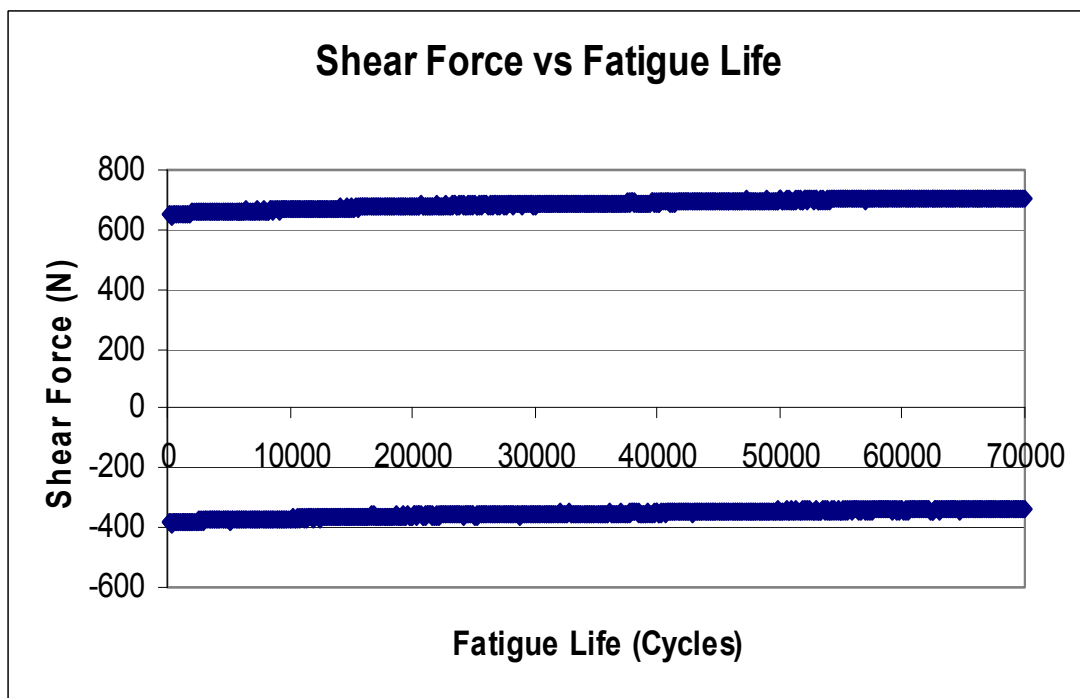
Figure 5.4 Shear Force vs. Fatigue Life for Test # 9 (Out-Phase) Axial Load 376-37 (MPa)
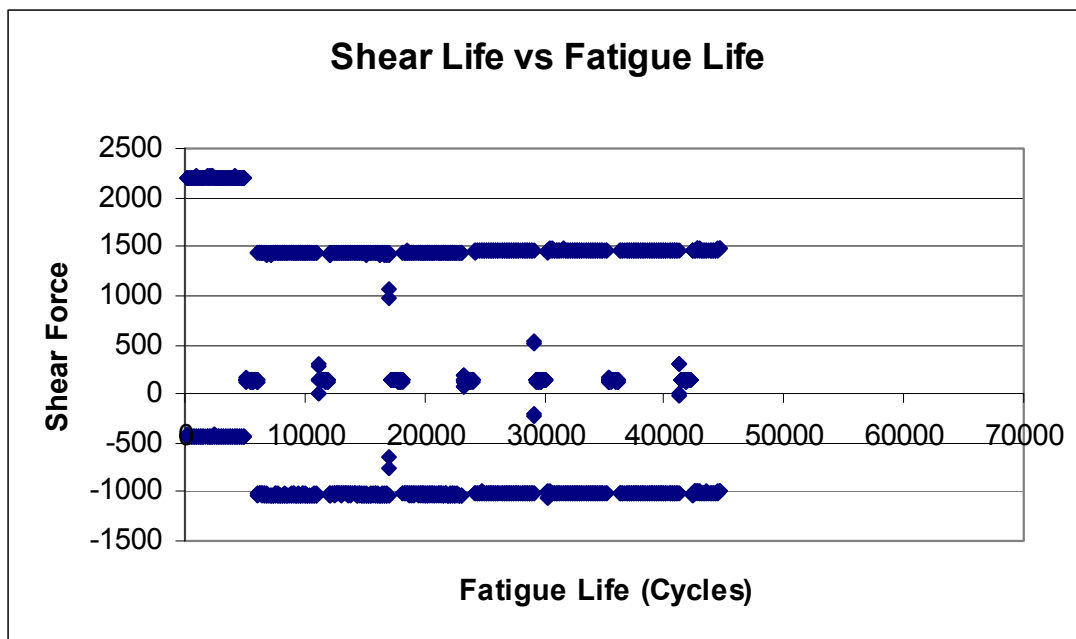
Figure 5.5 Shear Load vs. Fatigue Life for Test # 16 Combination of Fretting Fatigue & Plain Fatigue
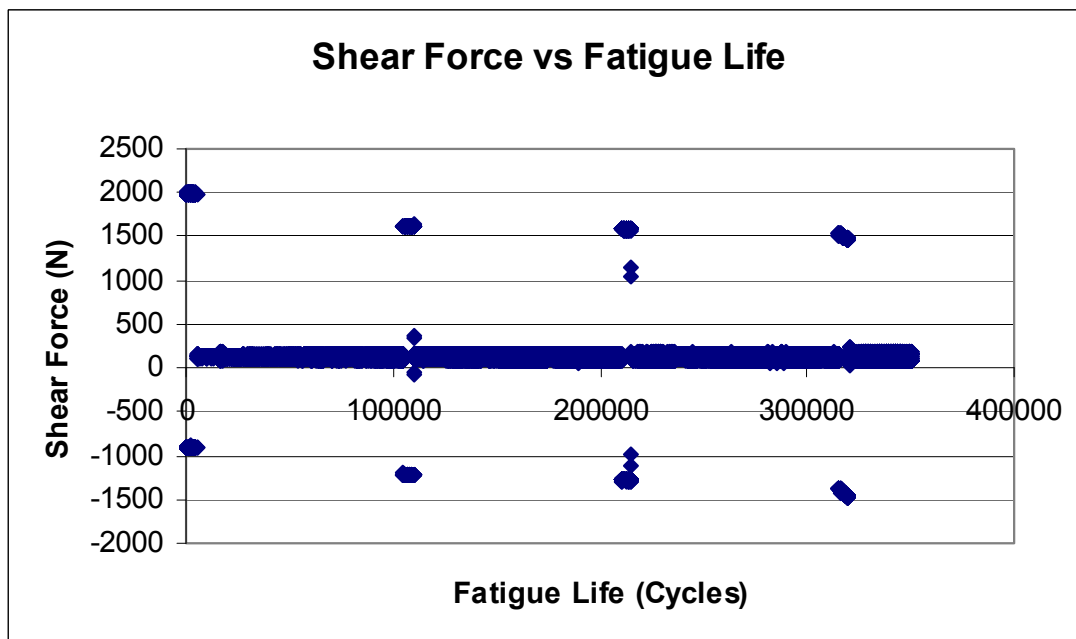
Figure 5.6 Shear Load vs. Fatigue Life for Test # 17 Combination of Fretting Fatigue & Plain Fatigue
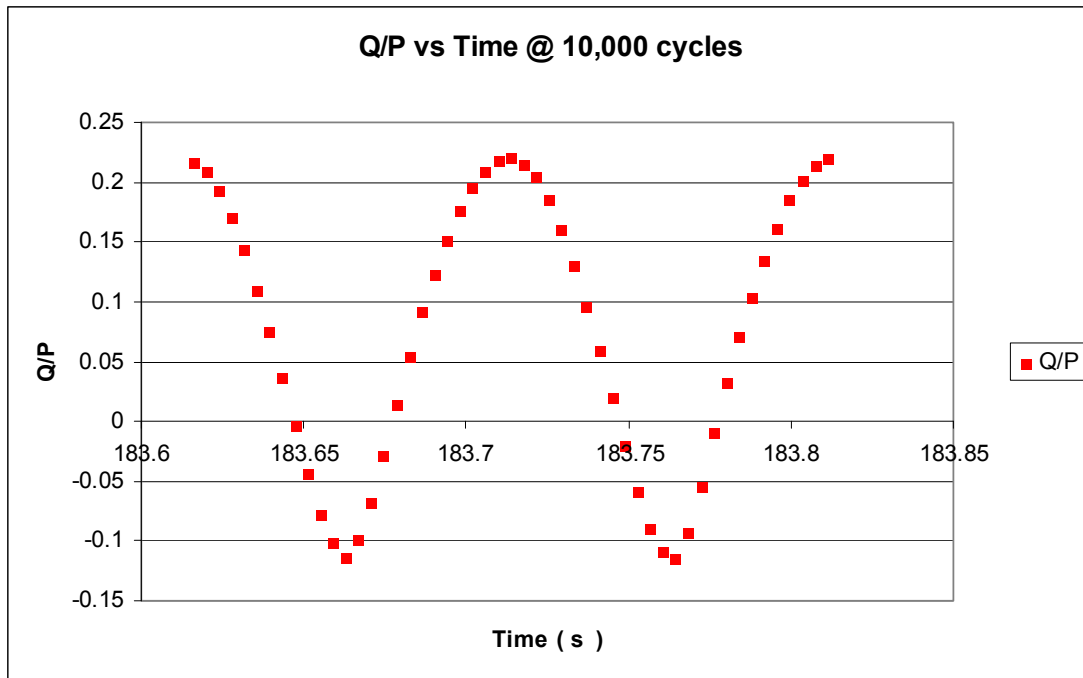
Figure 5.7 Q/P vs. Time for Test # 4 (Out-phase) at 10,000 cycles
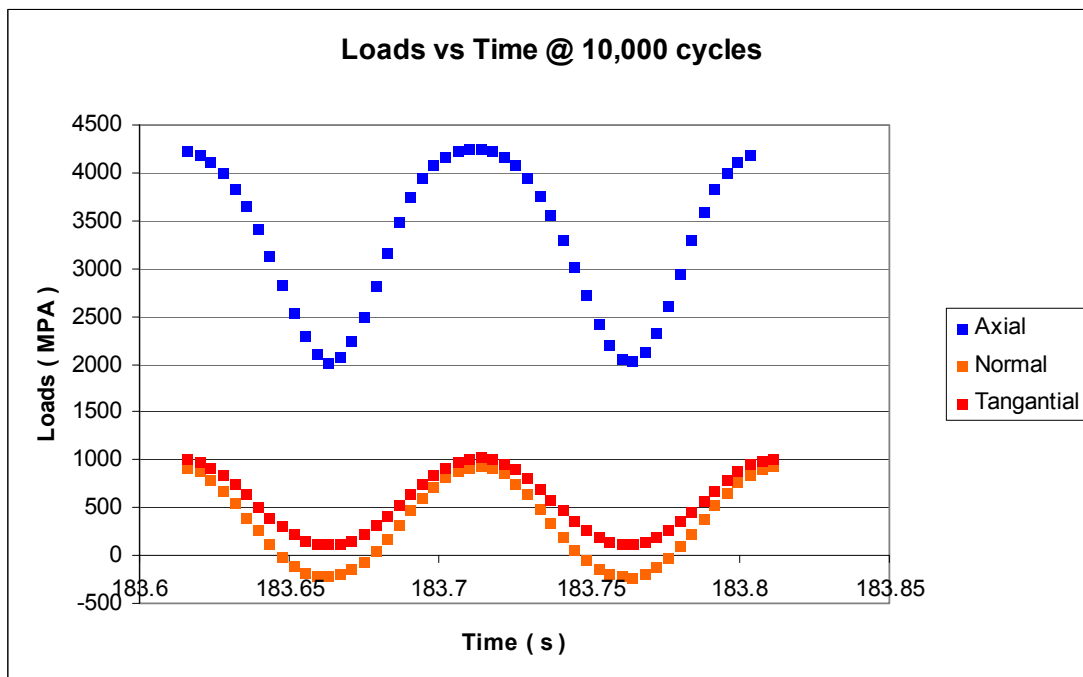
Figure 5.8 Axial Load vs. Time for Test # 4 at 10,000 Cycles, In-Phase Condition

88
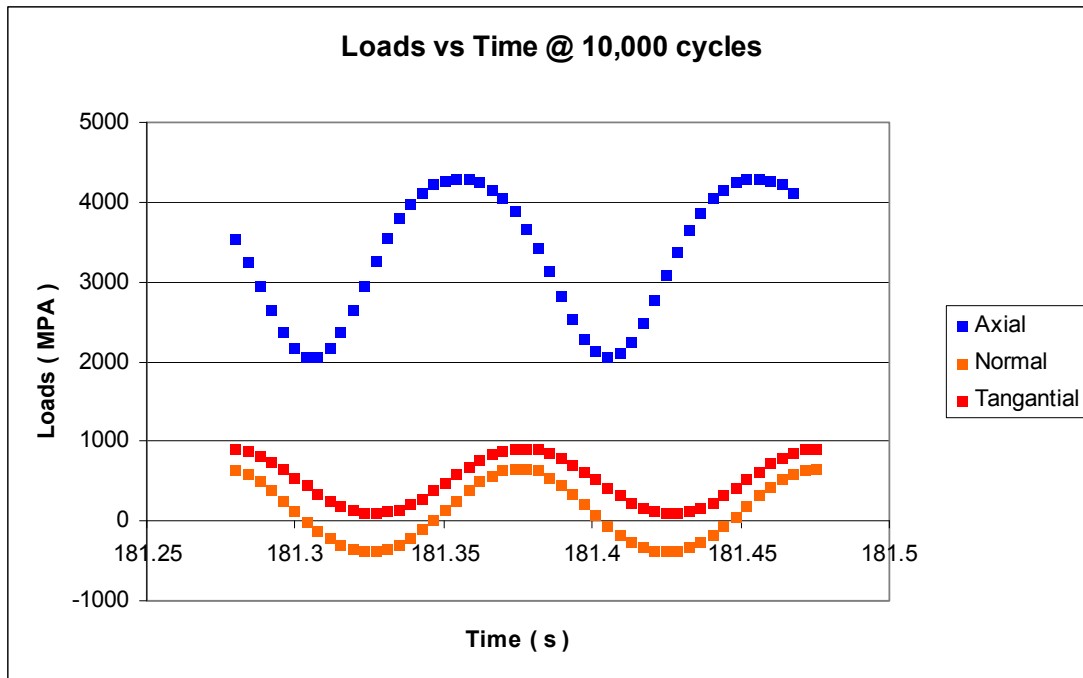
Figure 5.9 Axial Load vs. Time for Test # 9 at 10,000 Cycles, Out of Phase Condition
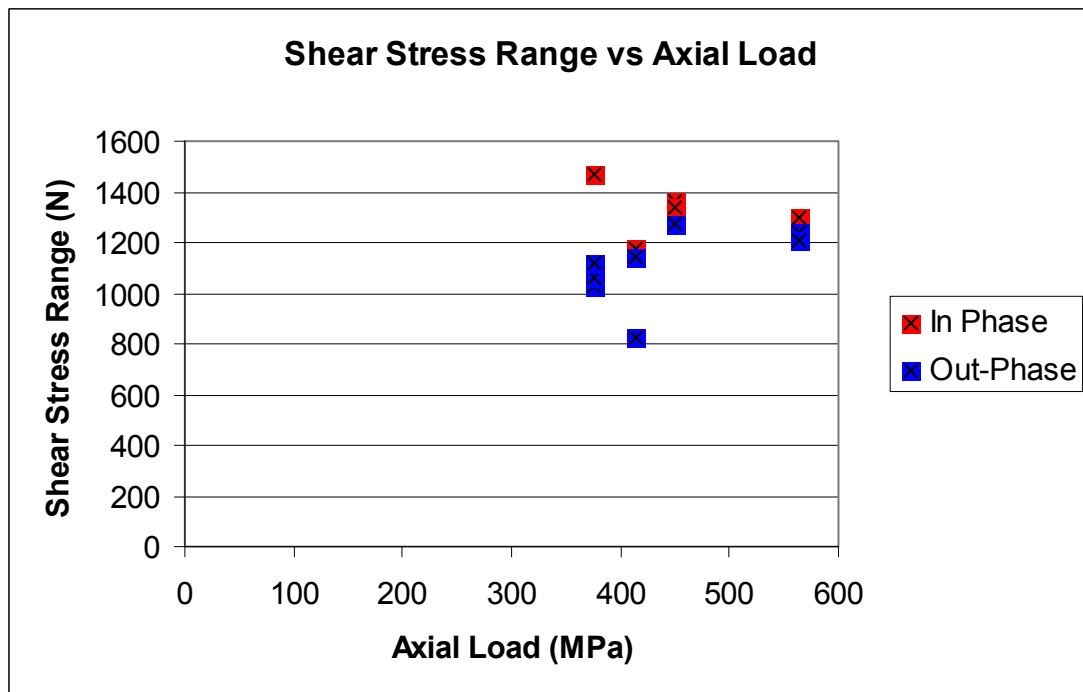
Figure 5.10 Shear Stress Range vs. Axial Load In-Phase and Out of Phase Condition
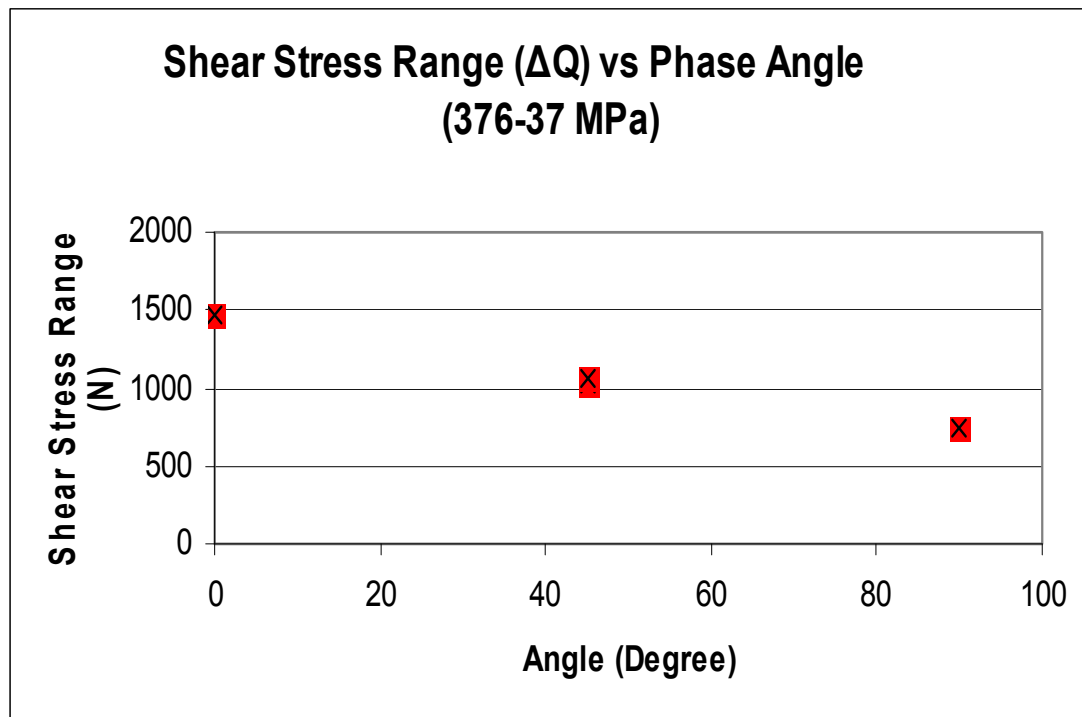
Figure 5.11 Shear Range vs. Phase Angle
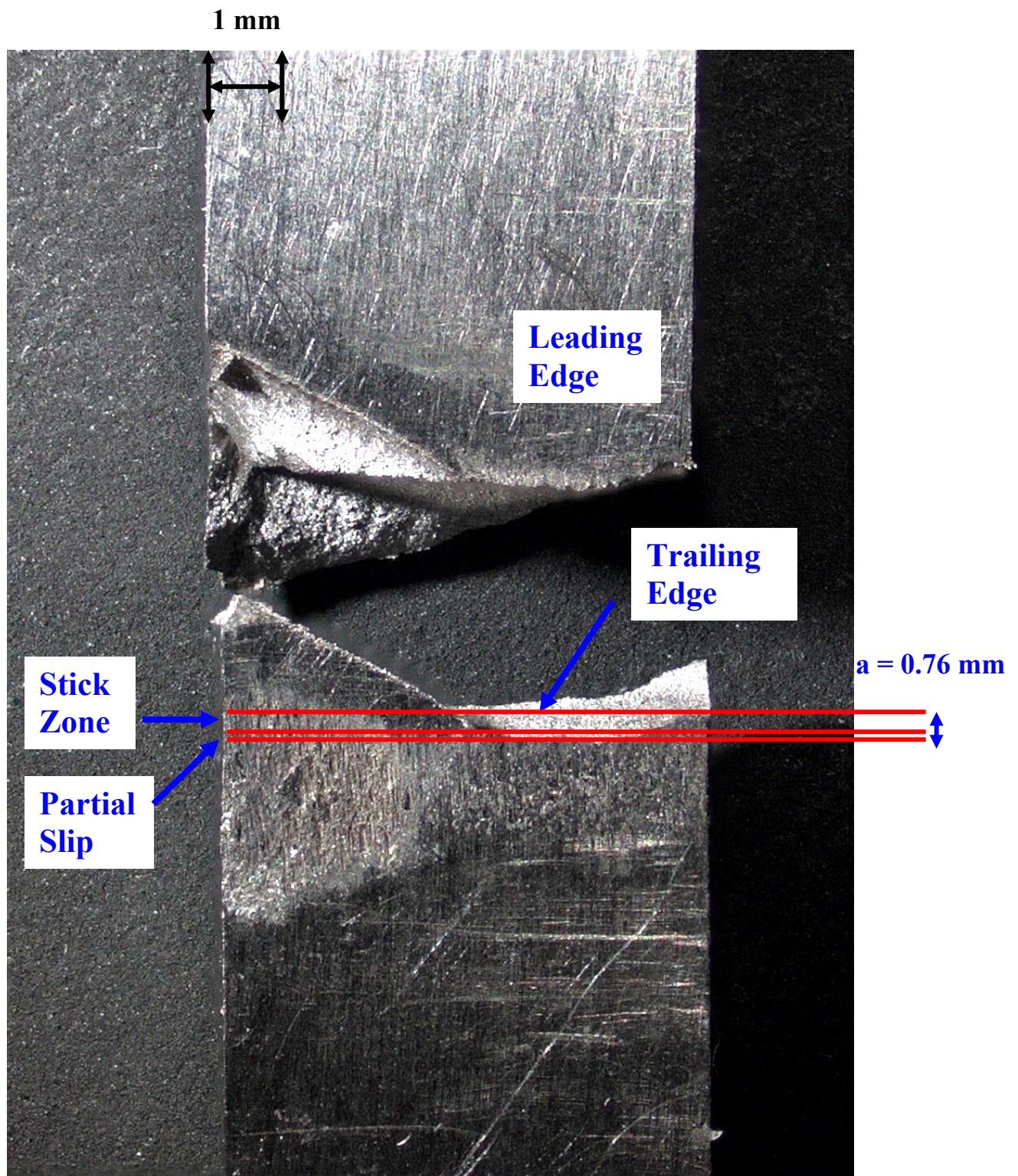
Figure 5.12 Partial Slip and Stick Zones for Test # 4
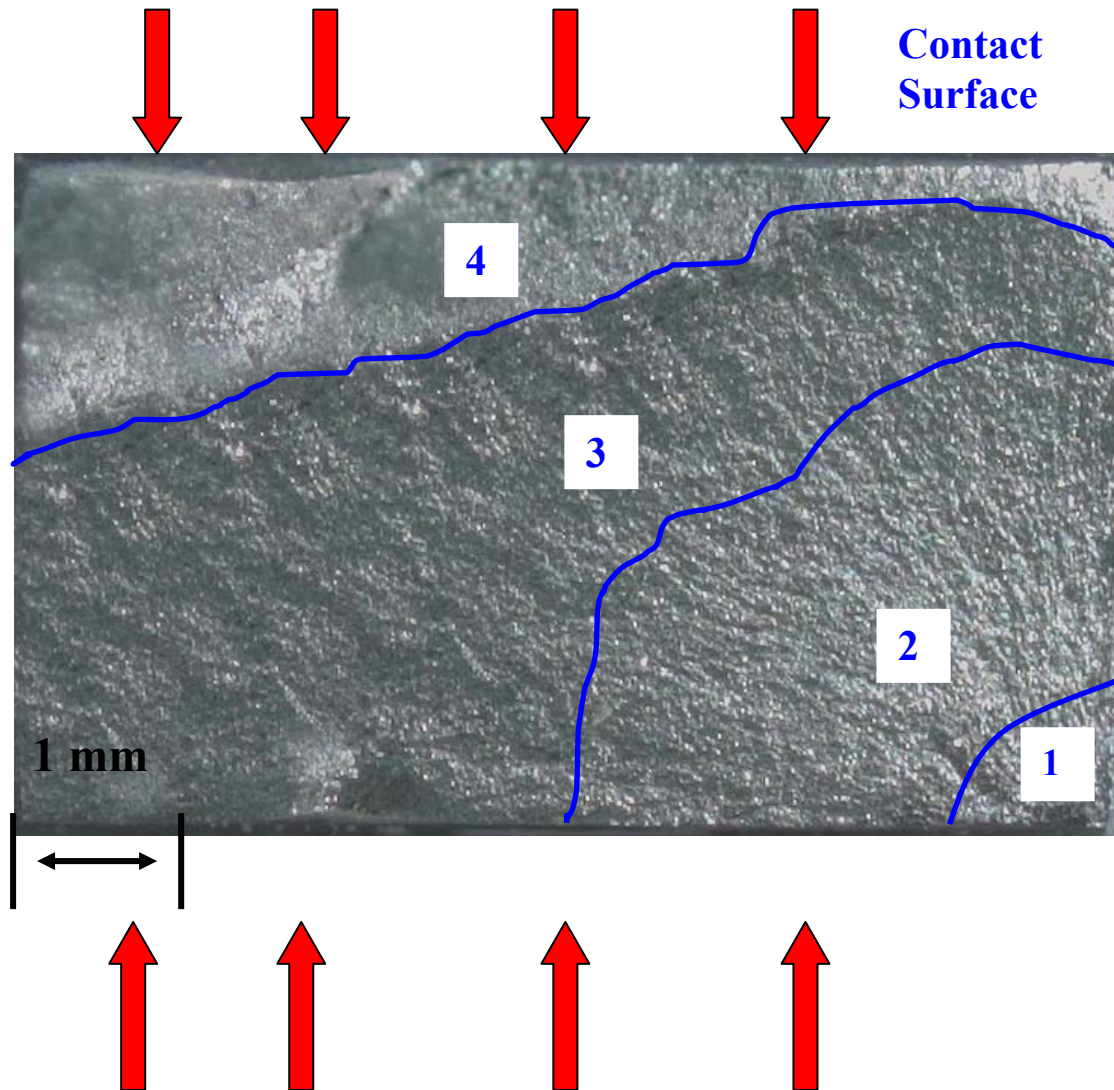
Figure 5.13 Fracture Surface Showing Four Distinguishable Regions
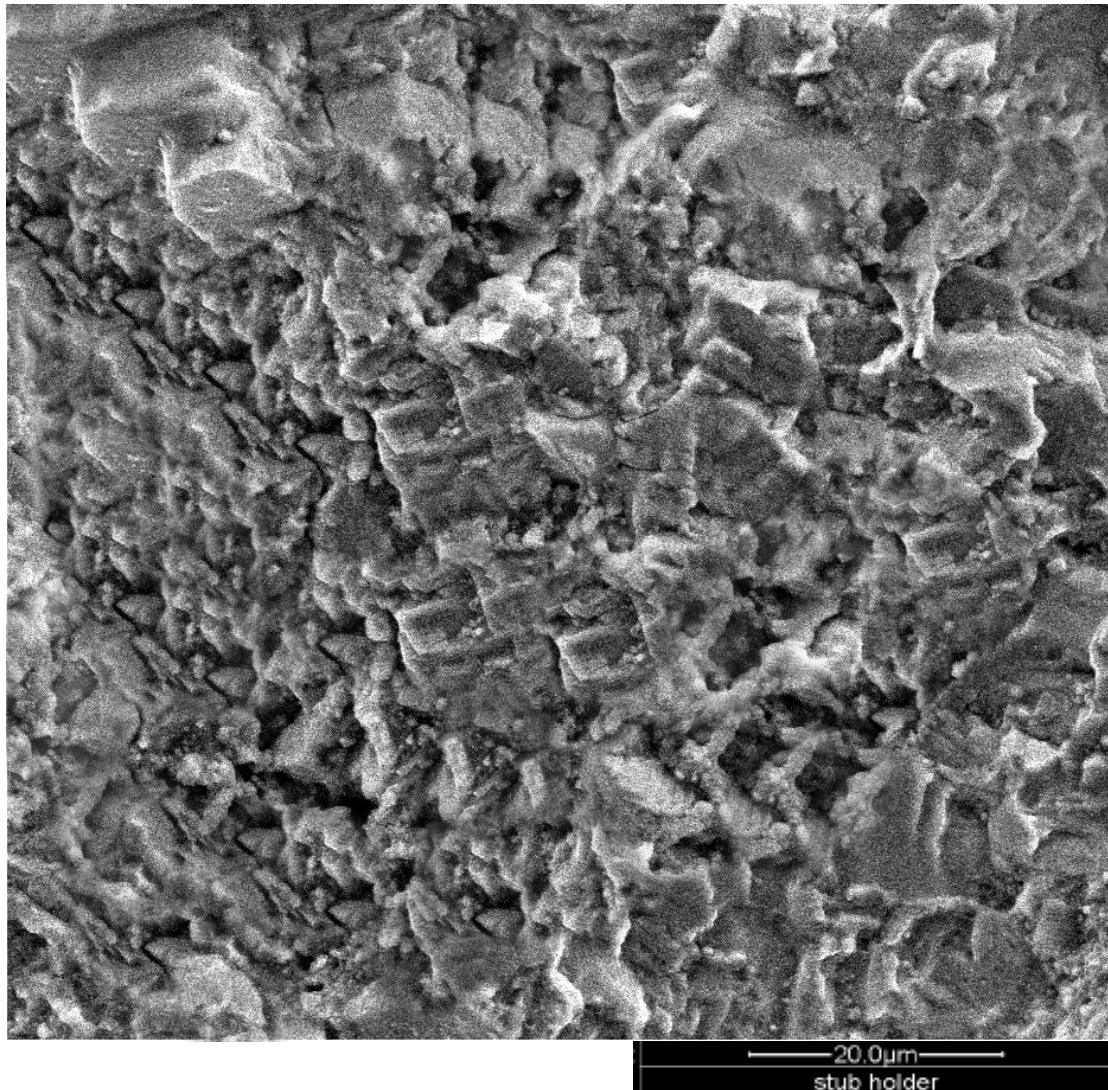
Figure 5.14 Region One Showing Debris
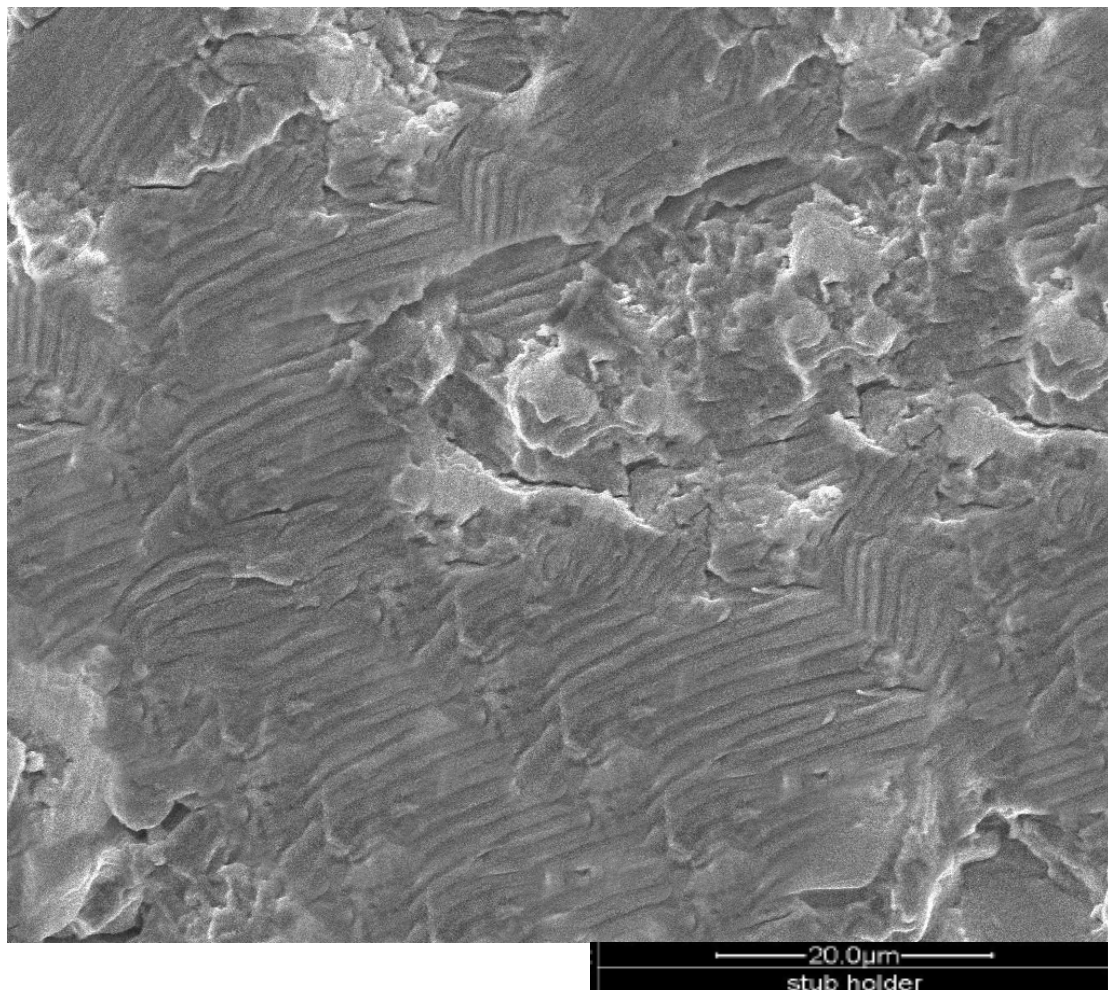
Figure 5.15 Region Two Showing Stiriations
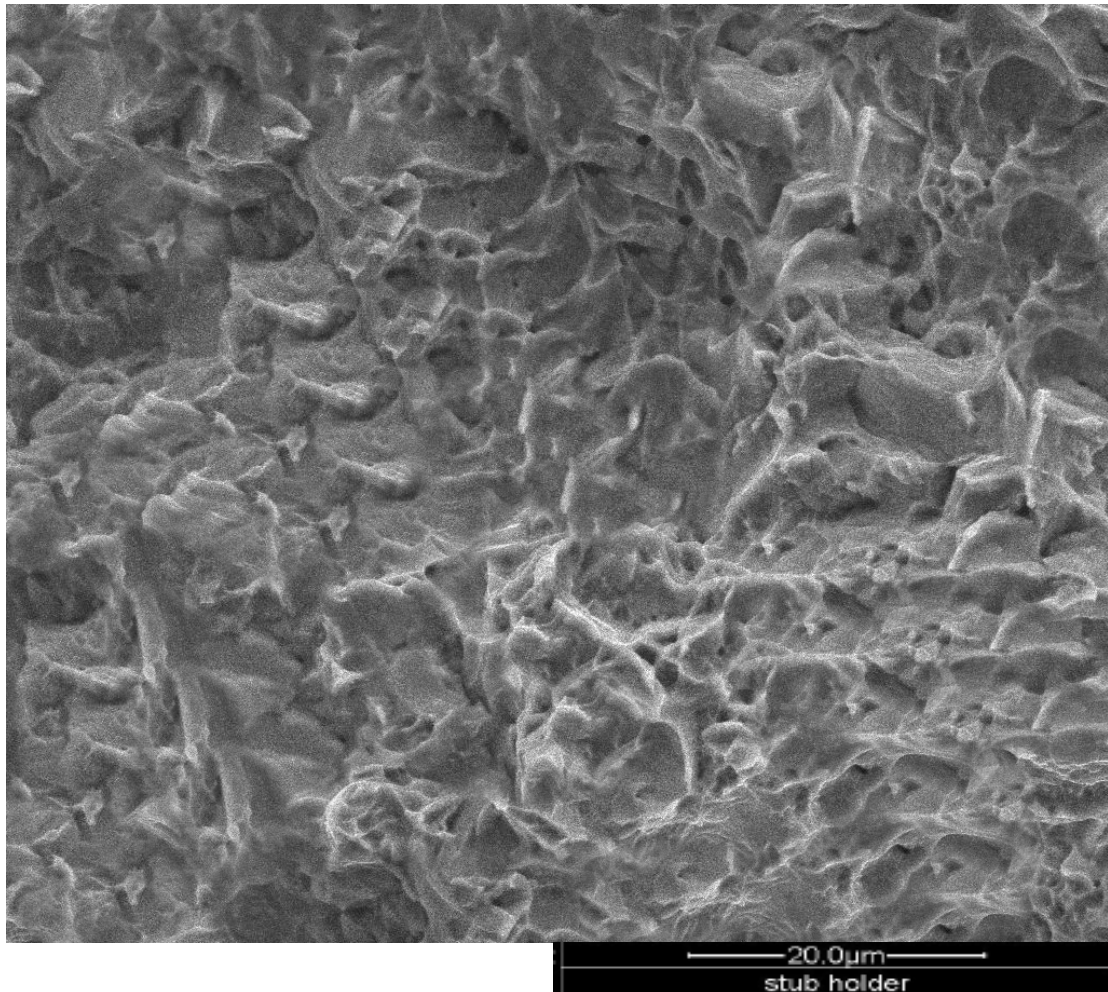
Figure 5.16 Region Three Showing Large Dimples
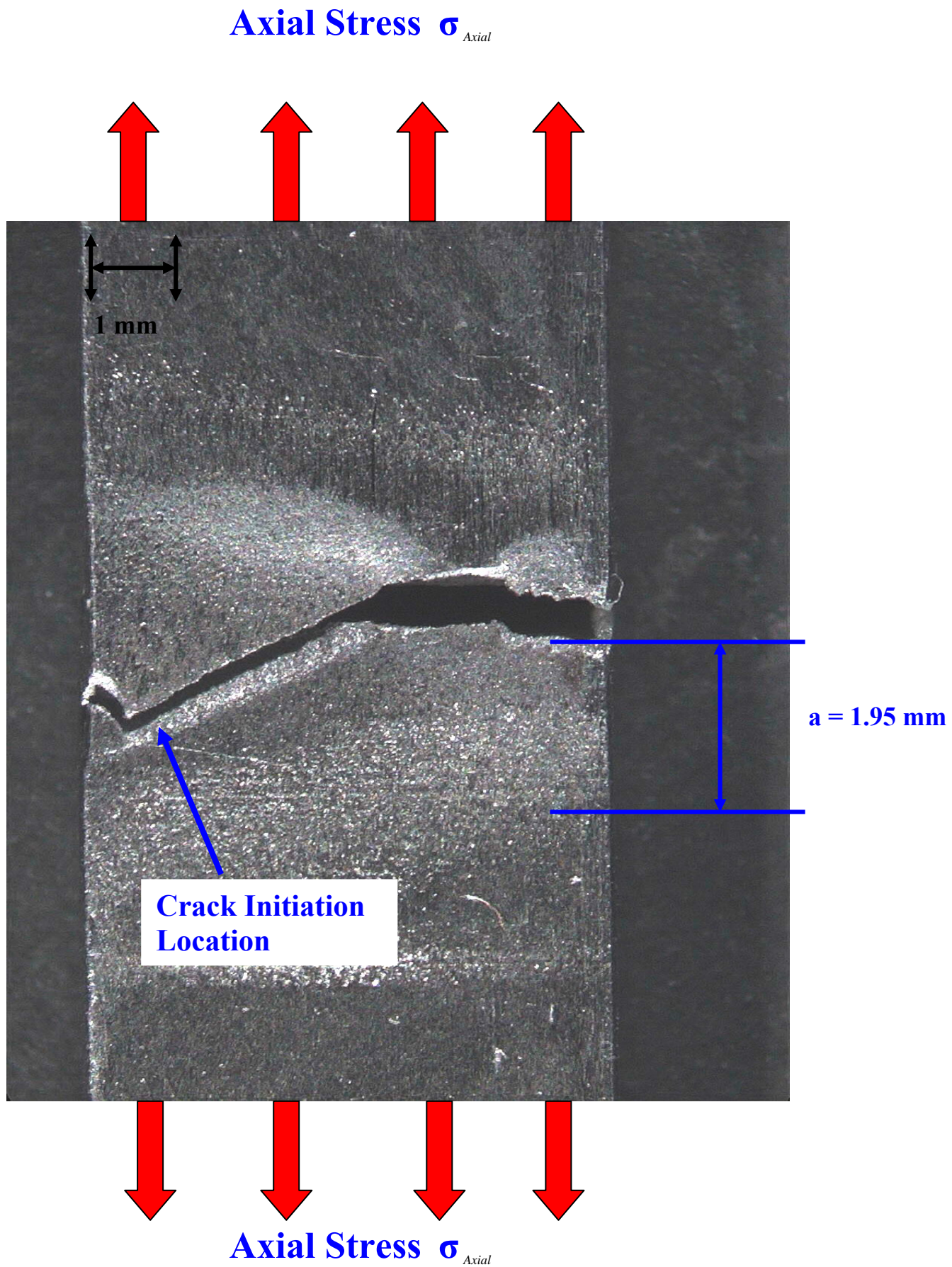
Figure 5.17 Crack Initiation Location For Test # 12
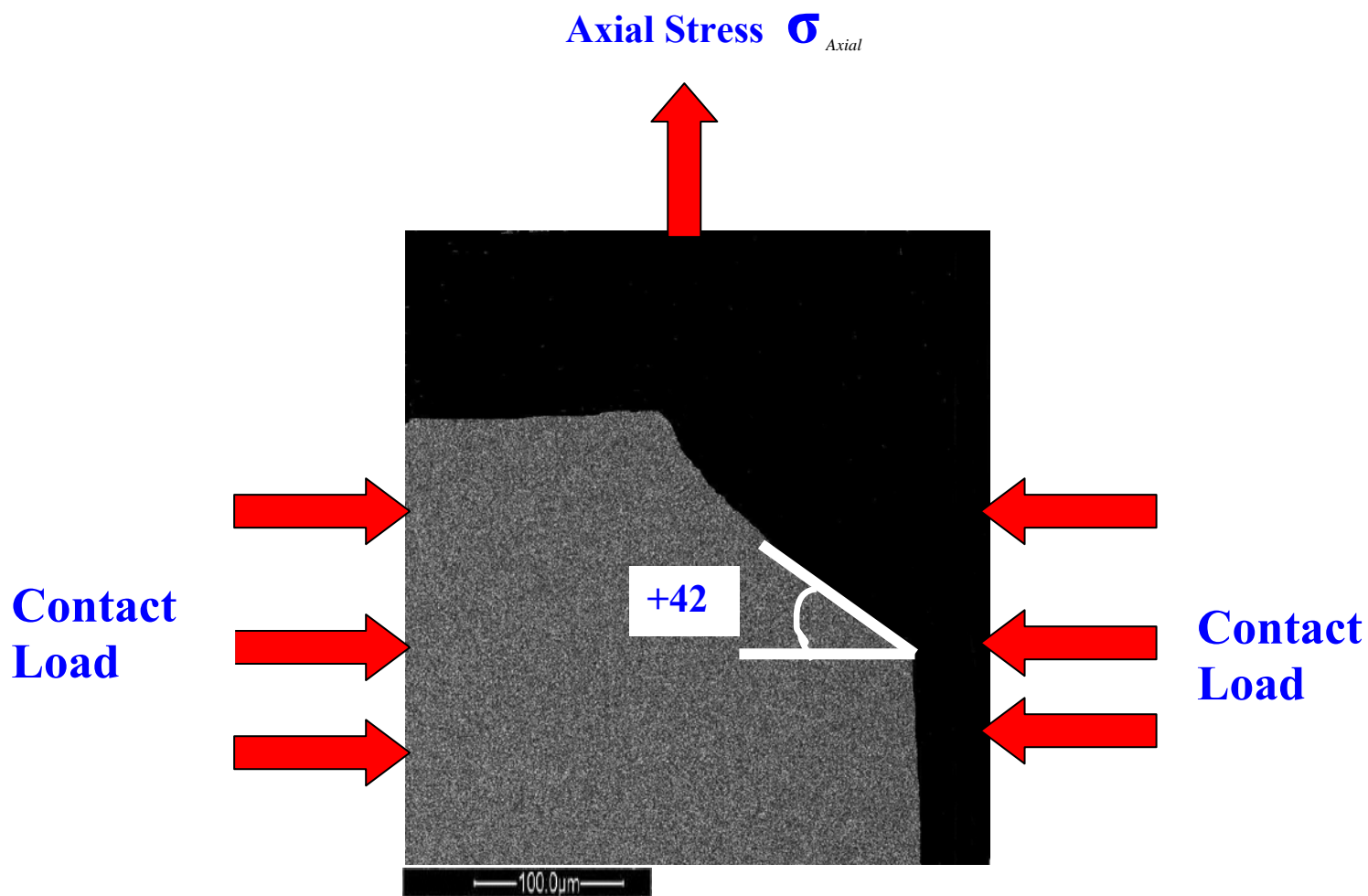
Figure 5.18 Crack Initiation Orientations for Test # 5
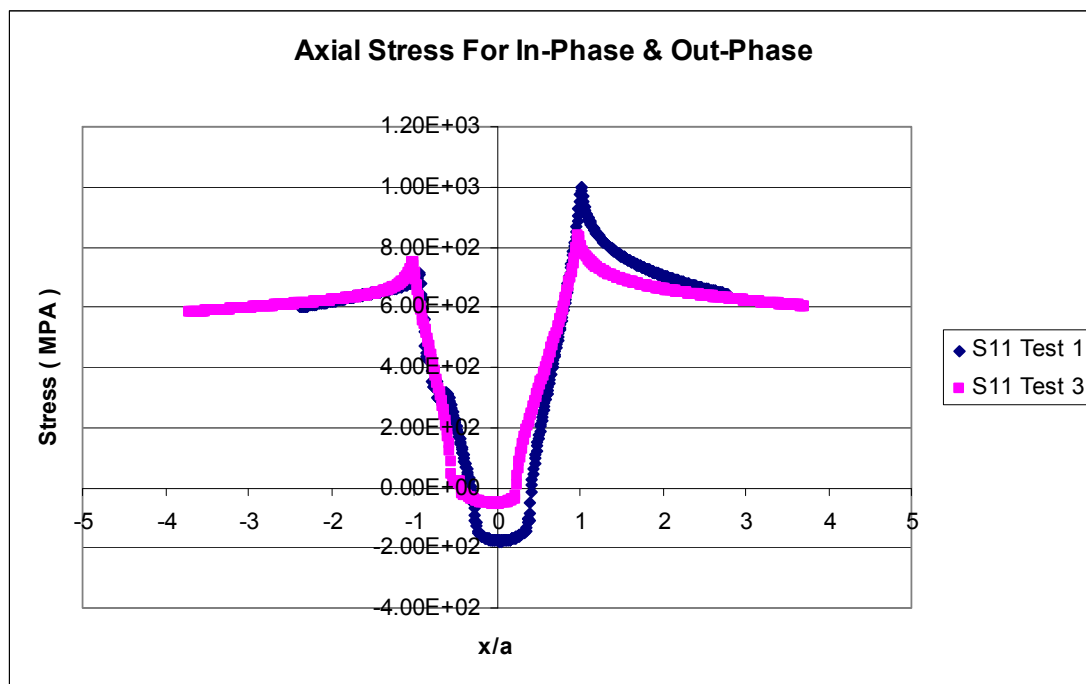
Figure 5.19 Stress Distribution of Axial Stress for Test # 1 & 3
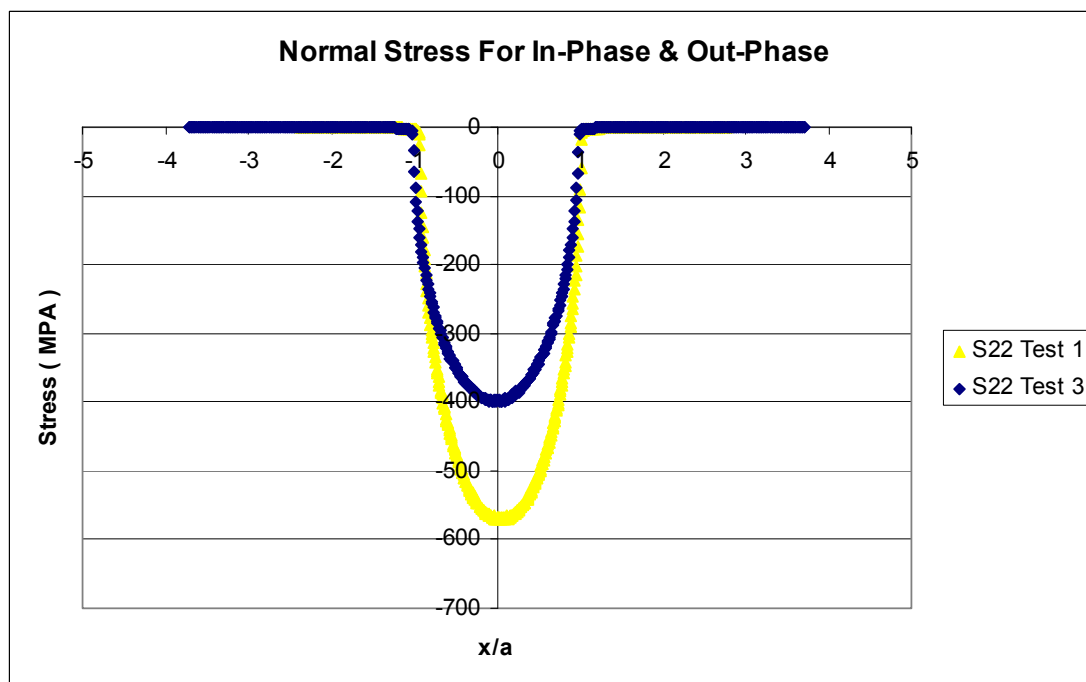
Figure 5.20 Stress Distribution of Normal Stress for Test # 1& 3
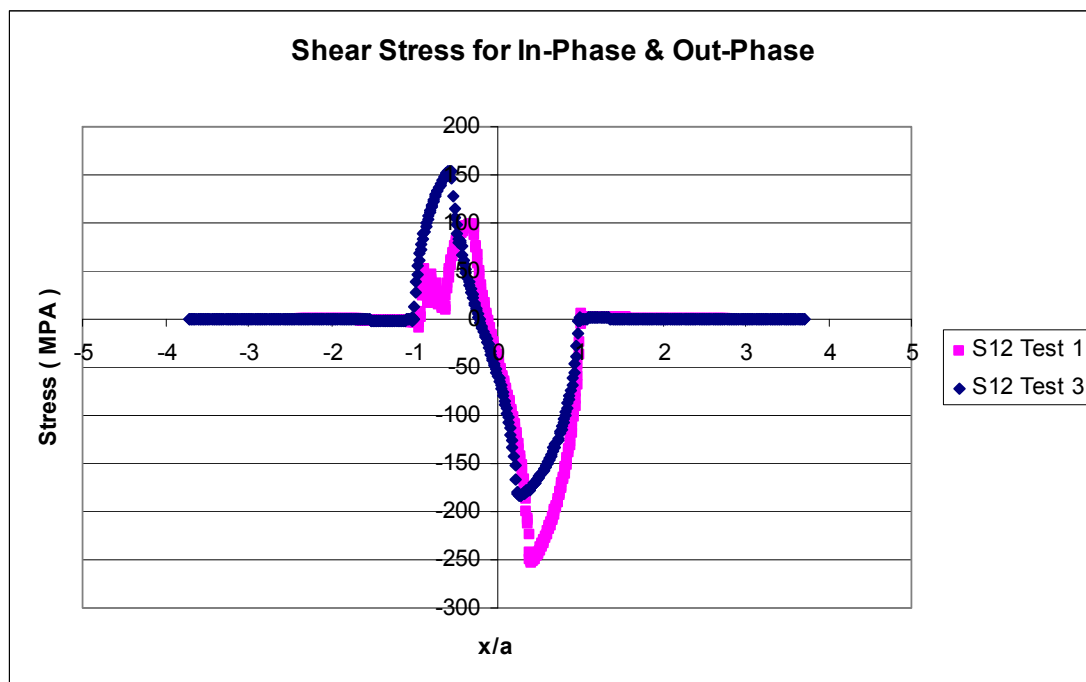
Figure 5.21 Stress Distribution of Shear Stress for Test # 1 & 3
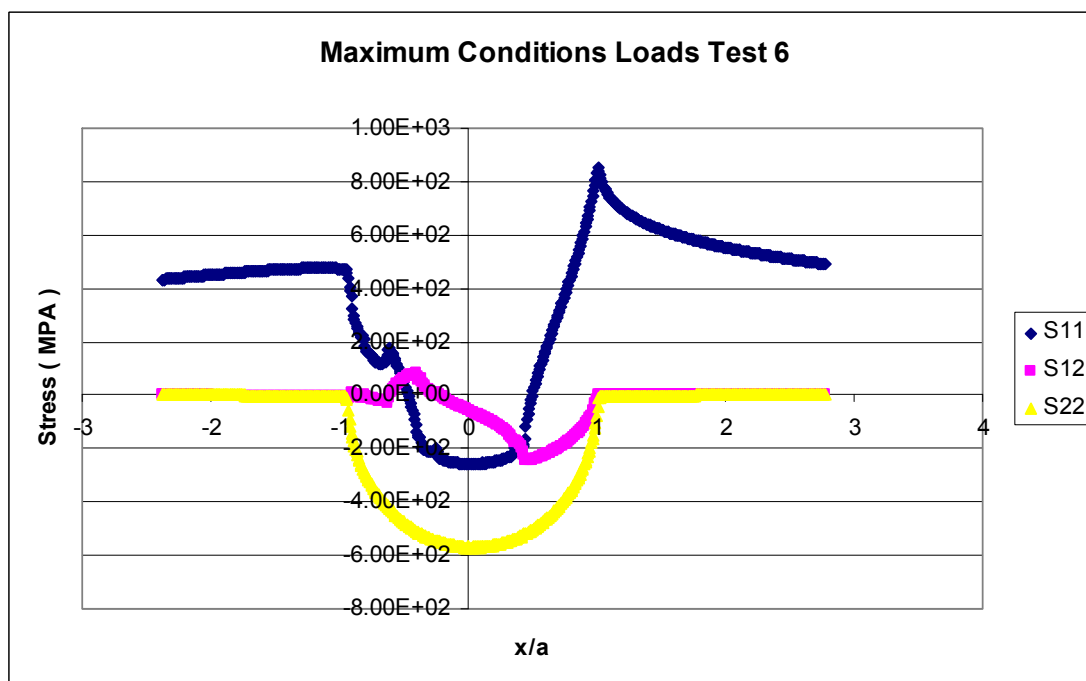
Figure 5.22 Stress Profiles at Maximum Condition for Test # 6 (Out-Phase)
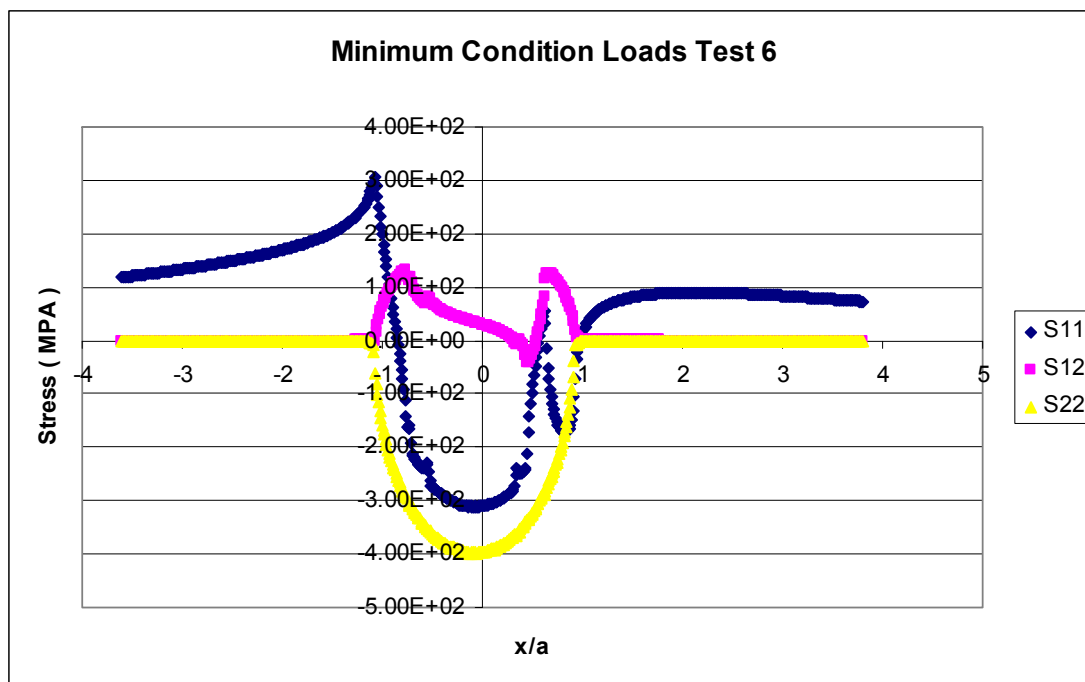
Figure 5.23 Stress Profiles at Minimum Condition for Test # 6 (Out-Phase)
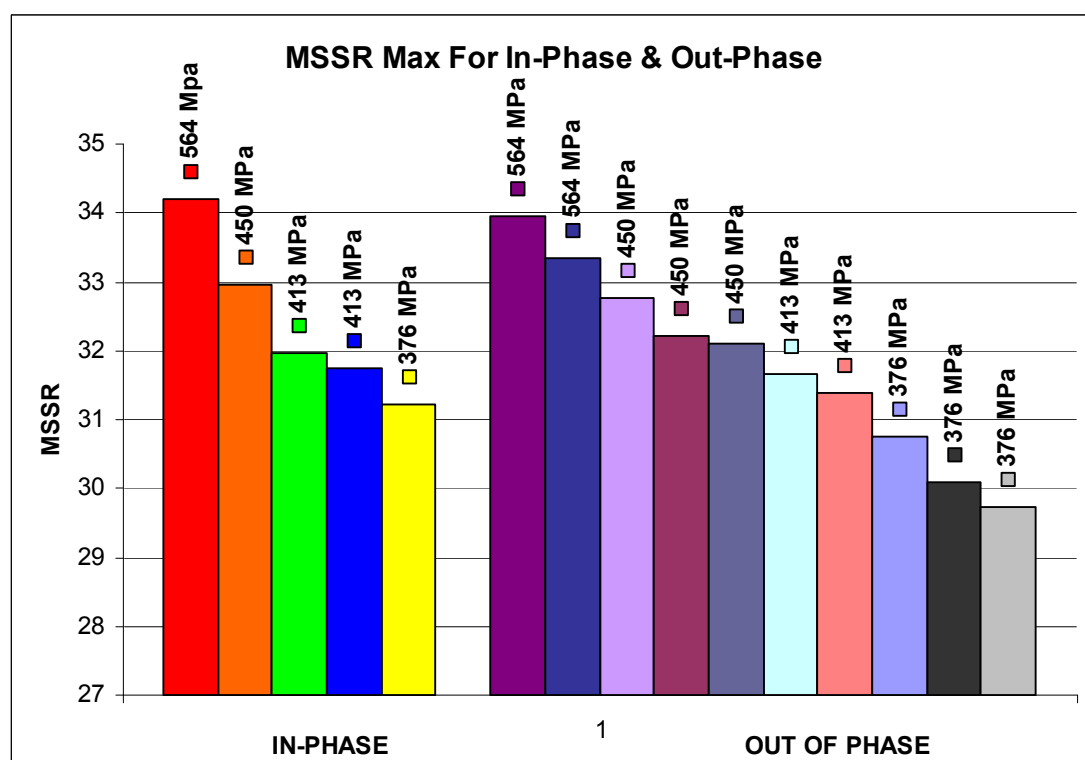
Figure 5.24 MSSR Values for In-Phase and Out of Phase Tests
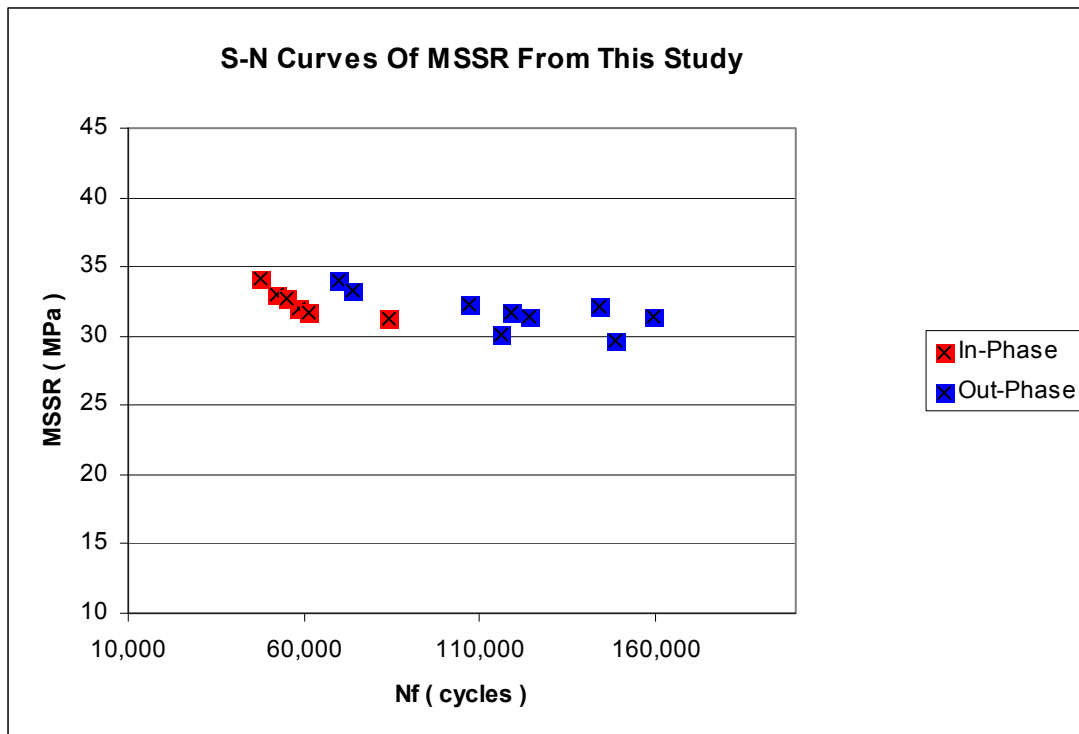
Figure 5.25 Maximum MSSR Values Vs Axial Stress for In-Phase & Out of Phase
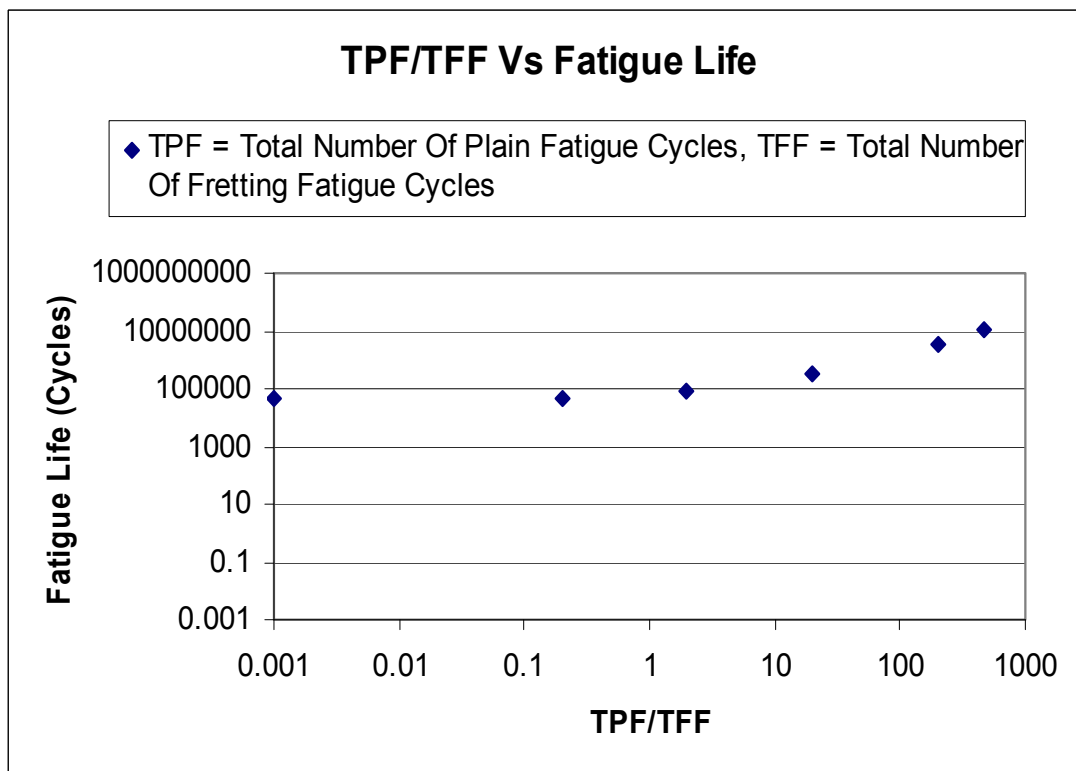
Figure 5.26 Combination of Fretting Fatigue & Plain Fatigue

101
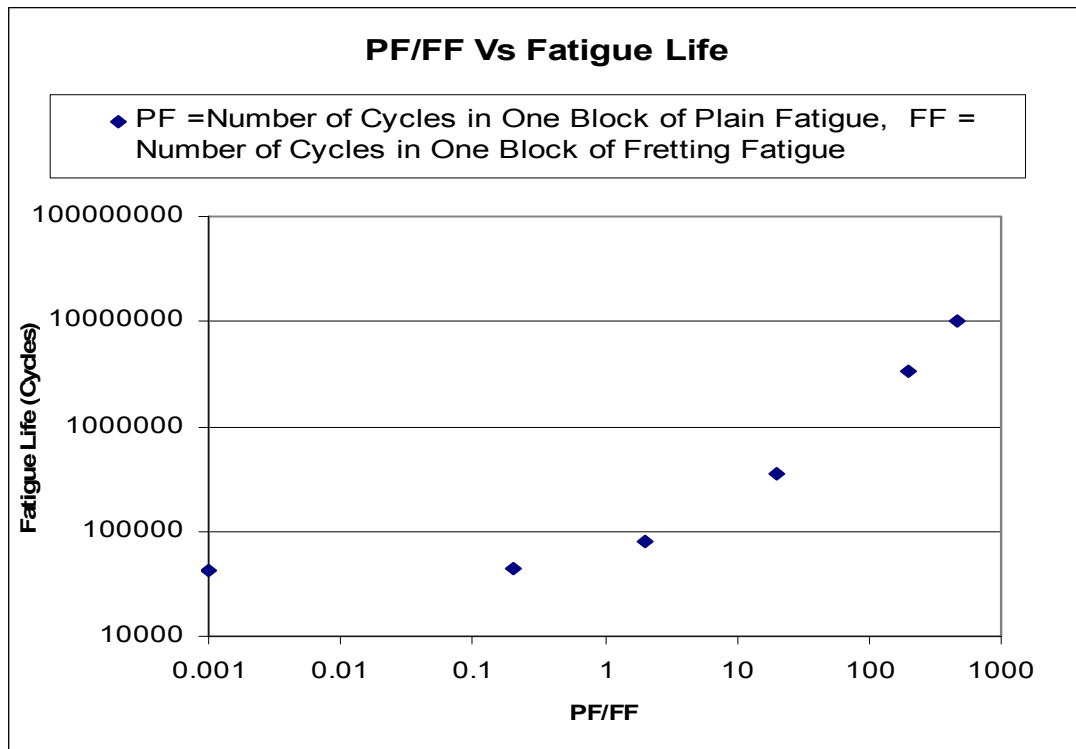
Figure 5.27 Combination of Fretting Fatigue & Plain Fatigue
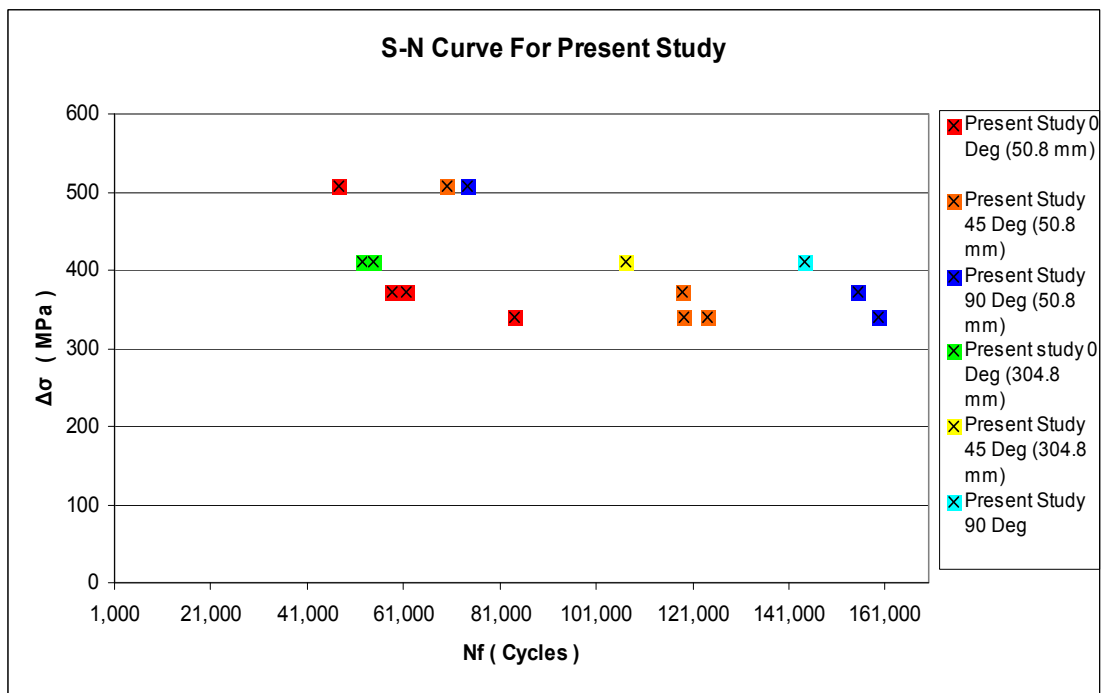
Figure 5.28 S_N Curve for Axial Stress Range for Present Study
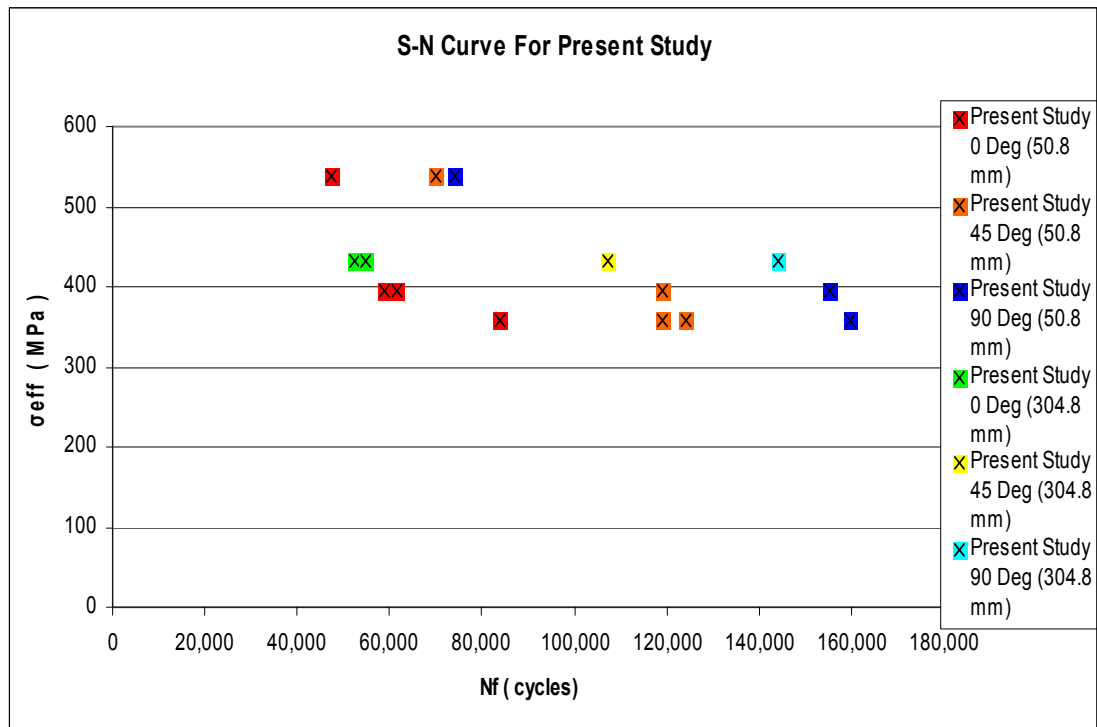
Figure 5.29 S_N Curve for Effective Stress for Present Study
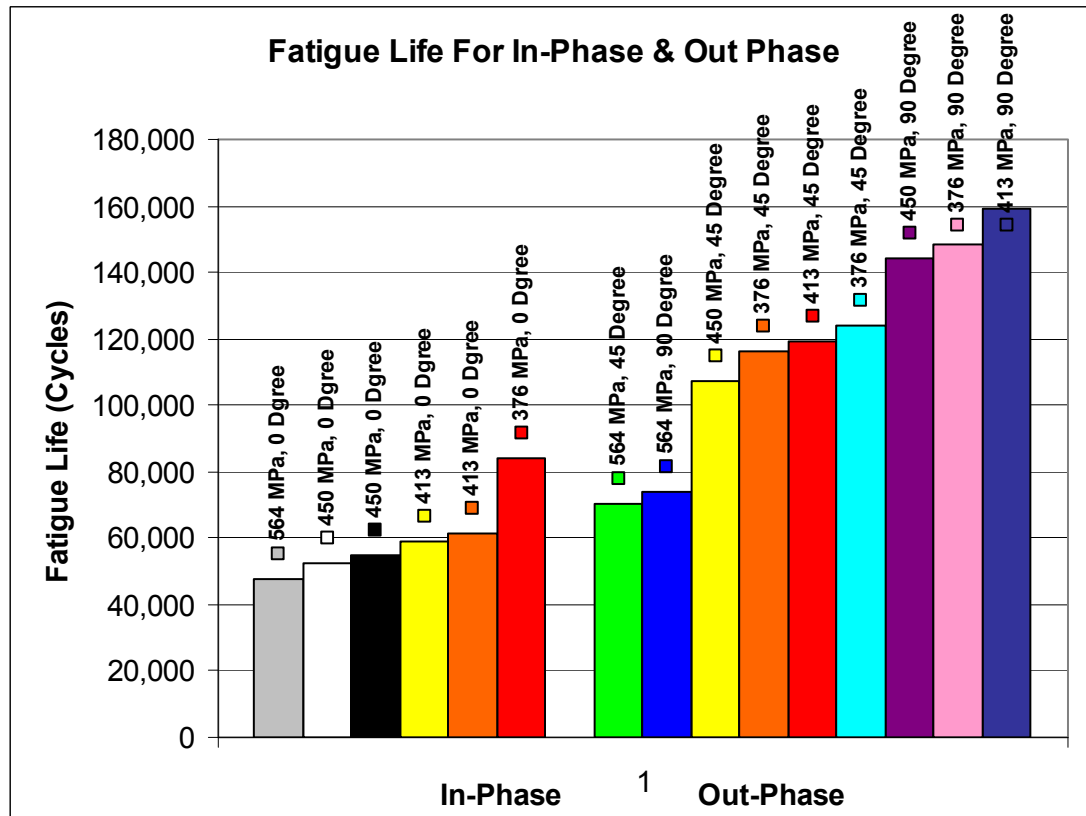
Figure 5.30 Fatigue Life for In-Phase & Out of Phase Tests

103
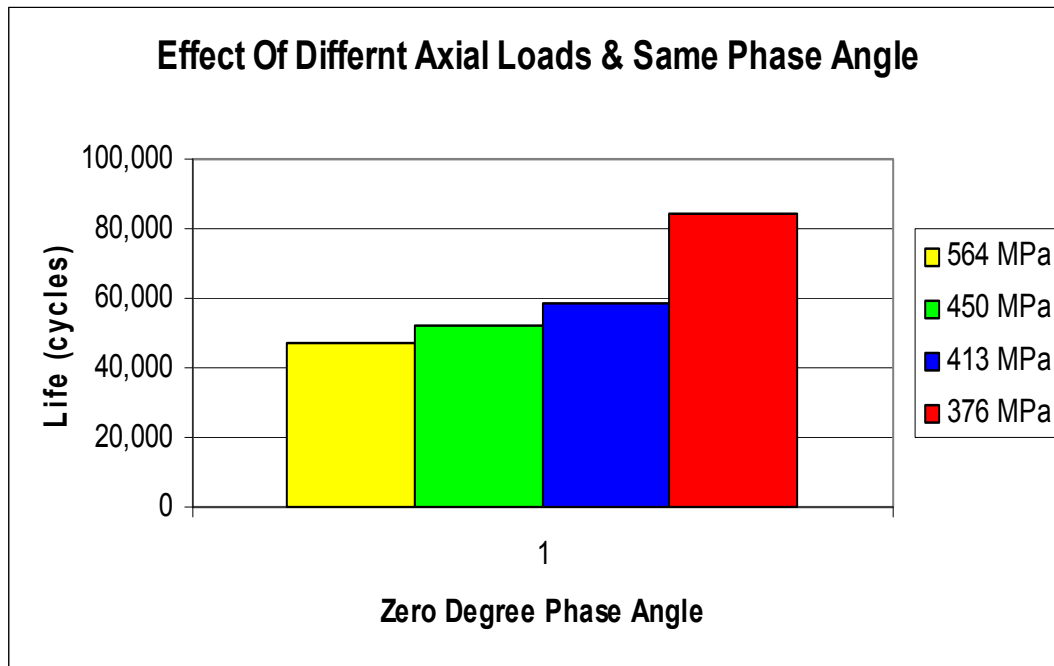
Figure 5.31 Effect of Phase Angle on Fretting Fatigue Life (Same Applied Axial Load)
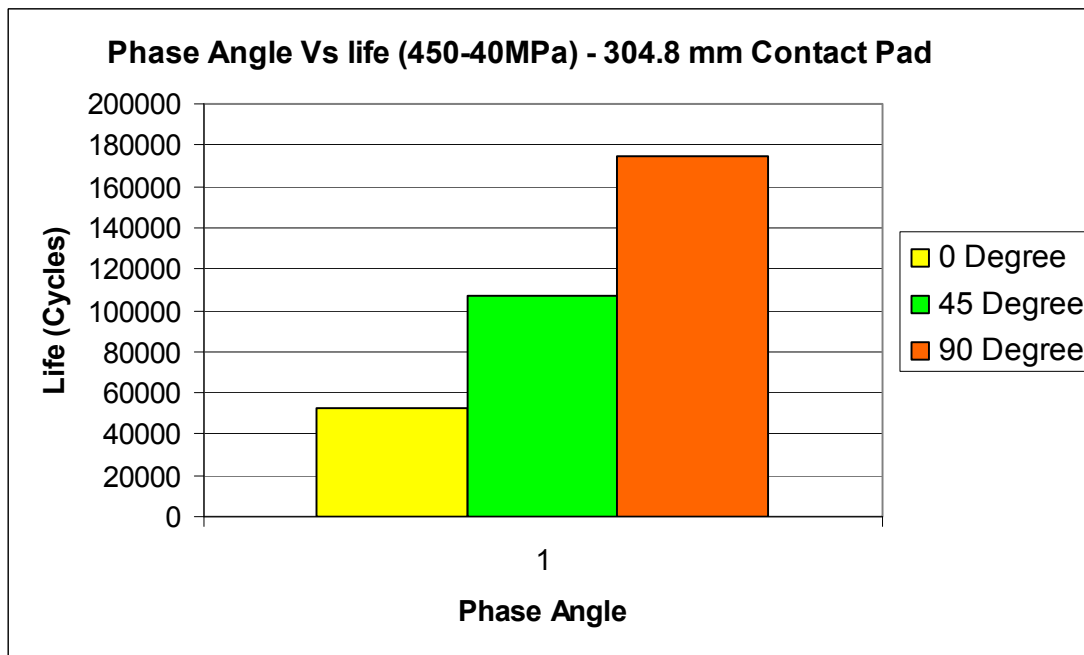
Figure 5.32 Effect of Phase Angle on Fretting Fatigue Life (Same Applied Axial Load)
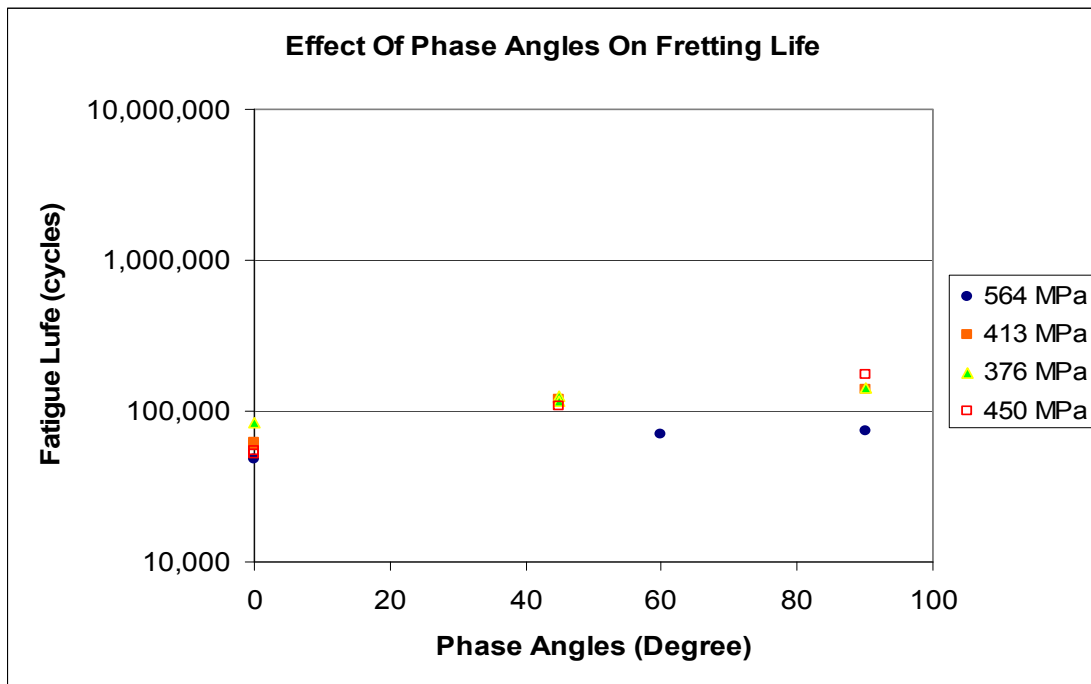
Figure 5.33 Effect of Phase Angle on Fretting Fatigue Life (Different Applied Axial Loads)
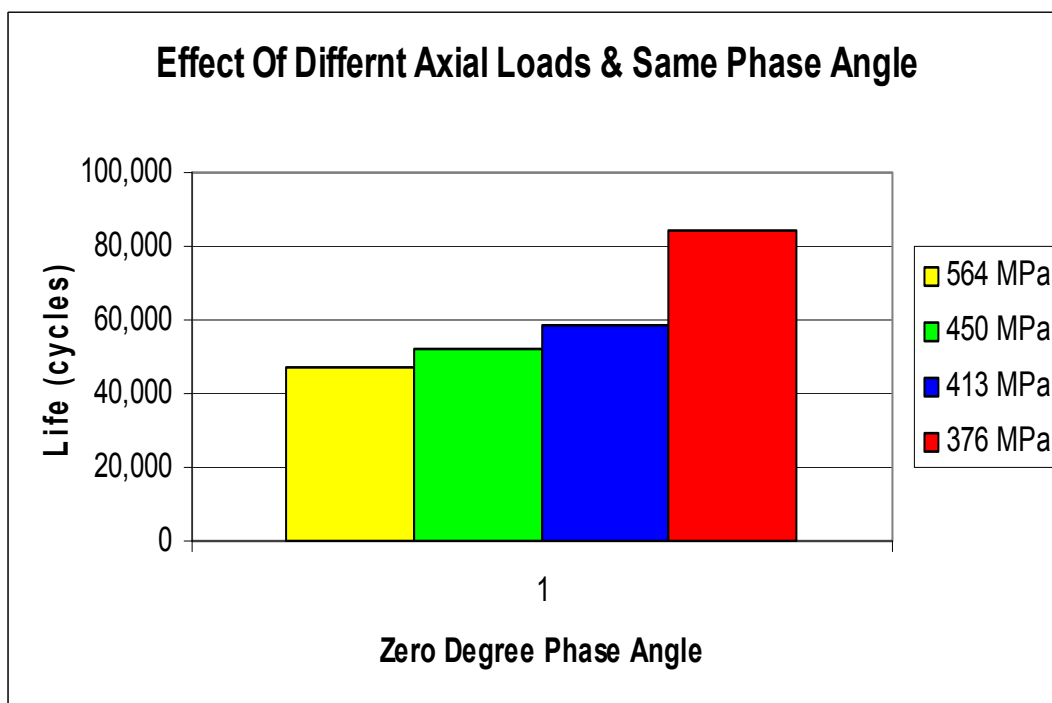
Figure 5.34 Effect of Different Axial Load (Same Phase - Angle 0 Degree)
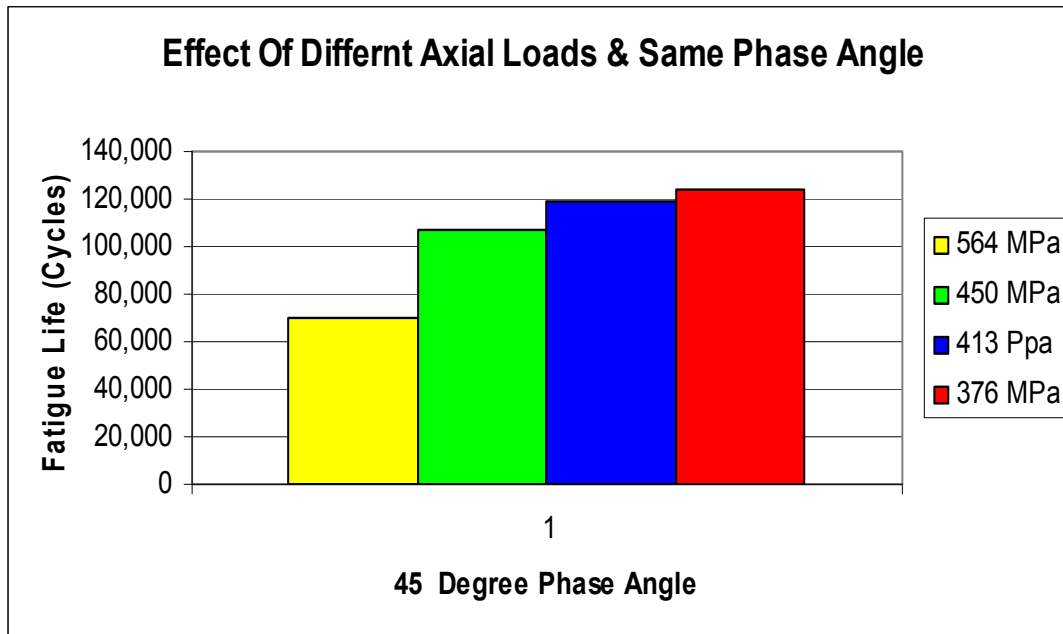
Figure 5.35 Effect of Different Axial Load (Same Phase - Angle 45 Degree)
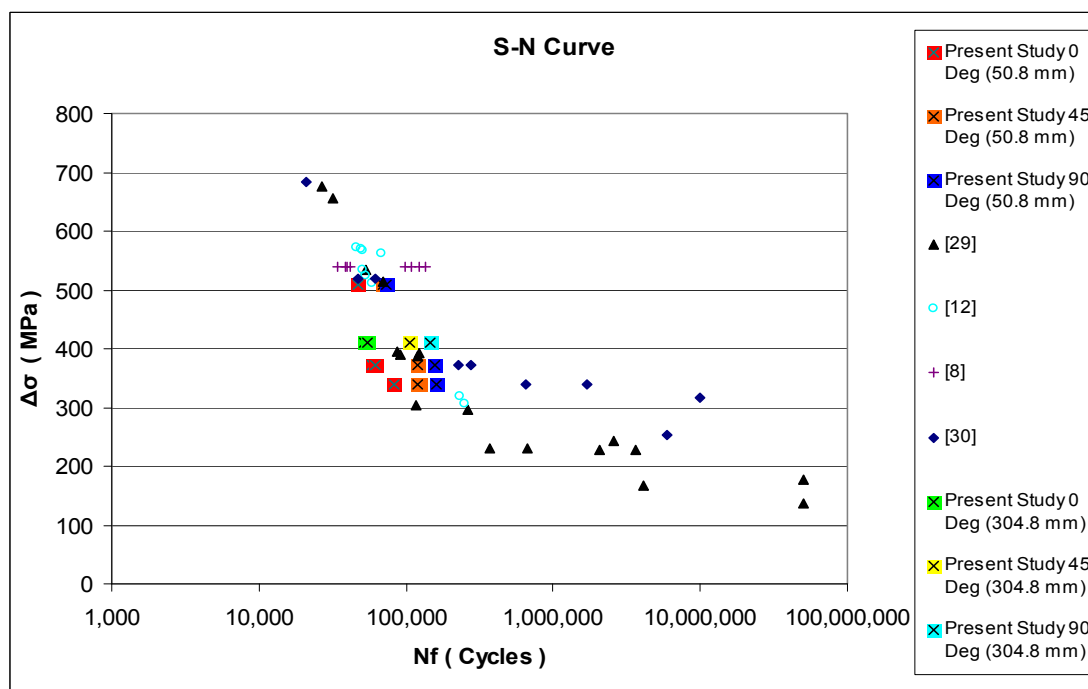
Figure 5.36 S_N Curve of Axial Stress Range from Present Study & Previous

Studies

106
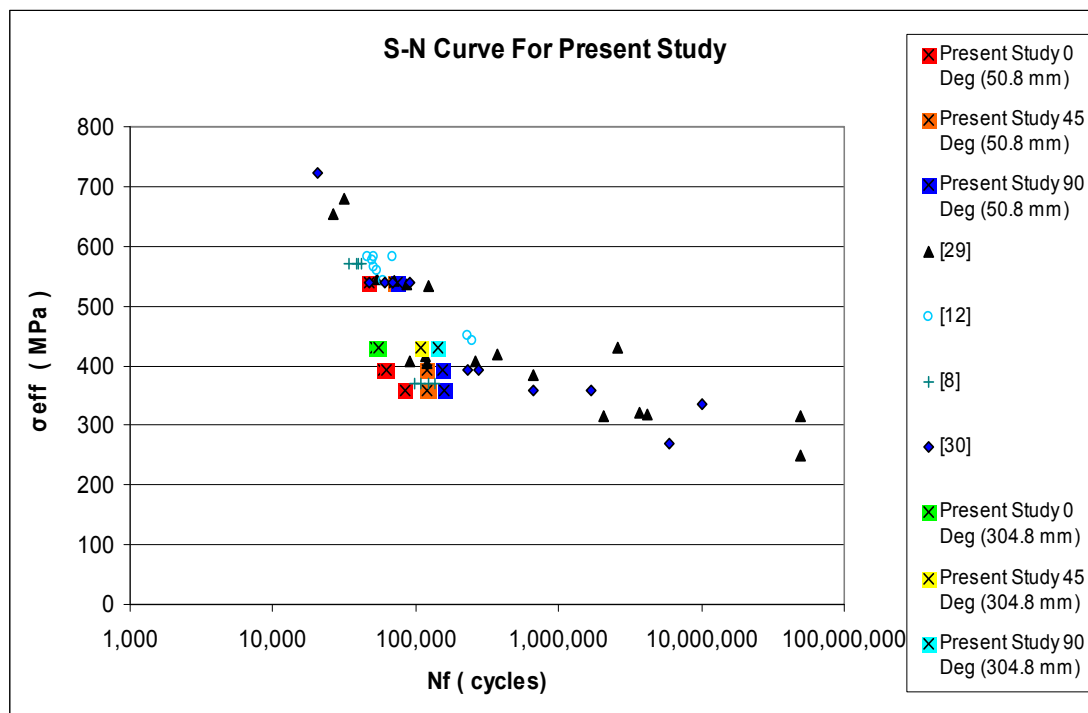
Figure 5.37 S_N Curve of Effective Stress from Present Study & Previous Studies
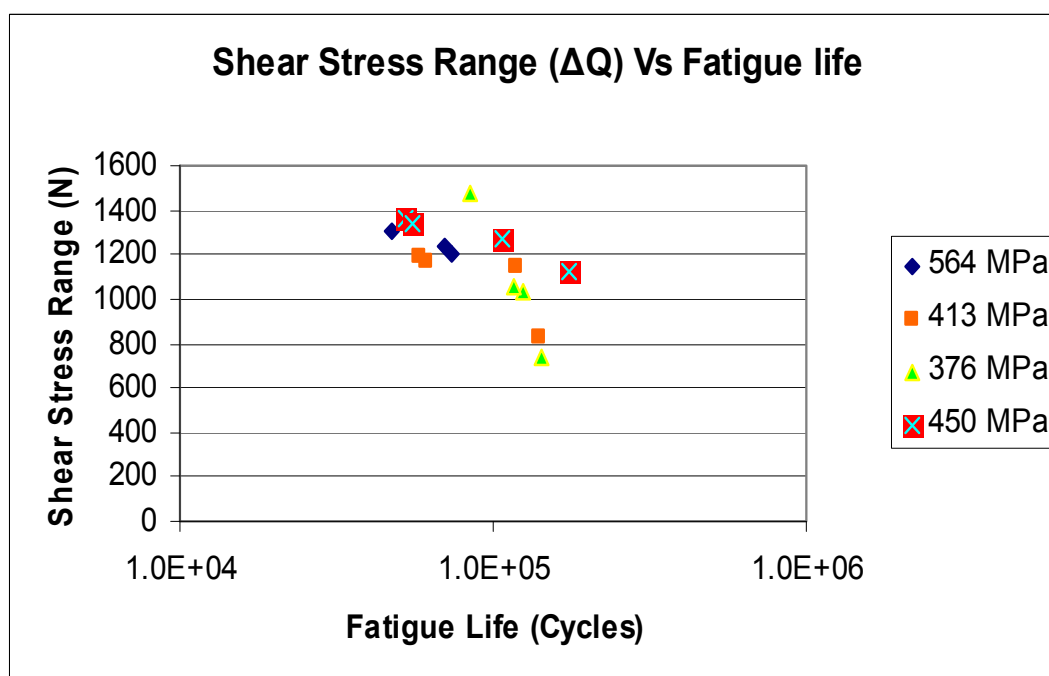
Figure 5.38 Effect of Shear Stress Range on Fatigue Life
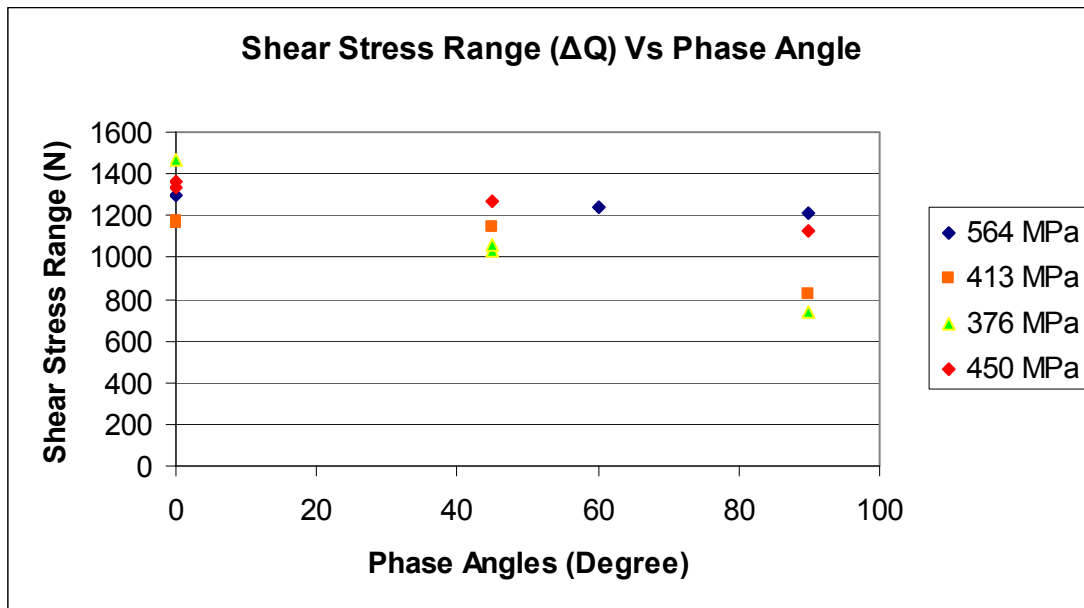
Figure 5.39 Effect of Phase Angles on Shear Stress Range
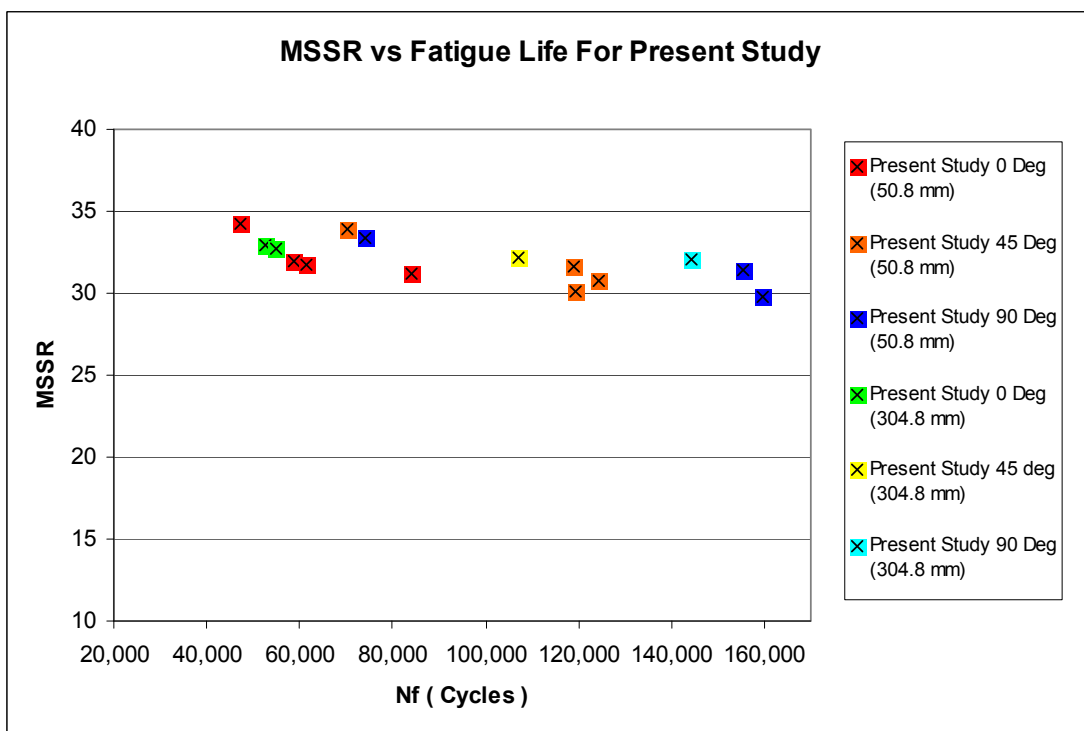
Figure 5.40 S_N Curve of MSSR from Present Study

108
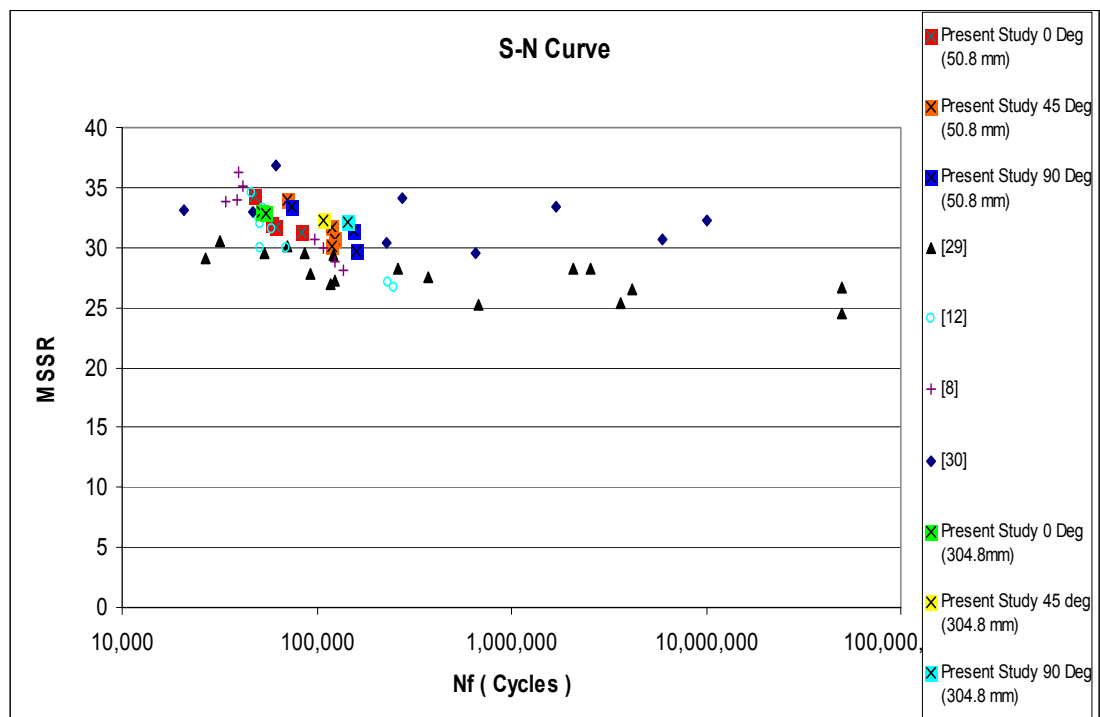
Figure 5.41 S_N Curve for MSSR Values from Present Study & Previous Studies

Table 5.1 Test Inputs & Results

Test	σ_{max} (MPa)	σ_{min} (MPa)	$\Delta\sigma$ (MPa)	P_{max} (N)	P_{min} (N)	θ deg	Q_{max} (N)	Q_{min} (N)	Q/P Max	N_f (Cycle)
1	564	56	508	4,448	2,224	0	410	-890	0.3733	47,421
2	564	56	508	4,448	2,224	45	819	-413	0.3211	70,118
3	564	56	508	4,448	2,224	90	611	-597	0.3034	74,168
4	413	41	372	4,448	2,224	0	934.1	-229.7	0.2223	58,574
5	413	41	372	4,448	2,224	0	939	-235	0.2234	61,578
6	413	41	372	4,448	2,224	45	754	-390	0.2052	118,960
7	413	41	372	4,448	2,224	90	110	-715	0.1655	159,422
8	376	37	339	4,448	2,224	0	1189	-283	0.1762	83,989
9	376	37	339	4,448	2,224	45	648	-383	0.142	124,238
10	376	37	339	4,448	2,224	45	680	-380	0.1345	116,238
11	376	37	339	4,448	2,224	90	58.3	-682.3	0.1107	158,555
12	450	40	410	4,448	2,224	0	1168	-198	0.3420	52,422
13	450	40	410	4,448	2,224	0	1086	-250	0.3411	54,889
14	450	40	410	4,448	2,224	45	1049	-221	0.2312	107,214
15	450	40	410	4,448	2,224	90	858	-264	0.2221	144,303
16	564	56	508	3,336	3,336	-	-	-	-	44,656
17	564	56	508	3,336	3,336	-	-	-	-	350,397

Table 5.2 Q/P Values Versus Different Phase Angles

Test Number	θ (deg)	Q/P (Max)
1	0	0.3733
2	45	0.3211
3	90	0.3034
4	0	0.2223
5	0	0.2234
6	45	0.2052
7	90	0.1655
8	0	0.1762
9	45	0.142
10	45	0.1345
11	90	0.1107
12	0	0.342
13	0	0.3411
14	45	0.2312
15	90	0.2221
16	-	-
17	-	-

Table 5.3 Contact Half-Width Values from Experimental Observations for Present Study

Test #	$\Delta\sigma_{axial}$ (MPA)	P_{max} (N)	P_{min} (N)	$a_{Experimental}$ mm	$A_{Theoretical}$ Mm
1	684	4448	2224	0.75	0.8055
2	518	4448	2224	0.78	0.8055
3	518	4448	2224	0.8	0.8055
4	372	4448	2224	0.76	0.8055
5	372	4448	2224	0.79	0.8055
6	339	4448	2224	0.82	0.8055
7	339	4448	2224	0.75	0.85
8	254	4448	2224	0.81	0.8055
9	518	4448	2224	0.76	0.8055
10	518	4448	2224	0.79	0.8055
11	518	4448	2224	0.77	0.8055
12	518	4448	2224	1.95	1.9609
13	518	4448	2224	1.92	1.9609
14	518	4448	2224	1.95	1.9609
15	316	4448	2224	1.94	1.9609
16	316	3336	3336	0.75	0.8055
17	316	3336	3336	0.78	0.8055

Table 5.4 MSSR Calculation from Present Study

Test	σ_{max} (MPa)	σ_{min} (MPa)	P_{max} (N)	P_{min} (N)	P_{Freq} (Hz)	N_f (Cycles)	$MSSR_{max}$
1	564	56	4,448	2,224	10	47,421	32.95
2	564	56	4,448	2,224	10	70,118	33.96
3	564	56	4,448	2,224	10	74,168	33.04
4	413	41	4,448	2,224	10	58,574	31.01
5	413	41	4,448	2,224	10	61,578	32.65
6	413	41	4,448	2,224	10	118,960	30.74
7	413	41	4,448	2,224	10	159,422	34.29
8	376	37	4,448	2,224	10	83,989	32.01
9	376	37	4,448	2,224	10	124,238	29.74
10	376	37	4,448	2,224	10	116,238	29.74
11	376	37	4,448	2,224	10	158,555	33.42
12	450	40	4,448	2,224	10	52,422	29.1
13	450	40	4,448	2,224	10	54,889	28.95
14	450	40	4,448	2,224	10	107,214	28.77
15	450	40	4,448	2,224	10	144,303	28.4

**Table 5.5 Combination of Fretting Fatigue and Plain Fatigue
(Data from Present Study Highlighted By Yellow Color)**

Number Of Cycles In One Block Of Plain Fatigue = PF	Number Of Cycles In One Block Of Fretting Fatigue = FF	PF/FF	Nf
10000000	0	10*10^16	10000000
0	42640	0.001	42640
200000	1000	200	3301122
1000	5000	0.2	44656
10000	5000	2	79695
100000	5000	20	350937
10028211	21320	470.3664	10049531

**Table 5.6 Combination of Fretting Fatigue and Plain Fatigue
(Data from Present Study Highlighted By Yellow Color)**

PF	FF	Nf	Number of Times PF & FF Occurred (Or one of them)	Total Number of PF Cycles = TPF	Total Number of FF Cycles = TFF	TPF/TFF
10000000	0	10000000	1	10000000	0	
0	42640	42640	1	0	42640	0.001
200000	1000	3301122	16.42	3284699	16423.5	200
1000	5000	44656	7.4	7442.667	37213.3	0.2
10000	5000	79695	5.31	53130	26565	2
100000	5000	350937	3.34	334225.7	16711.3	20
10028211	21320	10049531	1	10028211	21320	470.37

Table 5.7 Axial Stress Range & Effective Stress [8]

Test	σ_{max}	σ_{min}	$\Delta\sigma$	$\sigma_{eff \ (Mpa)}$	P_{max}	P_{min}	P_{Freq}	N_f
#	(MPa)	(MPa)	(MPa)	MPa	(N)	(N)	(Hz)	Cycles
1	600	60	540	572	2224	2224	0	34,072
2	600	60	540	572	4448	4448	0	39,434
3	600	60	540	572	4448	2224	2.5	41,400
4	600	60	540	572	4448	2224	30	39,004
5	270	-270	540	369	2224	2224	0	136,092
6	270	-270	540	369	4448	4448	0	98,072
7	270	-270	540	369	4448	2224	2.5	108,056
8	270	-270	540	369	4448	2224	30	124,417

Table 5.8 Axial Stress Range & Effective Stress [29]

Test	σ_{max}	σ_{min}	$\Delta\sigma$	σ_{eff} (Mpa)	P_{max}	P_{min}	P_{Freq}	N_f
#	MPa	MPa	MPa	MPa	N	N	Hz	Cycles
1	636	-40	675	653	1330	1330	0	26,700
2	700	44	656	679	1330	1330	0	31,600
3	552	18	534	544	1330	1330	0	53,400
4	566	53	513	542	1330	1330	0	70,600
5	687	291	396	536	1330	1330	0	86,200
6	425	35	389	408	1330	1330	0	91,900
7	538	233	305	416	1330	1330	0	118,000
8	416	29	388	403	1330	1330	0	121,000
9	686	294	392	533	1330	1330	0	124,000
10	529	232	297	408	1330	1330	0	262,000
11	687	456	231	420	1330	1330	0	371,000
12	582	351	231	384	1330	1330	0	672,000
13	413	186	227	315	1330	1330	0	2,080,000
14	686	442	244	431	1330	1330	0	2,560,000
15	420	191	229	320	1330	1330	0	3,660,000
16	540	372	168	319	1330	1330	0	4,140,000
17	507	331	176	315	1330	1330	0	50,000,000
18	410	273	137	250	1330	1330	0	50,000,000

Table 5.9 Axial Stress Range & Effective Stress [12]

Test	σ_{max}	σ_{min}	$\Delta\sigma$	σ_{eff}	P_{max}	P_{min}	P_{Freq}	N_f
#	MPa	MPa	MPa	MPa	N	N	Hz	Cycles
11	600	294	306	443	4448	2224	20	250,000
12	592	272	320	449	4448	2224	20	230,000
15	569	57	512	543	2224	2224	0	59,000
17	590	65	525	560	4448	4448	0	53,000
18	599	36	563	583	4448	2224	36	69,000
19	582	12	570	577	4448	2224	36	50,000
20	596	30	566	582	4448	2224	36	51,000
21	591	18	573	583	4448	2224	40	46,000
22	592	59	533	565	4448	2224	40	51,000

Table 5.10 Axial Stress Range & Effective Stress [30]

Test	σ_{max}	$\Delta\sigma$	σ_{eff}	P_{max}	P_{min}	P_{Freq}	Phase Angle	N_f
#	MPa	MPa	MPa	N	N	Hz	Degree	cycle
1	760	684	724	4448	2224	10	0	20,734
2	564	518	538	4448	2224	10	0	47,298
3	564	518	538	4448	2224	10	90	61,428
4	413	372	394	4448	2224	10	0	229,477
5	413	372	394	4448	2224	10	90	275,172
6	376	339	358	4448	2224	10	0	657,432
7	376	339	358	4448	2224	10	90	1,706,847
8	282	254	269	4448	2224	10	0	> 6 million
12	564	518	538	4448	2224	10	60	69,149
13	564	518	538	4448	2224	10	105	90,528
15	351	316	335	4448	2224	10	90	10,000,000

Table 5.11 Shear Stress Range & Fatigue Life from Present Study

Test	σ_{max} (MPa)	σ_{min} (MPa)	$\Delta\sigma$ (MPa)	P_{max} (N)	P_{min} (N)	θ deg	Q_{max} (N)	Q_{min} (N)	ΔQ (N)	N_f (Cycle)
1	564	56	508	4,448	2,224	0	410	-890	1,300	47,421
2	564	56	508	4,448	2,224	45	819	-413	1,232	70,118
3	564	56	508	4,448	2,224	90	611	-597	1,208	74,168
4	413	41	372	4,448	2,224	0	934.1	-229.7	1,164	58,574
5	413	41	372	4,448	2,224	0	939	-235	1,174	61,578
6	413	41	372	4,448	2,224	45	754	-390	1,144	118,960
7	413	41	372	4,448	2,224	90	110	-715	825	159,422
8	376	37	339	4,448	2,224	0	1189	-283	1,472	83,989
9	376	37	339	4,448	2,224	45	648	-383	1,031	124,238
10	376	37	339	4,448	2,224	45	680	-380	1,060	116,238
11	376	37	339	4,448	2,224	90	58.3	-682.3	741	158,555
12	450	40	410	4,448	2,224	0	1168	-198	1,366	52,422
13	450	40	410	4,448	2,224	0	1086	-250	1,336	54,889
14	450	40	410	4,448	2,224	45	1049	-221	1,270	107,214
15	450	40	410	4,448	2,224	90	858	-264	1,122	144,303
16	564	56	508	3,336	3,336	-	-	-	-	44,656
17	564	56	508	3,336	3,336	-	-	-	-	350,397

Table 5.12 MSSR Calculation [29]

Test	σ_{max} (MPa)	σ_{min} (MPa)	P_{max} (N)	P_{min} (N)	P_{Freq} (Hz)	N_f (Cycles)	$MSSR_{max}$
1	636	-40	1330	1330	0	26,700	29.1
2	700	44	1330	1330	0	31,600	30.5
3	552	18	1330	1330	0	53,400	29.6
4	566	53	1330	1330	0	70,600	30.1
5	687	291	1330	1330	0	86,200	29.6
7	538	233	1330	1330	0	118,000	27.8
8	416	29	1330	1330	0	121,000	26.9
9	686	294	1330	1330	0	124,000	29.4
10	529	232	1330	1330	0	262,000	27.2
11	687	456	1330	1330	0	371,000	28.2
12	582	351	1330	1330	0	672,000	27.5
13	413	186	1330	1330	0	2,080,000	25.3
14	686	442	1330	1330	0	2,560,000	28.2
15	420	191	1330	1330	0	3,660,000	25.4
16	540	372	1330	1330	0	4,140,000	26.5
17	507	331	1330	1330	0	50,000,000	26.6
18	410	273	1330	1330	0	50,000,000	24.5

Table 5.13 MSSR Calculation [12]

Test	σ_{max} (MPa)	σ_{min} (MPa)	P_{max} (N)	P_{min} (N)	P_{Freq} (Hz)	N_f (Cycles)	$MSSR_{max}$
11	600	294	4448	2224	20	250,000	26.7
12	592	272	4448	2224	20	230,000	27.1
15	569	57	2224	2224	0	58,600	31.5
17	590	65	4448	4448	0	53,000	33.3
18	599	36	4448	2224	36	69,000	29.9
19	582	12	4448	2224	36	49,500	32.6
20	596	30	4448	2224	36	50,700	29.9
21	591	18	4448	2224	40	46,000	34.5
22	592	59	4448	2224	40	51,000	32.0

Table 5.14 MSSR Calculation [8]

Test	σ_{max} (MPa)	σ_{min} (MPa)	P_{max} (N)	P_{min} (N)	P_{Freq} (Hz)	N_f (Cycles)	$MSSR_{max}$
1	600	60	2224	2224	0	34,072	33.88
2	600	60	4448	4448	0	39,434	36.32
3	600	60	4448	2224	2.5	41,400	35.07
4	600	60	4448	2224	30	39,004	33.97
5	270	-270	2224	2224	0	136,092	28.12
6	270	-270	4448	4448	0	98,072	30.64
7	270	-270	4448	2224	2.5	108,056	30.03
8	270	-270	4448	2224	30	124,417	28.84

Table 5.15 MSSR Calculation [30]

Test	σ_{max} (MPa)	σ_{min} (MPa)	P_{max} (N)	P_{min} (N)	P_{Freq} (Hz)	N_f (Cycles)	$MSSR_{max}$
1	760	76	4448	2224	10	20,734	*33.09*
2	564	56	4448	2224	10	47,298	*33.347*
3	564	56	4448	2224	10	61,428	*36.748*
4	413	41	4448	2224	10	229,477	*30.42*
5	413	41	4448	2224	10	275,172	*34.19*
6	376	37	4448	2224	10	657,432	*29.588*
7	376	37	4448	2224	10	1,706,847	*33.418*
8	282	28	4448	2224	10	> 6 million	*30.857*
9	564	56	3336	3336	0	42,640	*35.923*
12	564	56	4448	2224	10	69,149	*33.96*
13	564	56	4448	2224	10	90,528	*35.956*
15	351	35	4448	2224	10	10,000,000	*32.2*

VI. Conclusion and Recommendation

In this chapter, the summary of this study are presented. This chapter will include the conclusion of the analyzed and discussed results from this present study as well as recommendation for future work which can be accomplished based on the results those achieved in this present study.

6.1. Summary

There is a lot of work that has been accomplished to better understand the fretting behavior of the titanium alloy Ti-6Al-4V since this material is used in gas turbine engines. In previous studies, most of them assumed that the applied contact load is constant, while a little effort has been conducted under variable contact load. Trying to look into mechanics of components in the turbine engine fretting fatigue phenomenon is a very difficult area to study due to the complicated oscillatory movements at the contact region which result from the application of both the axial and the contact loads. These loads can be applied in any condition; variable contact load, in-phase, an alternate between plain fatigue and fretting fatigue, or phase lag between the axial and the contact load. In order to have a better understanding of the behavior of fretting fatigue, investigating the fretting fatigue with phase difference and combination of fretting fatigue and plain fatigue was the main objective of this present study.

Test # 16 and test # 17 were conducted under combinations between fretting fatigue and plain fatigue. In both tests; the contact load was kept constant at 3336 N, while the axial stress range was kept in between 564 MPa and 56 MPa. In addition, fifteen tests were conducted with phase difference between the applied axial load and the applied contact load. Eleven out of these fifteen tests were conducted using 50.8 mm pads while the rest were conducted using 304.8 mm pads. In these experiments; the maximum axial load was varied between 564 MPa and 413 MPa and the applied contact load was kept constant between 4448 N and 2224 N. Also, the selected phase angles were: 0 degree, 45 degree, and 90 degree. The frequency applied during the seventeen tests was 10 Hz.

All of the experiments were conducted by using Ti-6Al-4V alloy specimens, which has Poison's ratio of 0.33, modulus of elasticity of 126 GPa, and dimension of 3.81 mm thickness and 6.35 mm width. a computer controlled bi-axial servo-hydraulic machine was used to control the applied load condition and their frequencies and phase angle by using a peak valley compensator to reduce the variation between control and feedback signals. The outputs of various data were monitored and saved continuously until failure of the specimen occurred. The resulting tangential loads were found as the half difference between the lower axial loads and the upper grip loads. After the specimen failed, the contact half width of the failed specimen was determined by using the lower magnification microscope. After that, the Scanning Electron Microscope (SEM) was used to examine the fracture surface area, locate the crack initiation location, and measure the crack initiation orientation. And prior to SEM the contact half width of the failed specimen was determined by using the lower magnification microscope.

The loads recorded by the computer connected to the bi-axial servo-hydraulic machine were used as an input to the Finite Element Analysis (FEA) model. It was concluded in this study that the infinite half-space assumption was invalid. This is where the importance of FEA lies since this was the requirement of the FEA which doesn't require a finite half-space assumption. Therefore, the commercial software ABAQUAS was used to conduct the FEA in this study. In order to prevent gross slip, the maximum contact load was always applied initially at the first, and in step 2 the maximum axial load with the corresponding tangential load were applied. The maximum calculated Q/P from this study was around 0.5, therefore; the coefficient of friction was selected for all tests to be 0.5 for FEA, the maximum load condition was used here at the maximum axial load condition for in-phase or phase difference.

MSSR was adopted in this study as the most effective parameter in predicting the fretting fatigue life, and the crack initiation location and orientation. The FEA outputs were used as an input into the MSSR calculation. Also, the shear stress range and the axial stress range were investigated to determine their effect on the fatigue life and the crack initiation mechanism. In the present study, local stress range was not taken into consideration for both the shear stress range and the axial stress, but rather both were formulated on the global axial and tangential stresses.

6.2. Conclusions

In this section, the effect of the combination between the fretting fatigue and the plain fatigue on the fretting fatigue behavior, the effect phase difference between the

126

axial and the contact loads, and the effect of using different contact pads will be discussed in this section.

6.2.1 Combination between Fretting and Plain Fatigue

1. The resulted tangential load converged to the same magnitude when the contact load reapplied after the plain fatigue condition .Also, the steady state condition has been met after a few hundreds of fretting fatigue cycles each time the fretting fatigue condition started after plain fatigue condition.

2. Domination of plain fatigue cycles increases the life of titanium alloy while domination of fretting fatigue cycles decreases the life of titanium alloy.

3. There is no history effect as long as the total cycles are the same. This means that there will be no effect on fretting fatigue life whether some of fretting fatigue was applied at first and continued by plain fatigue and the process kept alternating or finishing all fretting fatigue cycles first followed by plain fatigue.

6.2.2. Phase Difference

1. Steady state condition of the fretting fatigue variables were met after a few hundreds of fretting fatigue cycles. These fatigue variables are the applied axial and contact loads, the tangential load, and the coefficient of friction.

2. The crack initiation location always occurred at or very near the trailing edge of the contact region where $x/a \approx +1$ along the x-direction. This observation occurred in test one through fifteen, which have been conducted under in-phase as well as phase difference conditions.

3. The maximum magnitude for the Q/P ratio under fretting fatigue condition barely reached 0.4.The greatest value of Q/P was found to be at the in-phase condition, while the least value at the out of phase condition. This conclusion indicates that the out of phase condition has less friction than other conditions and the in-phase condition has the most friction.

4. Fretting fatigue life increases as shears stress range, ΔQ, increases. This observation is valid despite of phase angle condition, in-phase or out of phase condition.

5. Shear stress range, ΔQ, for out of phase condition is les than that of in-phase condition.

6. Shear stress range, ΔQ, decreases as the phase angle increases.

7. At different axial load conditions and same phase angle, fretting fatigue life decreases when axial stress increases.

8. Fretting fatigue life increases when the phase angle increases for the same applied axial load condition.

9. Fretting fatigue life for out of phase condition is higher than that of in-phase condition for the same axial load.

10. There was no effect from the applied contact load on the tangential load except on it magnitude and the tangential load was varying in the same manner as the axial load.

11. It was noticed that the stress range of the out of phase condition is less than that of the in-phase condition.

12. Fretting fatigue life increases as axial stress range decreases, for both in-phase and out of phase conditions.

13. It was concluded that the S_N curve for the axial stress range did not collapse the data together, rather three segregated curves were formed which reflect that using axial stress range as a predictive parameter for this present study is not effective. This is due to the reason that axial stress range does not account do contact stresses.

14. It was concluded that S_N curve for the effective stress did not collapse the data together, rather three segregated curves were formed which reflect that using effective stress as a predictive parameter for this present study is not effective. This is due to the reason that effective stress does not account do contact stresses.

15. Four distinguishable regions were found in the fracture surface; debris at region 1, striation at region 2, large dimples at region 3, and catastrophic fracture at region 4.

16. The crack initiation orientation angle for the in-phase condition and out of phase condition was around 45 degree which is close to the previous studies.

17. It can be concluded using FEA that the maximum local axial stress magnitude for the out of phase condition is less than the in-phase.

18. MSSR values increases as axial stress increases.

19. MSSR values for out of phase condition was found to be slightly more than that of the in-phase condition, yet the difference is very small and trivial.

20. MSSR values increases as fretting fatigue life decreases at a given stress level.

21. MSSR parameter was very effective in predicting the crack initiation location and the crack initiation orientation for present study. This is due to the fact that MSSR parameter takes into consideration both normal and shear stress and is independent of pad geometry.

22. The crack initiation location, that was determined from the MSSR, for experiments using 50.8 mm pads, was at x/a = 1.1 for the in-phase condition and at out of phase condition. On the other hand, for experiments using 3.4.8 mm pads, crack imitation location was at x/a = 0.99.

23. Comparing results from test conducted with in-phase condition to those tests conducted under out-phase conditions; the phase difference improved the fatigue life. Fretting fatigue life increases when phase angles increases.

6.2.3 Pad Geometry Effect on Fatigue Life

It was noticed that changing the radius of the cylindrical pads from a high curvature value 50.8 mm to merely flat pads 304.8 mm did have different effect on the fatigue life. Changing the pad radius from 50.8 mm to 304.8 mm did decrease the fretting fatigue life.

6.3. Recommendations for Future Work

This present study was concentrated on the investigation of the effect of phase difference between the axial and the contact load and the combination between the fretting fatigue and the plain fatigue on the behavior of fretting fatigue on titanium alloy. This work was done with both 50.8 mm and 304.8 mm radius cylindrical-end pads with axial and contact load frequency of 10 Hz. The followings are some recommendations for further studies:

1. Investigating the fretting fatigue behavior under phase difference between the axial and contact load under elevated temperature will be a very worthy study since interesting subject to study the operating temperature inside the engine is very high comparing to the room temperature.

4. The axial and contact load frequency was 10 Hz, however; in reality aircraft engine has a frequency that much greater than that. Therefore, it will be worthy to do a study that investigates the effect of in phase as well as in phase conditions under high frequency.

5. Environmental corrosion and its effect of fretting fatigue is another interesting field to look at and study. In some countries, like the Kingdom of Bahrain, where fighter aircraft are exposed to high humidity and high salt content in the environment knowing it's a small island and most the major air force base lies next to the sea, the effect of environmental corrosion on fretting fatigue will be a critical study.

6. Aircraft engines includes various material other than titanium, so it will be worthy to conduct the same effect of fretting fatigue as well phase difference using other metals.

7. One of the most important procedures to improve the material performance and the fatigue life of the material is the shot peening, so it will be worthy to

conduct the same effect of fretting fatigue as well phase difference using

titanium alloy treated by shot-peening.

Bibliography

1. D. Hills and D. Nowell. *Mechanics of Fretting Fatigue*, Kluwer Academic Publishers, Netherlands, 1994.

2. K. Chan and Y. Lee. *Ruiz Program*, South West Research Institute, Personal Communication, 1998.

3. K. Iyer and S. Mall. "Effects of Cyclic Frequency and Contact Pressure on Fretting Fatigue under Two-level Block Loading," *Fatigue Fract. Engng. Mater. Struct.*, 23: 335-346 (2000).

4. D. Hills, D. Nowell, and A. Sackelfield. "Surface Fatigue Considerations in Fretting Interface Dynamic, Proceedings of the 14th Leeds-Lyon Symposium on Tribiology, D. Dawson, C. M. Taylor, M. Godet, D. Berthe Eds. Elsevier, Amsterdam, 1988.

5. C.D Lykins, S. Mall, and V.K Jain. "A Shear Stress Based Parameter for Fretting Fatigue Crack Initiation," *Fatigue and Fracture of Engineering Materials and Structures*, 24: 461-473 (2001).

6. K. Iyer and S. Mall. "Analysis of Contact Pressure and Stress Amplitude Effects on Fretting Fatigue Life," *Journal of Engineering Materials and Technology*, 123:85-93 (January 2001).

7. S.A. Namjoshi, S. Mall, V.K. Jain, and O. Jain. "Effects of Process Variables on Fretting Fatigue Crack Initiation in Ti-6Al-4V," *Journal of Strain Analysis*, 37, No.6: 535-542 (2002).

8. Chia-hwa Lee. "Effect of variable contact load on fretting fatigue behavior of shot-peened and un-peened titanium alloy", Thesis AFIT/GAE/ENY/04-D01, Dec 2004M.H.

9. C.D Lykins, S. Mall, and V.K Jain. "A Shear Stress Based Parameter for Fretting Fatigue Crack Initiation," *Fatigue and Fracture of Engineering Materials and Structures*, 24: 461-473 (2001).

10. S. A. Namjoshi, S. Mall, V. K. Jain, and O. Jin. "Fretting Fatigue Crack Initiation Mechanism in Ti-6Al-4V," *Fatigue Fract Engng Master Struct*, 25: 955-964 (2002).

11. MADHI. " Fretting fatigue behavior of Nickel alloy IN-100," Thesis AFIT/GAE/ENY/06-M22, March 2006.

12. A.J. Jutte. "Effect of a Variable Contact Load on Fretting Fatigue Behavior of Ti-6Al-4V," Thesis, Air Force Institute of Technology, Wright-Patterson Air Force Base, Ohio, 2004.

13. H. Lee, O. Jin, and S. Mall. "Fretting Fatigue Behaviour of Shot-peened Ti-6Al-4V at Room and Elevated Temperature," *Fatigue Fract Engng Master Struct*, 26: 1-12 (2003).

14. H. Lee, S. Mall. "Stress Relaxation Behavior of Shot-peened Ti-6Al-4V under Fretting Fatigue at Elevated Temperature," *Materials Science and Engineering* A366: 412-420 (2004).

15. R.B. Waterhouse and M.K. Dutta. "The Fretting Fatigue of Titanium and Some Titanium Alloys in a Corrosive Environment," *Wear*, 25: 171-175 (1973).

16. M.H. Wharton and R.B. Waterhouse. "Environmental Effects in the Fretting Fatigue of Ti-6Al-4V," *Wear*, 62:287-297 (1980).

17. D.W. Hoeppner, A.M. Taylor, and V. Chandrasekaran. "Fretting Fatigue Behavior of Titanium Alloys," In: Fretting Fatigue: Advances in Basic Understanding and Applications. Eds. Y. Mutoh, S.E. Kinyon, and D.W. Hoeppner. West Conshohocken PA: ASTM International (2003).

18. L.C. Lietch. "Fretting Fatigue Behavior of the Titanium Alloy Ti-6Al-4V under Seawater Conditions," Master's thesis, AFIT/GMS/ENY/04-M02, Air Force Institute of Technology, Wright-Patterson Air Force Base, Ohio, 2004.

19. H.I. Yuksel. "Effects of Shot-peening on High Cycle Fretting Fatigue Behavior of Ti-6Al-4V," MS Thesis AFIT/GAE/ENY/02-12. Air Force Institute of Technology (AU), Wright-Patterson AFB OH, December 2002.

20. L. Coffin, Jr. "A Study of the Effects of Cyclic Thermal Stresses on a Ductile Metal," Trans. ASME, 76: 931-950 (1954).

21. S. Manson. "Behavior of Materials under Conditions of Thermal Stress," *NACA Technical Report* TN 2933 (1953).

22. O. Basquin. "The Exponential Law of Endurance Tests," *Am. Soc. Test. Mater Proc.*, 10: 625-630 (1910).

23. K. Walker. "The Effect of Stress Relation during Crack Propagation and Fatigue for 2024-T3 and 7075-T6 Aluminum," Presented to subcommittee E-9V Winter Meeting (Feb 1969).

24. S. Mall, V.K. Jain, S. Namjoshi, and C.D. Lykins. "Fretting Fatigue Crack Initiation Behavior of Ti-6Al-4V," *Standard Technical publication 1425*, ASTM International (2003).

25. M. Szolwinski, and T. Farris. "Mechanics of Fretting Fatigue Crack Formation", *Wear*, 93-107 (1996).

26. R. Neu, J. Pape, and D. Swalla-Michaud. "Methodologies for Linking Nucleation and Propagation Approaches for Predicting Life under Fretting Fatigue", Fretting Fatigue: Current Technology and Practices, ASTM 1367, D. Hoeppner, V. Chandrasekaran and C. Elliot, Eds. American Society for Testing and Materials.

27. W.N. Findley. "Fatigue of Metals under Combination of Stresses," *Trans ASME*, 79: 1337-48 (1975).

28. Maganizer, R. S. examination of Contact Width on Fretting Fatigue. Ph.D. dissertation, Graduate School of Engineering, Air Force Institute of Technology (AFIT), WPAFB, March 2002. AFIT/GAE/ENY/02-8.

29. C.D Lykins, S. Mall, and Douglas. "An Investigation of Fretting Fatigue Crack Initiation Behavior of the Titanium Alloy Ti-9Al-4V," PhD.dissertation, University of Dayton, December 1999

30. Al-Majali. "Effect of Phase Difference between Axial and Contact Loads on Fretting Fatigue Behavior of Titanium Alloy," Thesis AFIT/GAE/ENY/06-S02, September2006.

Vita

Captain Abdulla Ahmed Al-Noaimi holds a Bachelor of Science in Aerospace Engineering since 1999 and he graduated with Cum Laude Honors from Embry Riddle Aeronautical Engineering University, Dayton Beach, U.S.A.

His first assignment was at the Fighter Wing Maintenance Squadron at Shaikh Isa Air Force Base, Kingdome of Bahrain, as a maintenance officer in the F-16 Flight Line. In 2002 he attended the Air Force Maintenance Officer Course AMOC at Sheppard Air Base in Texas, USA. In 2004, he became the F-16 Flight Line Commander and worked in this position for two years. During his service at the Royal Bahraini Air Force he did manage several positions which includes; F-16 Flight line, Maintenance Back Shops, Maintenance Training, and Maintenance Control. In September 2006, he entered the Graduate school of Engineering and Management, Air Force Institute of Technology. Upon Graduating with a Master of Science degree in Aeronautical Engineering, he will be assigned back to Sheikh Isa Air Force Base to resume his job as the F-16 Flight Line Commander.

REPORT DOCUMENTATION PAGE

1. REPORT DATE *(DD-MM-YYYY)* 21-03-2008	2. REPORT TYPE **Master's Thesis**	3. DATES COVERED *(From – To)* January 2006 – March 2008

4. TITLE AND SUBTITLE **IVESTIGATION INTO FRETTING FATIGUE UNDER CYCLIC CONTACT LOAD AND IN CONJUNCTION WITH PLAIN FATIGUE OF TITANIUM ALLOY**	5a. CONTRACT NUMBER
	5b. GRANT NUMBER
	5c. PROGRAM ELEMENT NUMBER
6. AUTHOR(S) Al-Noaimi, Abdulla, Capt, Royal Bahraini Air Force	5d. PROJECT NUMBER
	5e. TASK NUMBER
	5f. WORK UNIT NUMBER

7. PERFORMING ORGANIZATION NAMES(S) AND ADDRESS(S) Air Force Institute of Technology Graduate School of Engineering and Management (AFIT/EN) 2950 Hobson Way, Building 640 WPAFB OH 45433-7765	8. PERFORMING ORGANIZATION REPORT NUMBER AFIT/GAE/ENY/08-M30

9. SPONSORING/MONITORING AGENCY NAME(S) AND ADDRESS(ES)	10. SPONSOR/MONITOR'S ACRONYM(S)
	11. SPONSOR/MONITOR'S REPORT NUMBER(S)

12. DISTRIBUTION/AVAILABILITY STATEMENT
APPROVED FOR PUBLIC RELEASE; DISTRIBUTION UNLIMITED.

13. SUPPLEMENTARY NOTES

14. ABSTRACT

Fretting fatigue is the surface damage that occurs at the interface between two components that are under going a small amplitude oscillatory movements. It results in a reduction of the material life comparing to the plain fatigue. Most of the previous works were accomplished under a constant applied contact load and a little effort has been done under a variable contact load, while none of these studies have taken the phase difference between the axial and the contact load. The primary goal of this study is to investigate the effect of phase difference between axial and contact loads on fretting fatigue behavior of Ti-6Al-4V alloy and to determine the behavior of this material under combination of fretting fatigue and plain fatigue. The frequency of both axial and contact loads was the same .i.e. 10 Hz. During the variable contact load condition; only the axial stress range and the phase angle were varying. Cracks were always found to initiate on the contact surface and near the trailing edge for all tests. The software program, ABAQUAS, was used in finite element analysis to determine the contact region state variables such as stress, strain, and displacement. The fatigue parameters; such as the stress range, effective stress, and modified shear stress range (MSSR) were analyzed to predict the fatigue life. The out of phase condition was found to increase the fatigue life of 20 % to 30% in life with low cycles and up to 150 % at life with high cycles. As the application ratio of plain fatigue to fretting fatigue increases the life will increase. The MSSR parameter was effective in predicting the fatigue life, crack initiation location, and crack initiation orientation.

15. SUBJECT TERMS
Fatigue, Fretting, Titanium Alloys, Out of phase, Combination.

16. SECURITY CLASSIFICATION OF:			17. LIMITATION OF ABSTRACT	18. NUMBER OF PAGES	19a. NAME OF RESPONSIBLE PERSON Dr. Shankar Mall, AFIT/ENY
REPORT U	ABSTRACT U	c. THIS PAGE U	UU	156	19b. TELEPHONE NUMBER *(Include area code)* (937) 255-3636X4587; e-mail: shankar.mall @afit.edu